PROCESS AND STRUCTURAL HEALTH MONITORING OF ADVANCED FIBRE REINFORCED COMPOSITES USING OPTICAL FIBRE SENSORS

Abilash Kumar Kochumulappon Raghavan Nair

A thesis submitted to the University of Birmingham for the degree of

DOCTOR OF PHILOSOPHY

School of Metallurgy and Materials

College of Engineering and Physical Sciences

University of Birmingham

July 2014

ABSTRACT

The focus of this research programme was to design, optimise and deploy a practical multi-measurand sensor (MMS) for process monitoring of glass and carbon fibre preforms in an autoclave. The MMS design was based on the optical fibre-based extrinsic Fabry-Perot interferometric (EFPI) strain sensor. The EFPI sensor consisted of a pair of cleaved optical fibres, with a defined gap (Fabry-Perot cavity) that were housed in a precision bore capillary. The optical fibres were secured to the capillary via two fusion joints. The distance between the fusion joints represents the gauge length. Interferometric interrogation was used to measure the cavity length hence, permitting the strain to be determined. The basic EFPI sensor design was modified in the following manner to enable multi-measurand monitoring.

Firstly, a fibre Bragg grating (FBG) was inscribed on one of the optical fibres that were destined to be housed in the capillary; the end-face of this cleaved optical fibre was sputter coated with Au/Pd to produce a reflective surface. This FBG is in a relatively strain-free condition and as such, it only responds to temperature. Secondly, a technique was developed to manufacture optical-quality end-faces of the capillary and this too was sputter coated with Au/Pd. Thirdly, secondary cleaved optical fibres were packed around the lead-in optical fibre of the EFPI sensor with a defined (secondary) cavity. These secondary cavities acted as pseudo cuvettes to contain the liquid of interest thus, permitting transmission/reflection FTNIR spectroscopy. Finally, cleaved secondary optical fibres were also secured to the lead-in fibre and these served as

Fresnel reflection sensors. The interrogation of the MMS was carried out using a conventional fibre-coupled multi-channel FTNIR spectrometer. The feasibility of monitoring the following parameters simultaneously during the processing of glass and carbon fibre preforms was demonstrated: (i) strain; (ii) temperature; (iii) cross-linking kinetics; and (iv) refractive index.

This thesis is dedicated to my family.

ACKNOWLEDGEMENTS

I would like to take this opportunity to thank Professor Gerard Fernando for his able guidance and encouragement throughout the progress of this work. The fruitful discussions with him have taught me the method of designing, executing and analysing the problems in a true scientific spirit.

I would like to thank Universities UK and School of Metallurgy and Materials for the overseas research studentship award. I am very much thankful to Dr Christophe Paget (Airbus, UK) for the funding and support. I would also like to thank Dr Stephen Kukureka for his support.

I am grateful to Dr Venkata Machavaram for his help and support throughout the course of this research. Appreciation is due to my colleagues in the Sensors and Composites group for their help and support. I would also like to thank Dr Ramani Mahendran, Dr Dee Harris, Dr Shafiq Irfan, Dr Liwei Wang, Ms Claire Wait, Mr Samuel Ojo, Mr Fran Nieves, Mr Richard Murray, Mr Sebastian Ballard, Mr Sebastian Hellmann, Mr Mark Paget and Mr Frank Biddlestone for their help during my work. I sincerely thank Mrs Anne Cabezas and Mrs Kay Jones for their constant support.

I am glad to extend my thanks to Dr Mathew Philip (London Metropolitan University, London), Dr Anil Kumar P V (Head, Polymer Engineering Department, STAS, Mahatma Gandhi University, India), Dr S Radhakrishnan (Deputy Director, National

Chemical Laboratory, Pune, India), Mr Eapen Mathew (M M A H S S Maramon, Kerala, India), Mrs Saroj Sharma (The Female Health Company, London), Mr Marcus Hancock, Mr Andrew Turner and Mrs Dawn Sparks (Dunlop Aircraft Tyres Limited, Birmingham) for their constant support.

I would also like to thank the technical staff and colleagues at the School of Metallurgy and Materials, University of Birmingham for their help.

I am truly indebted to my late father Mr Raghavan Nair for his eternal blessings. Finally, I would like to express my deepest gratitude and love for my beloved mother Mrs Retnamma K K, sisters Mrs Asha R Nair and Mrs Ambily R Nair, wife Dr Sreedevi G V and daughter Miss Kalyani A Nair for their endless support, encouragement and prayers.

TABLE OF CONTENTS

LIST OF FIGURES

LIST OF TABLES

ABBREVIATIONS

AFRC	Advanced fibre reinforced composite
ASE	Amplified spontaneous emission
CFRP	Carbon fibre reinforced plastic
DGEBA	Diglycidyl ether of bisphenol-A
DSC	Differential scanning calorimetry
EFPI	Extrinsic Fabry-Perot interferometric
ETFE	Ethylene tetrafluoroethylene
FBG	Fibre Bragg grating
FTNIR	Fourier transform near-infrared
MMS	Multi-measurand sensor
OFS	Optical fibre sensor
OSA	Optical spectrum analyser
PEEK	Poly(etheretherketone)
PI	Polyimide
PS	Photo-sensitive
PTFE	Poly(tetrafluoroethylene)
RI	Refractive index
SMF	Single-mode fibre
T_g	Glass transition temperature

1 INTRODUCTION

Advanced fibre reinforced composites (AFRCs) are being used increasingly as engineering materials in high performance, light-weight structural applications. This is mainly due to their advantageous properties such as low density, high strength-to-weight ratio and design flexibility [1]. The specific properties (property of interest divided by density) of AFRCs are superior to those of other engineering materials [2, 3]. Hence, they are being widely used in a variety of engineering applications including aerospace, automotive, marine and civil engineering [1, 2, 3, 4, 5].

Typically, AFRCs are made by embedding reinforcing fibres in a matrix phase. The mechanical properties are generally dictated predominantly by the properties of the reinforcing fibres used. However, the matrix dominated properties such as compressive strength, inter-laminar shear strength and hygro-thermal behaviour are influenced by the rate and degree of cross-linking during processing [2].

With reference to AFRCs and thermoset-based resin systems, it is generally accepted that the chemical conversion of the monomers can be influenced by parameters such as: (i) the chemical integrity of the constituent components of the resin; (ii) the moisture content; and (iii) the rate of heating. Furthermore, thermosetting reactions are exothermic and therefore, efficient thermal management is important especially for large and thick laminated preforms. When the composite is cooled down to ambient from its processing temperature, residual stresses can develop in the material. This is

due to the thermal expansion mismatch of the components [4, 5]. The development of process-induced residual strain is of significant concern as they can introduce damage in AFRCs in the form of matrix cracks and delaminations [2, 6, 7]. Moreover, the cross-linking reactions in thermosetting resins result in shrinkage as new covalent bonds are formed. Therefore, it is important to monitor the cross-linking kinetics, residual strain and temperature during processing and to establish cross-correlation between processing conditions and performance of composites.

From an application point of view, there is a significant interest in monitoring the structural integrity of AFRCs [6, 7, 8]. For example, in aerospace structures, impact damages can be induced by bird-strikes, damage from debris or dropped tools. The real-time monitoring and evaluation of damage mechanisms within the composite structures are essential to increase its reliability and long-term durability. Furthermore, this will ease the service maintenance of the structural components when used in a dynamic environment [1, 2].

Optical fibre-based sensors can be used as an ideal candidate for process and performance (structural health) monitoring of engineering composites and structures [2, 4, 6-8, 13, 15]. The main advantages include their immunity to electromagnetic interference as well as their relative light-weight compared to conventional electrical-based sensors. Hence, they can be deployed in the areas where electrical-based sensors would fail or require expensive protection/shielding [2, 5].

Unlike conventional electrical-based sensors, optical fibre-based devices can be used to monitor a wide range of measurands including strain, temperature, pressure, humidity, vibration, chemical composition and acoustic emission. Moreover, optical fibre sensors (OFS) can be multiplexed to be used for remote monitoring [5, 10, 11].

Previous researchers have developed different types of optical fibre sensors to optimise the processing of composites. However, the majority of the fibre optic-based sensor systems reported to-date for process monitoring have been single, or at the most, dual measurand systems [8, 10, 11, 15, 19, 21, 22, 28, 29]. In the context of the current work, optical fibre extrinsic Fabry-Perot interferometric (EFPI) sensors, fibre Bragg grating sensors (FBG), Fresnel reflection sensors, chemical sensors and multi-measurand sensors (MMS) are used for process monitoring. EFPI sensors are used to monitor the strain whereas FBG sensors are used simultaneously to monitor the strain and temperature. Fresnel reflection and chemical sensors are used to monitor the cross-linking characteristics of the resin system. However, unlike the other sensors, MMS are used to monitor four independent measurands simultaneously: strain, temperature, relative concentration of specified functional groups in the resin system and refractive index.

1.1 Aims of the study

The overall aim of this research is to design, develop and deploy optical fibre sensors (OFS) for process and structural health monitoring of AFRCs. The primary measurands

of interest are strain, temperature, relative concentrations of specified chemicals and refractive index for process monitoring.

The specific aims of this project are as follows:

(i) To design and optimise multi-measurand sensors for the autoclave-based processing of composites;

(ii) To study the temperature dependencies of the extrinsic Fabry-Perot interferometric sensors and fibre Bragg grating sensors, and to establish the annealing conditions for the sensors;

(iii) To monitor simultaneously the strain and temperature during autoclave processing and post-processing of carbon and glass fibre reinforced composite laminates using EFPI and FBG sensors ; and

(iv) To investigate the strain anomalies of acrylate-coating on the optical fibres during the autoclave-based processing and post-processing of carbon and glass fibre reinforced composite laminates.

1.2 Structure of the thesis

This thesis is structured in the following manner:

Chapter 1 provides an overview of the research.

Chapter 2 presents the literature review of the current research relating to the process and structural health monitoring of fibre reinforced composite materials. It covers an introduction to AFRC's and optical fibre sensors including the sensor operating

principles that contribute to this research. Critical reviews of the cross-linking mechanism of epoxy/amine resin systems, followed by optical fibre sensors relevant to this research.

Chapter 3 details the experimental aspects of the research, including descriptions of the materials and instruments used and the procedures adopted. The fabrication of the optical fibre sensors are detailed first, followed by descriptions of the experimental techniques used for process and structural health monitoring of fibre reinforced composites.

Chapter 4 presents the results obtained using the experimental procedures detailed in Chapter 3 and a discussion of the results.

Chapter 5 summarises the overall conclusions drawn from this study and the recommendations for future research.

2 LITERATURE REVIEW

2.1 Introduction

AFRCs consist of three components; a reinforcing fibre phase, a matrix phase and a fibre-matrix interface [2, 4]. The fibres carry the majority of the load imposed on the composite whilst the matrix transfers the load to the fibre and secures the position of individual fibres within the composite.

The reinforcing phase can be short or continuous fibres. Typical examples of reinforcing fibres include graphite, glass, silicon carbide, polyolefins, aliphatic and aromatic polyamides. The matrix phase can be thermoplastic, thermoset, metal or ceramic. Typical examples of matrices used in the manufacture of AFRCs include epoxy, polyester, phenolic, cyano-acrylate and polyetheretherketone (PEEK). Selected properties of reinforcing fibres and matrix systems are summarised in Table 2.1.

Thermoset resin systems usually consist of a low-molecular weight resin and a compatible cross-linking agent or hardener. When the resin and hardener are mixed, they form a low viscosity liquid that undergoes a chemical reaction under the influence of heat/light to form a highly cross-linked solid that cannot be reprocessed on reheating. High-performance thermosetting resins such as epoxy/amine resin systems are widely used as matrices in AFRCs [4].

The prepreg materials/reinforcing fibres and the resin systems used in this research were: (i) unidirectional carbon/epoxy prepreg; and (ii) woven E-glass/epoxy resin. Therefore, further information is reviewed for these materials.

The cross-linking mechanism associated with the epoxy/amine-based resin system is presented in the next section. A critical review of optical fibre sensors relevant to the current research are presented in the following sections of this chapter.

Table 2.1 Selected properties of reinforcing fibres and matrix systems [2, 4].

Material	Density (Kg m^{-3})	Young's Modulus (GPa)	Tensile Strength (GPa)	Failure Strain (%)	Thermal Expansion (10^{-6} K^{-1})	Diameter (μm)	Max. service temperature (°C)
E-Glass fibres	2560	76	2	2-2.6	5	10-16	650
S-Glass fibres	2490	86	4.4	2-2.5	2.3	7-10	700
Quartz fibres	2200	73	3.6	2-2.5	0.54	9-14	1050
High modulus carbon fibres	1950	330-350	2.3-2.6	0.5-0.7	-0.7	7-10	*
High strength carbon fibres	1750	220-240	3.0-3.3	1.3-1.4	-0.4	7-10	*
Polyaramid (Kevlar ^{TM}-49)	1450	130-140	2.8-3.0	2.3-2.4	-2	12-14	400
Polyethylene	970	85-99	2.7-3.2	3.5-3.7	-10	27-38	Melts at 130 ºC
Silicon carbide fibres	3000	400	2.4	0.6	4	7-10	---
Aluminium	2700	70	0.2-0.6	6-20	24	---	---
Titanium	4500	110	0.3-1	4-12	9	---	---
Mild steel	7800	208	0.4		17	---	---
Aluminium oxide (Al_2O_3)	3800	380	0.5	0.1	8	---	1200
Epoxy	1200	3-7	0.035-0.1	1-3	60	---	80-150
PEEK	1250-1300	3.6	0.15-0.18	50	47	---	120
Polyester	1200-1500	2-4.5	0.04-0.09	2	100-200	---	---
Cyanate ester	---	22-26	0.4-0.7	---	---	---	177
Polyimide	1400	2.1-2.8	0.08-0.12	6-8	45-56	---	>260

* The upper service temperature for carbon fibre would depend on the actual matrix system and the test environment.

2.2 Epoxy resin

Epoxy resins are used widely in diverse applications such as surface coatings, adhesives, printed circuit boards and fibre reinforced composites [12, 13, 15-18]. Epoxy resins are characterised by the possession of two or more epoxide groups or oxirane rings per molecule, the structure of which is given in Figure 2.1.

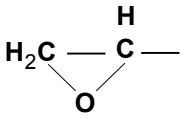

Figure 2.1 Structure of an epoxide group.

Epoxy resins are produced commercially by reacting epichlorohydrin and bisphenol-A. Previous researchers have reviewed the chemistry of epoxy resins in detail [12-19]. The most common type of epoxy resin is the diglycidyl ether of bisphenol-A (DGEBA).

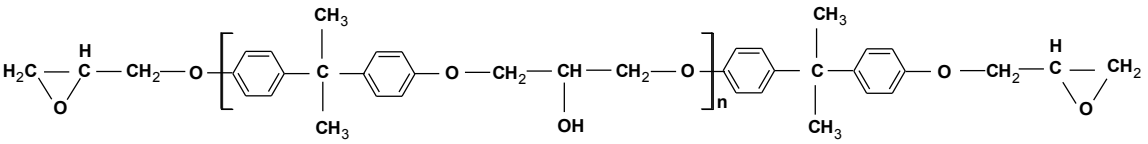

Figure 2.2 General chemical structure of diglycidyl ether of bisphenol-A epoxy resin [12].

Values of *n* vary from 0 to 12, giving a wide range of physical forms from low viscosity liquids to tack-free solids [2]. Cross-linking agents and/or catalysts are used to promote cross-linking of epoxy resin. Examples of such cross-linking agents are aliphatic and

aromatic amines, anhydrides and polyamides [20]. The structure of an aliphatic amine hardener – poly(oxypropylene)diamine used in this research is shown in Figure 2.3.

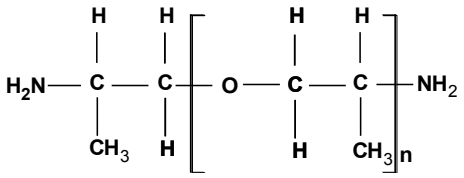

Figure 2.3 Chemical structure of poly(oxypropylene)diamine [20].

2.2.1 Cross-linking of epoxy resins

The epoxide ring is highly strained and reactive [2, 9]. This allows the resin to be cross-linked with a variety of cross-linking agents such as multi-functional primary and secondary amines. Generalised representations of the cross-linking reactions for a typical epoxy/amine resin system are presented in Figure 2.4 (Equations 2.1 and 2.2). Equation 2.1 shows the initial reaction between the epoxy and amine functional groups; here the primary amine is converted to a secondary amine along with the formation of a hydroxyl functional group. The secondary amine (Equation 2.2) is thus capable of reacting with a further epoxy functional group. Cross-linking reactions of this nature result in the conversion of the liquid or semi-solid monomer to a highly cross-linked and insoluble solid.

(i) Primary amine-epoxy addition

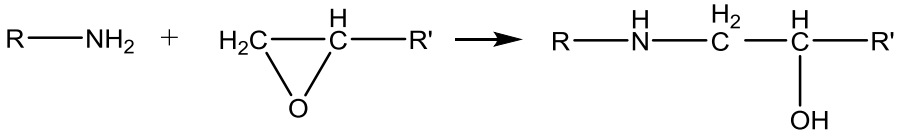

(2.1)

(ii) Secondary amine-epoxy addition

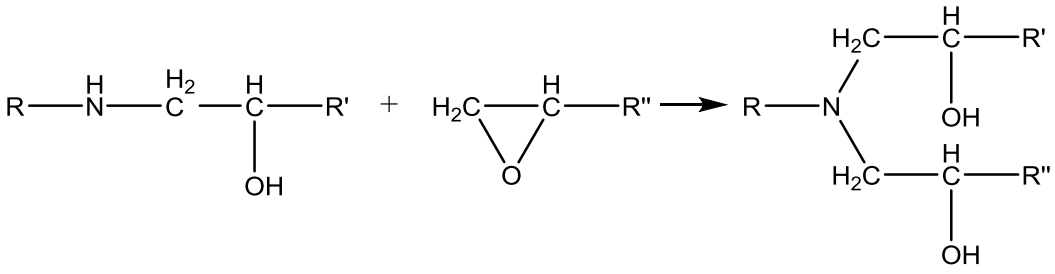

(2.2)

(iii) Etherification (epoxy/hydroxyl addition)

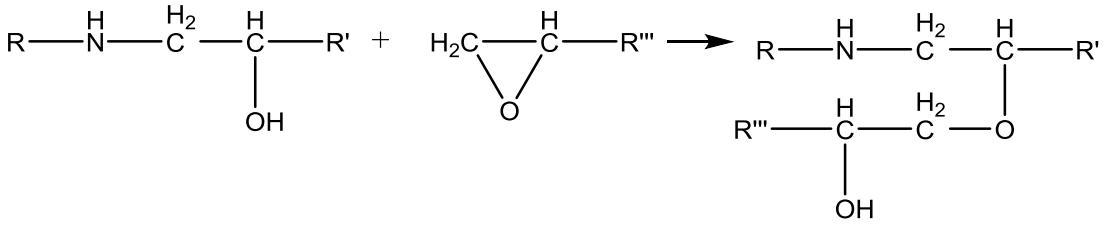

(2.3)

(iv) Epoxy homo-polymerisation

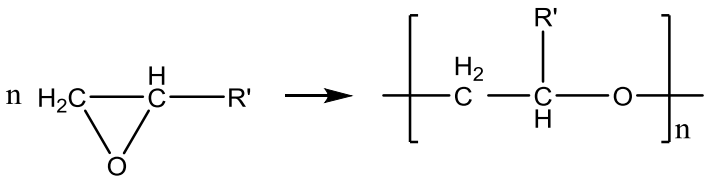

(2.4)

Figure 2.4 Generalised reaction scheme for an epoxy/amine resin system [4].

Side-reactions are also possible depending on the stoichiometry, processing temperature and the nature of contaminants present. Two such side reactions are shown in Figure 2.4 (Equations 2.3 and 2.4); reaction of this nature can add complexity to the analysis and interpretation of the cross-linking kinetics. With reference to the design of the sensor systems to facilitate real-time process monitoring of composite preforms, Equations 2.1 and 2.2 illustrated in Figure 2.4 can be used to define the basic requirements.

This section has presented an overview of the generalised reaction scheme for various possible reactions between epoxy-amine systems. The resin undergoes changes in its thermal, physical and optical properties during the reaction, due to the formation of cross-linked networks. Optical fibre-based sensors can be used to monitor these changes in real-time. A brief introduction of optical fibres is presented in the following section.

2.3 Introduction to optical fibres

Optical fibres are cylindrical waveguides that transmit light along its length by total internal reflection. Optical fibres essentially consist of a core, cladding and a protective coating as highlighted in Figure 2.5. The refractive index of the core is higher than that of the cladding and the light is propagated along the core.

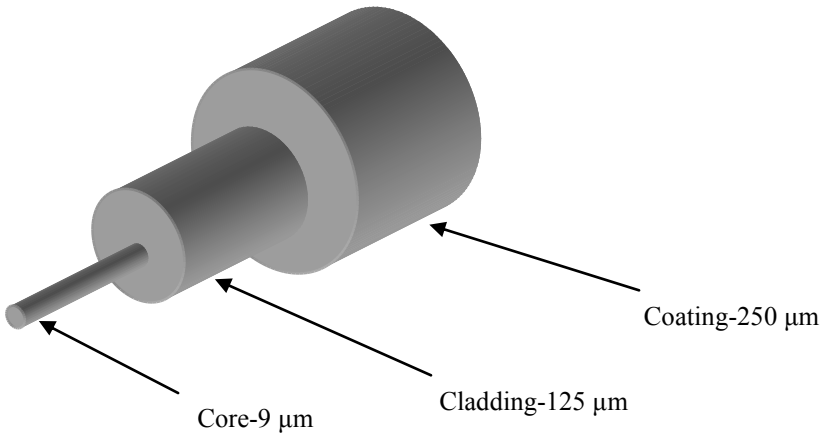

Figure 2.5 Schematic illustration of a single-mode optical fibre showing the diameters of individual components.

A protective coating of polyacrylate or polyimide on the cladding imparts adequate protection during handling and operation. Single-mode or mono-mode optical fibres support a single mode of light propagation path while multi-mode fibres support many propagation paths. The core diameter of a single-mode optical fibre is generally between 7-12 μm whilst that of a multi-mode optical fibre is around 50 μm [5].

2.4 Process monitoring of composites

The development of residual stresses in composites during processing is mainly due to: (i) cross-linking-induced shrinkage of the polymer matrix, and (ii) the thermal expansion mismatch of the constituent materials used. The cross-linking-induced residual stresses are developed due to the shrinkage of the resin during cross-linking. When cooled back to ambient, the difference in thermal expansion rates of the fibre and the matrix result in the build-up of thermally-induced residual stresses in the layers of the composite [26, 28, 31, 37, 45, 46, 50]. It is also known that other factors such as resin-loss from the surface plies when bleeder-fabrics are used, and tool/preform interactions can also contribute to the residual fabrication stresses [26, 28]. These stresses may be sufficiently large enough to cause dimensional instability and they can have an adverse influence on the short and long-term mechanical properties of the composite structures [5, 6, 7]. Moreover, residual stresses can introduce micro-failures, such as matrix cracking and delamination in AFRCs [54, 55]. In short, residual stress development affects the macro-mechanical properties of composite materials and, therefore, it is essential to study the evolution of strain during processing.

2.4.1 Process monitoring using embedded optical fibre sensors

Previous researchers have reported and demonstrated that optical fibre sensors can be used to monitor a wide range of measurands including humidity [5], strain [4, 8, 10, 11, 19], pressure [76, 77], temperature [52, 53, 55, 57-60, 74, 73], vibration [58], chemical composition [62, 69, 84-90, 92, 95] and acoustic emission [64, 65, 67, 68, 73, 104]. With reference to Figure 2.4, since the chemical reactions result in the formation of covalent bonds between the reacting functional groups, the resin system shrinks during chain extension and cross-linking [18, 20, 24]. Shrinkage of the matrix is a concern because it can lead to debonding. A number of techniques have been developed to quantify the magnitude of the shrinkage of thermosetting resins [25, 28, 29, 31, 36]. Optical fibre-based sensors have also been used to monitor the development of strain in preforms during processing, including the following: extrinsic fibre Fabry-Perot interferometric (EFPI) sensors [31, 37, 40, 45, 46, 56]; and (ii) fibre Bragg gratings (FBG) [10, 11, 19, 26, 27, 35, 36, 41].

With reference to monitoring the cross-linking kinetics of the resin systems used for the manufacture of composites, it is essential to monitor the heat-transfer characteristics in and out of the cross-section of the preform [18, 21]. The cross-linking reactions are exothermic and hence it is necessary to monitor and manage the thermal gradients within the composite preform during processing [31, 36, 37, 45, 46, 50, 51, 54]. It is necessary to monitor the temperature in close proximity to where the cross-linking data are obtained; this will enable to cross-correlate the temperature rise in the preform due to the exothermic nature of the reactions illustrated in Equations 2.1 and 2.2.

Conventional K-type thermocouples and embedded FBG temperature sensors are used to monitor the temperature during processing and post-processing of the composite laminates.

In this research, EFPI and FBG sensors are the two main types of embedded optical fibre sensors used for residual strain and temperature measurements in composites. Hence, a detailed review is presented for these devices.

2.4.1.1 Process monitoring of composites using EFPI sensors

With reference to Figure 2.6, when a broadband light source is launched into the lead-in fibre, a portion of the light is reflected from the end of the lead-in fibre (R_1). The transmitted light travels through the cavity, and is partially reflected at the reflector fibre end-face (R_2). The light reflected from the two surfaces is transmitted back through the lead-in fibre as shown in Figure 2.6. These reflections, called Fresnel reflections, undergo interference to produce fringes of superposition [24].

This interference fringe as shown in Figure 2.7, is used to calculate the Fabry-Perot cavity length, *d*, using the formula [22, 24]:

$$d = \frac{n\lambda_1\lambda_2}{2000(\lambda_2 - \lambda_1)}\mu m \tag{2.5}$$

where *n* is the number of fringes between λ_1 and λ_2 wavelengths in nm.

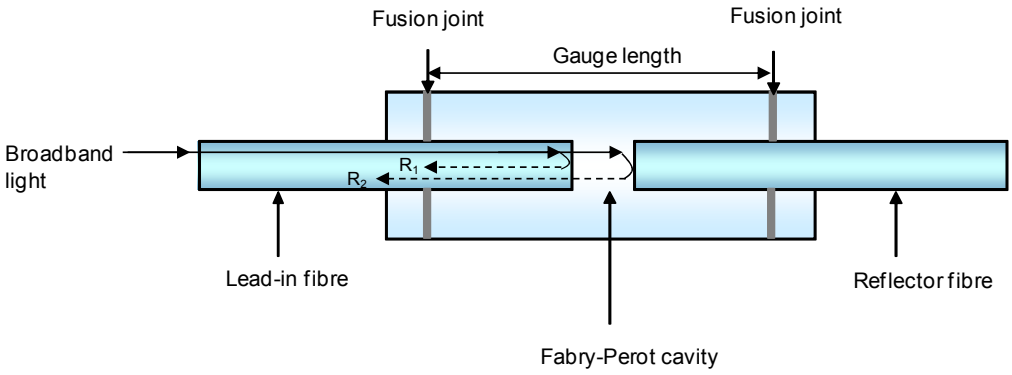

Figure 2.6 Schematic illustration of an extrinsic Fabry–Perot interferometric sensor.

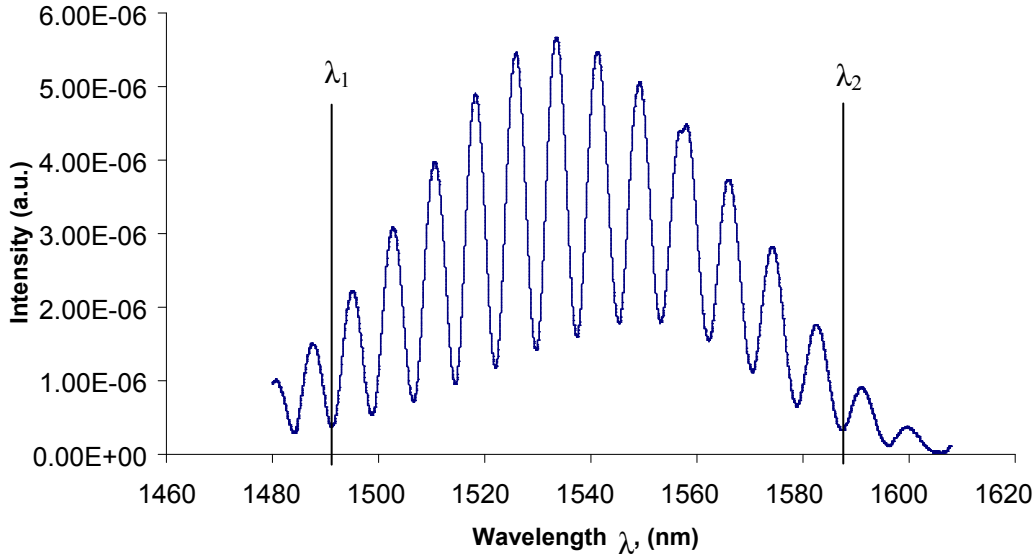

Figure 2.7 Interference fringes obtained from an EFPI sensor with a cavity length of 150 μm.

When the EFPI sensor is subjected to mechanical and/or thermal strains, the cavity length of the sensor will change. This will result in a change in the path-length of the Fresnel reflections [24]. The change in the cavity length can be calculated from the new interference pattern, which can be expressed as [8]:

$$\Delta d = L\varepsilon + A\,\Delta T \tag{2.6}$$

where ε is the strain experienced by the sensor, L is the gauge length, ΔT is the change in temperature, A is the coefficient of thermal expansion in the sensing region.

$A = L(\alpha_s - \alpha_f)$ where α_s and α_f are the coefficient of thermal expansion of the silica capillary and optical fibre, respectively [8]. The coefficients of thermal expansion of the optical fibre and the silica capillary are similar ($0.55 \times 10^{-6}\ ^{o}C^{-1}$) [8]. The free-ends of the silica fibres and the capillary undergo thermal expansions in opposite directions. This cancels the effect of thermal expansion of the two components on the cavity length when the sensor is not embedded in the composite. Therefore, A can be ignored in most applications. Thus, the strain of the sensor is calculated according the following Equation [35]:

$$\varepsilon = \frac{\Delta d}{L} \tag{2.7}$$

Liu *et al.* [56] demonstrated the feasibility of measuring residual strain using EFPI sensors. Two EFPI sensors were embedded between ply numbers 2 and 3 (sensor 1) and 8 and 9 (sensor 2) in a cross-ply $[0, 90_2, 0_2, 90, 0, 90]_s$ carbon/epoxy laminate. Residual strain values of 90 με and 550 με in sensor 1 and sensor 2, respectively were reported. They observed uncertainty in these measurements as they could not establish the actual orientation of the sensor in relation to the reinforcing fibre directions. However, they

demonstrated that EFPI sensors can be used to measure the residual strain in composite laminates.

Jinno *et al.* [31] reported the real-time monitoring of strain during the autoclave-based processing of carbon fibre reinforced composites using EFPI sensors. They observed an exotherm at the start of the isothermal period, which was 20 °C higher than the isothermal temperature. After 20 minutes, isothermal conditions were attained. They observed that it was difficult to differentiate the cross-linking-induced and thermally-induced shrinkage during the cross-linking of the composite.

Lawrence *et al.* [37] reported that EFPI sensors can be used for monitoring *real-time* strain during processing of 20-ply unidirectional and $[0_5/90_5]_S$ cross-ply carbon/epoxy laminate. They embedded two EFPI sensors between ply numbers 10 and 11 in the 0°and 90° directions of the unidirectional laminate. In the cross-ply laminate, two EFPI sensors were embedded between ply numbers 3 and 4, and 10 and 11, in parallel to the reinforcing fibres. The laminates were cured in a hot-press. In the first phase, the temperature was increased to 115 °C and held for an hour. They reported that the magnitude of the observed stress during the first heating phase was negligible due to the reduction in resin viscosity. The temperature was further increased to the cross-linking temperature (175 °C) in the second phase and held for two hours. In the final phase, the composite was cooled-down to room temperature and the magnitude of the residual strain due to the thermal contraction of the matrix was evaluated.

During the cool-down cycle, a compressive residual strain value was reported in the 0°and 90° directions of the unidirectional and cross-ply laminates. The residual strain values are summarised in Table 2.2. Lawrence *et al.* [37] reported that the magnitude of the thermally-induced strain was higher than the cross-linking-induced strain. It is apparent from Table 2.2 that there is a significant difference between the residual strain measurements from the sensors embedded in the 0° and 90° directions in the unidirectional laminate. They explained that the matrix was restrained from shrinking in the 0 ° direction due to the presence of reinforcing fibres in that direction. Alternatively, there were no restrictions for the matrix to shrink in the 90° direction, which resulted in a high compressive residual strain. In the cross-ply laminate, the magnitude of the residual strain measured in the 0° direction was lower than the 90° direction. The observed variation in residual strain was said to be due to (i) the misalignment of the sensor and (ii) the variation in adhesion between the sensor and the laminate [37].

Table 2.2 Compressive residual strain values of unidirectional and cross-ply carbon/epoxy laminates reported by Lawrence *et al.* [37].

Laminate sequence	**Compressive residual strain measurement**	
	0° direction	**90° direction**
Unidirectional 20 ply	-65 με	-4600 με
Cross-ply $[0_5/90_5]_S$	-450 με	-580 με

Fernando pointed out the main advantages of the EFPI sensors as [5]:

- sensitive to axial strain but not transverse strain,

- negligible temperature sensitivity,
- higher mechanical strength compared to intrinsic fibre Fabry–Perot sensors.

The main disadvantages include,

- relatively large diameter,
- difficulty in accurately measuring the gauge length of the sensor.

2.4.1.2 Process monitoring of composites using FBG sensors

The principle of the fibre Bragg grating sensor is based on the measurand-induced shift in the Bragg peak reflection. This is related to the spacing of the index of perturbation of the grating and the refractive index of the core [10, 26]. According the Bragg condition, the Bragg wavelength can be expressed as [53]:

$$\lambda_B = 2n\Lambda \tag{2.8}$$

where λ_B is the Bragg grating wavelength, Λ the grating periodic spacing, n is the refractive index of the fibre core. When an external mechanical or thermal deformation is subjected onto the grating area, the Bragg reflection peak will shift with changes in either n or Λ. Therefore, monitoring the wavelength of this narrow band spectrum will serve to determine the strain and temperature environment to which the optical fibre is subjected. The Bragg wavelength shift caused by the change of strain ($\Delta\varepsilon$) and change of temperature (ΔT) can be expressed in the form [26]:

$$\frac{\Delta\lambda_B}{\lambda_B} = \left(\alpha_{fibre} + \xi\right)\Delta T + (1 - p_e)\varepsilon = K_T\Delta T + K_\varepsilon\Delta\varepsilon \tag{2.9}$$

where $K_T = (\alpha_{fibre}+\xi)$ and $K_\varepsilon = (1-p_e)$. $\alpha = (1/\Lambda)(\partial\Lambda/\partial T)$ is the thermal expansion coefficient, $\xi = (1/n)(\partial n/\partial T)$ is the thermo-optic coefficient and p_e is an effective photo-elastic constant [10, 26]. K_T and K_ε are the wavelength-temperature sensitivity and wavelength-strain sensitivity factors, respectively.

For a germanium-boron (GeO_2-B_2O_3) co-doped fibre, the wavelength-strain sensitivity factor (K_ε) and the wavelength-temperature sensitivity factor (K_T) is $0.77\text{x}10^{-6}$ $\mu\varepsilon^{-1}$ and $6.00\text{x}10^{-6}$ °C^{-1}, respectively [26, 53].

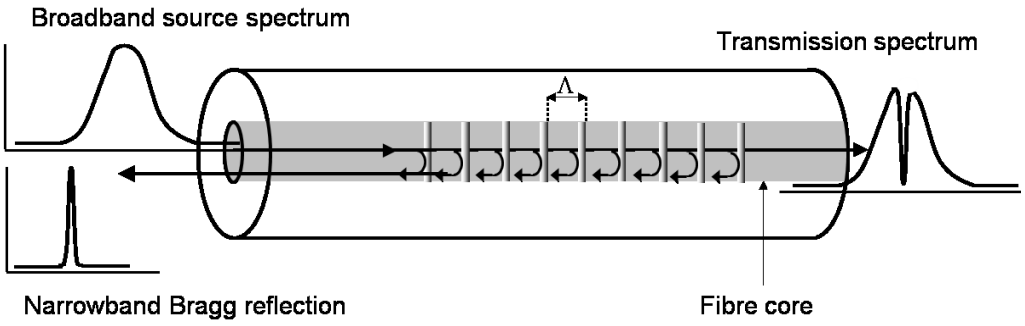

Figure 2.8 Principle of operation of an optical-fibre Bragg grating [81].

The fabrication of the FBG sensor is based on the periodic modulation of the refractive index within the fibre core. This is achieved by irradiating the fibre with an interference pattern produced by high intensity ultra-violet laser beams through a phase-mask. The laser beams are diffracted by the phase-mask and an interference pattern is produced as shown in Figure 2.9 [10]. This interference pattern is used to photo-imprint a refractive index modulation in the fibre [10].

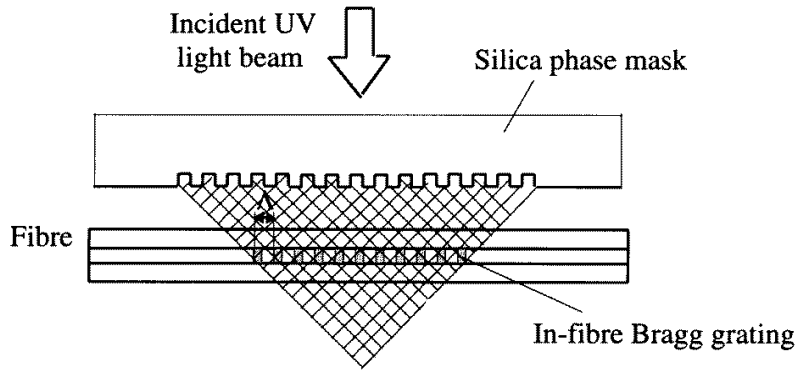

Figure 2.9 Schematic illustration of the phase-mask technique for inscribing an FBG in an optical fibre [10].

Generally, fibre reinforced composites are processed in the range of 120-180 °C and the quality and performance of the composite section is largely determined by various processing parameters such as heating rate, dwell time, cooling rate, pressure and tool plate material [26, 28]. Residual stresses will develop during these processing operations and will affect the performance of the composite parts.

Oliveira *et al.* [26] reported the build-up of internal stresses during cross-linking of carbon-epoxy composites in an autoclave as a function of the tool plate material. The experiment concentrated on unidirectional $[0_4]$ and cross-ply laminates $[0_2/90]_s$ on four different moulds namely aluminium, steel, carbon foam and carbon-epoxy composite. The strain measurement was undertaken using embedded FBG sensors with a gauge length of 4 mm.

They did not observe any broadening of the FBG peak before and after embedding in unidirectional laminates, and this was said to be because of the uniform transverse strain

along the optical fibre in the vicinity of the grating. On the contrary, in cross-ply laminates, broadening of the resonance peak was observed due to strain-induced birefringence in the optical fibre.

Higher strain values were reported for the unidirectional laminates cross-linked on aluminium and steel moulds [26]. However, in the case of the composite and carbon foam moulds, the relative maximum strains recorded were 20 and 44 με respectively for the unidirectional laminates. This was attributed to their low thermal expansion coefficient.

Montanini *et al.* [47] reported on real-time monitoring of process-induced residual strain and temperature in glass fibre/epoxy composites using fibre Bragg grating sensors. Two Bragg gratings with different peak wavelengths (1541 nm and 1549 nm) were inscribed on a single fibre (SMF-28). One of these sensors (FBG-temperature) was sealed in a capillary to decouple the temperature from strain. Thus, this sensor was in a strain-free condition allowing the temperature to be measured during cross-linking. A K-type thermocouple was also embedded adjacent to the FBG-temperature sensor as an independent reference.

Three angle-ply laminates (12, 18 and 24 plies) of dimensions 130 x 100 mm were fabricated. In sample-1 (12-plies), the sensors were embedded between the third and fourth plies of the laminate. In the case of sample-2 (18 plies), the sensors were embedded between the sixth and seventh plies, whereas in sample-3 (24 plies), the

sensors were embedded between the ninth and tenth plies. After manual lay-up, the laminates were vacuum-bagged and cured in a temperature-controlled oven at 80 °C for 240 minutes. A pressure of 30 kPa was applied using a vacuum bag.

They reported an increase in the residual strain and temperature when the number of layers of the composite laminate increased from 12 to 24 plies. They also found that the datasets obtained from the FBG-temperature sensor and the thermocouple was in good agreement (±2 °C). However, embedding more FBGs in different locations/layers within the laminates would have given more experimental evidence for the evolution of the fabrication strain and temperature during cross-linking.

Mulle *et al.* [46] reported the monitoring of residual strains in an autoclave using embedded FBGs in an eight-ply carbon/epoxy unidirectional laminate. The thickness of each ply was 0.26 mm. FBGs were embedded between plies 2-3 and 7-8 in a unidirectional 8-ply laminate. An FBG sensor for monitoring strain and an encapsulated FBG for monitoring temperature were positioned parallel to the fibre direction at each location as shown in Figure 2.10.

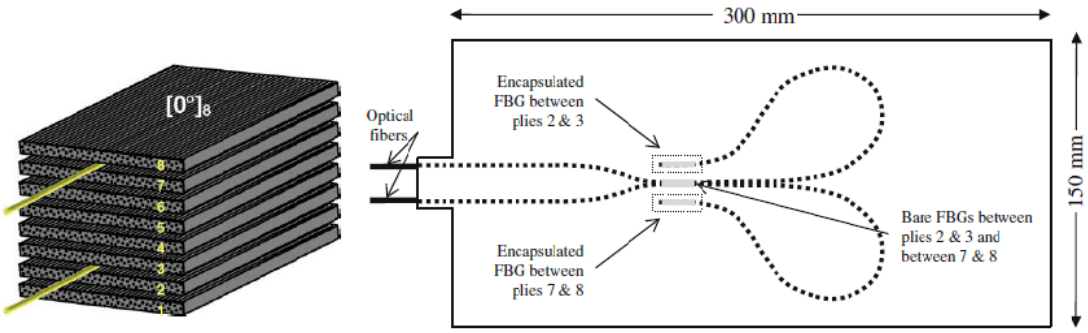

Figure 2.10 Schematic illustration of the location of the embedded FBGs in an eight-ply unidirectional laminate [46].

They observed a reduction in the strain before the onset of gelation. They explained that this could be due to compaction of the laminate when the vacuum and pressure was applied. However, this explanation requires further clarification as the magnitude of the measured strain was found to be higher in this initial stage when compared to the cool-down phase. The FBG embedded in between plies 2 and 3 showed a compressive strain compared to the one embedded in between plies 7 and 8. They proposed that this could have been due to the magnitude of the differential thermal behaviour of the steel mould and the ply that was in contact with the mould being higher than that compared to the top plies of the laminate.

Mulle *et al.* [46] concluded that the evolution of strain during autoclave-based curing of the composite laminate is related to the rheology of the resin system used. They also pointed out that the onset of gelation is the key point for the development of the fabrication strain. However, the magnitude of cure-induced strain appeared to be higher than the thermally-induced strain and this requires more clarification.

Kuang *et al.* [45] reported the influence of manufacturing variables on the functionality and hence the final profile of the FBG spectrum. The sensors were embedded in thermoset and thermoplastic (fibre/metal laminate) advanced composite materials. Thermoplastic-based fibre metal laminates (FML) were made with alternating layers of aluminium sheets of 300 μm thickness and glass fibre reinforced polypropylene prepregs of 500 μm thickness (E-glass content 60% w/w, 35%v/v Plytron from Borealis Ltd., Norway). Thermoset prepregs of glass fibre/epoxy (S2 glass fibre, 3M^{TM} Scotch ply^{TM} SP 250 S29) and carbon fibre/epoxy (Tenax J 12K from Cytec Fiberite Ltd.) were used.

They observed two distinctive peaks in the angle-ply specimens. This was due to the non-uniform strain distribution in the grating region caused by the asymmetric loading of the FBG during consolidation. It was also found that the grating in these specimens consists of two smaller sections with a uniform period and/or refractive index profile. However, the shapes of the spectrum in all the unidirectional specimens were unperturbed. This was due to the absence of any off-axis fibres in the unidirectional laminates and hence the possibility of asymmetric strain was minimised.

The peak distortion in the cross-ply laminates was considerably less than that of the angle-ply specimens. This was due to the fact that the sensor was shielded from the fibres in the neighbouring 90º ply which can reduce any radial compressive strain exerted on the grating. However, they found an observable difference in the spectra of

these samples even though the stacking sequence was identical. Hence, they pointed out the fact that other manufacturing variables such as sensor movement, resin flow, fibre movement etc. along with the lay-up sequence can have considerable impact on the final shape of the spectrum.

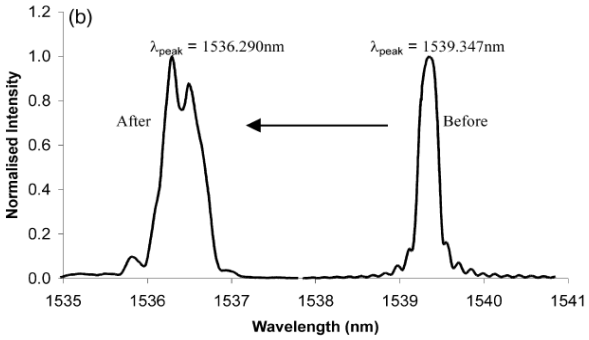

Figure 2.11 An FBG spectrum highlighting peak distortion after processing due to asymmetric sensor loading [45].

Kuang *et al.* [45] highlighted the significance of embedding the FBG sensors in the same direction as the adjacent composite plies to avoid any strain anomalies. Overall, they examined the cause of strain anomalies in terms of stacking sequence reasonably well. However, further work is essential to provide more experimental evidence of other causes for peak splitting such as sensor-fibre movement and resin flow.

Kang *et al.* [48] reported the simultaneous measurement of thermal strain and temperature of carbon fibre reinforced composites that were exposed to the low-earth orbit space environment for three months. Fibre Bragg grating sensors were used for

this experiment and the low-earth orbit conditions such as high vacuum, ultraviolet and thermal cycling were simulated in a thermal vacuum chamber.

A pair of FBGs were used; one for measuring the thermal strain and the other for the temperature. FBG used for the temperature measurement was capillary-sealed to decouple temperature from strain.

The sensors were embedded transversely in between the 8^{th} and 9^{th} plies of a 16-ply carbon/epoxy laminate of dimension: 150 x 70 x 2 mm. They reported that the thermal strain in the transverse-direction was higher compared to that in the fibre-direction and therefore, this can be related to the dimensional stability of the composite laminate [48].

Temperature and strain were measured simultaneously and the coefficient of thermal expansion (CTE) of the composite laminate was calculated after 0, 200, 400, 600, 800 and 1000 thermal cycles. One thermal cycle took 2 hours to complete; so the experiment was carried out for a total of 2000 hours (3 months) to complete 1000 thermal cycles.

A baseline data were acquired from one thermal cycle without using vacuum and ultraviolet in the vacuum chamber. They reported that there was no abrupt change in the CTE of the composite plate even after 1000 thermal cycles. However, when compared to the baseline results, they observed a decrease in CTE all over the temperature range. They explained this could be due to other factors such as moisture desorption, matrix cracking etc by the simulated environmental effects. SEM images confirmed this

argument, as they identified matrix cracks in the SEM images as a result of the low-earth orbit environment.

Kang *et al.* [48] concluded that FBG sensors can be used for simultaneous temperature and strain measurements in space environments for a long time. This work also highlights the possibility that FBG sensors can be used for real-time health monitoring of space craft. However, it would be better to provide more experimental evidence for the factors that cause changes in CTE during continuous thermal ageing.

Kang *et al.* [50] reported the measurement of strain and temperature during cross-linking of graphite/epoxy laminates using EFPI-FBG sensors. A schematic illustration of the sensor configuration used is presented in Figure 2.12. A unidirectional, a cross-ply and a fabric laminate were used for the experiment. Two EFPI-FBG sensors were embedded in each of these laminate in both parallel and perpendicular directions to the reinforcing fibres as shown in Figure 2.13. The strain and temperature of the laminates were monitored simultaneously during cross-linking in an autoclave. K-type thermocouples were also embedded in each laminate to monitor the temperature during cross-linking.

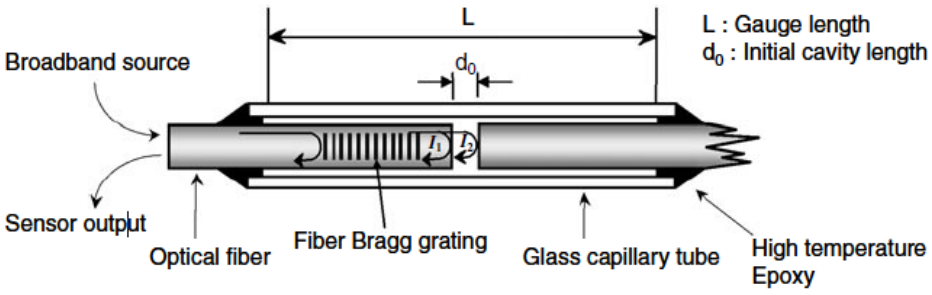

Figure 2.12 The schematic illustration of the EFPI-FBG sensor [50].

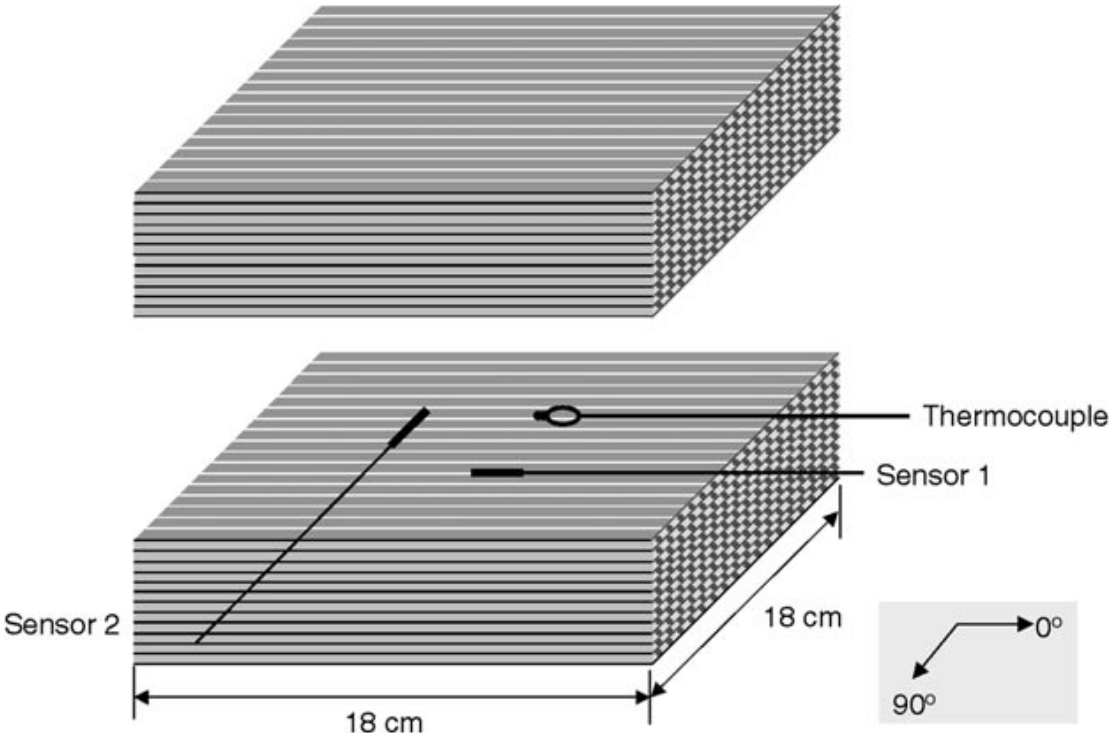

Figure 2.13 The location of FP-FBG sensors in a unidirectional laminate [50].

The laminates were cured in an autoclave at 130 ºC for 2 hours. For the unidirectional specimen, a large compressive residual strain was observed in the transverse direction. They explained that this was due to the fact that the transverse direction is matrix-dominated and therefore exhibit large thermal shrinkage in that direction during the cooling-phase.

Lower compressive strain values were reported for the fabric laminate compared to the other two. In the cross-ply and the fabric laminates, they observed almost similar compressive strain values in the 0 and 90° planes. However, these strain values were larger than that of the strain observed in the longitudinal direction of the unidirectional specimen.

Kang *et al.* [50] recommended a lower cross-linking temperature to decrease the residual strain in the composites as the residual strain is mainly induced by the thermal expansion mismatch of the matrix and the fibre, and the resin shrinkage during cross-linking and cooling period. However, this is not found to be economical as low temperature curing requires longer processing time.

Though Kang *et al.* [50] demonstrated the *in-situ* monitoring of strain and temperature during cross-linking of composites using EFPI-FBG combination sensors, it would have been valuable to discuss the reasons for the lower compressive strain values observed in the cross-ply and the fabric laminates, compared to the unidirectional laminate.

Pal *et al.* [57] studied the non-linear temperature dependence of fibre Bragg grating sensors from room temperature to 500 ºC. Gratings of type I and type IIA were inscribed on three different types of photo-sensitive fibres, namely B-Ge co-doped, Ge-Er co-doped and Ge-Sn-Er co-doped. The FBGs written on B-Ge fibre were tested up to 250 ºC whereas those written on the other two types of fibres were operated up to 500

ºC. Annealing of the sensors was carried out prior to the experiment in order to avoid the temperature-induced irreversible changes of the Bragg wavelength. FBGs inscribed on B-Ge co-doped fibre (type-I and type IIA) were annealed at 275 ºC for 8 hours whereas the gratings written on Ge- Er (type-I and type IIA) and Ge-Sn-Er (type-I) co-doped fibres were annealed at 525 °C for the same duration.

Pal *et al.* [57] observed that the Bragg wavelength change for all the FBGs were quite consistent over a number of repeated temperature cycles. The data were fitted to linear as well as higher order polynomial, in each case. Considering the linear fit to experimentally measured data, the temperature sensitivity of the different gratings was found to be varied from 10.69 to 14.61 pm/°C.

Vieira *et al.* [66] examined the sensor sensitivity as a function of the grating length and coating material when embedded in carbon fibre reinforced polymer (CFRP) laminates, during cross-linking. Uncoated and acrylate-coated FBG sensors with grating lengths of 5 mm and 10 mm were used for the study. Spectral broadening was observed in uncoated 10 mm FBG sensors due to the non-uniformity of strain field around the grating.

2.4.1.3 Process monitoring of composites using multi-measurand sensors

A multi-parameter sensing concept for strain, temperature and vibration was reported by Rao *et al.* [58]. The feasibility of using an EFPI sensor design for monitoring strain in

tandem temperature logging via fluorescence-decay has also been demonstrated by Liu *et al.*[60]. Rao *et al.* [59] also used laser ablation to create a cavity on the end-face of a fibre but in this instance, it was spliced to a long-period fibre grating for obtaining simultaneous information on the applied strain and temperature. An independent temperature calibration followed by the application of strain was used to demonstrate simultaneous monitoring of strain and temperature.

Singh *et al.* [40] reported the feasibility of multiplexing a number of EFPI sensors where the interrogation was carried out using a Fourier transform infrared spectrometer. Liu *et al.* [61] used a spline-fitting routine to deconvolute the combined EFPI and FBG signals, when using a low-resolution of low-cost CCD spectrometer, to overcome the ambiguity in determining the shift of Bragg resonance and the interference fringes of the EFPI under the simultaneous influence of strain and temperature. The cross-talk was found to be not significant with the measurement technique that was used. Ferreira *et al*. [96] decoupled the FBG signal from the combined EFPI and FBG signals by passing the signal through a Bragg grating that was similar to that used within the sensor head. Machavaram *et al.* reported the development of intrinsic Fabry-Perot cavities in optical fibres using an excimer laser [97], and hydrofluoric acid (HF) etching [98]. Another work reported by Li *et al*. [76] was on an HF-etched intrinsic Fabry-Perot cavity in conjunction with an FBG sensor to enable simultaneous monitoring of strain and temperature. The strain and temperature sensitivities of the FP cavity and the FBG were established independently. A summary of selected EFPI/FBG-based multi-measurand sensor designs used for process-monitoring is presented in Table 2.3.

Table 2.3 Summary of the EFPI/FBG-based multi-measurand sensors used for process monitoring [55, 59, 61, 76, 77, 90, 96-100, 104].

Authors/Year	Sensor design	Applications
Liu *et al.* (1997) Bogetti *et al.* (1992) Kang *et al.* (2003)	EFPI cavity formed by means of a cleaved single mode fibre and an FBG inscribed at the end of the cleaved fibre and housed within a capillary	Strain and temperature sensing in composites
Ferreira *et al.* (1998)	FP cavity formed by means of FBG inscribed fibre and a movable mirror	Temperature and displacement in a test rig
Jin *et al.* (1998)	Intrinsic FP cavity formed by fusion splicing two single mode fibres to a short section of capillary	Strain and temperature in composite
Li *et al.* (2011)	Intrinsic FP cavity formed by fusion splicing HF etched and cleaved single mode fibre FBG	Strain and temperature in a test rig
Bremer *et al*. (2009)	FP cavity formed by means of an FBG inscribed fibre and silica diaphragm at the end of a capillary	Pressure and temperature in a test rig
Bae *et al.* (2012)	FP cavity formed by means of an FBG inscribed fibre and polymer diaphragm at the end of a UV-curable resin mould	Pressure and temperature in a test rig
Rao *et al.*(2007)	Intrinsic FP cavity formed by means of an ablated cavity on cleaved end spliced to a LPG inscribed fibre	Strain and temperature in a test rig
Cusano *et al.*(2000)	Combination of Fresnel reflection sensing and temperature using FBG via wavelength division multiplexer	Temperature, strain and refractive index

In summary, this section has presented the significance of process monitoring of composites using optical fibre-based sensors. The use of FBG and EFPI sensors to

monitor the development of strain and temperature during processing of the composites was reviewed.

2.5 Cross-linking monitoring using optical fibre sensors

2.5.1 Cross-linking monitoring using Fourier transform near-infrared spectroscopy

Data on the quantitative depletion of the epoxy and amine functional groups can be obtained by transmission and reflection near-infrared spectroscopy [4]. In these techniques, the absorbance bands associated with a non-reacting functional group (one that does not take part in the cross-linking reactions) is used to normalise the absorbance associated with the reactive functional groups [25]. With reference to Equations 2.1 and 2.2 given in Figure 2.4, the C-H absorbance band is generally used to normalise the absorbance bands associated with the epoxy, primary and secondary amine functional groups. Therefore, during the cross-linking reaction of an epoxy/amine resin system, the degree of conversion of a specific functional group as a function of reaction time can be determined using the change in concentration of the functional group in the mixture. According to the Beer-Lambert relationship, the peak area related to an absorption band is linearly proportional to the concentration of the corresponding functional group in the mixture [83,84].

$$A_\lambda = \varepsilon_\lambda l c \tag{2.10}$$

where A_λ is absorption band at the wave length, λ, ε_λ is molar absorptivity at wavelength, λ, l is the thickness of the sample and c is the concentration. Therefore, the

degree of conversion of epoxy functional groups with respect to a non-reacting chemical group (in most high-performance epoxy systems, this is generally the aromatic C-H group) can be determined using the equation below [80]:

$$\alpha = 1 - \left(\frac{A_{EP,t} / A_{ref,t}}{A_{EP,0} / A_{ref,0}} \right) \tag{2.11}$$

where α is the conversion, $A_{ref,0}$ and $A_{ref,t}$ refer to the areas of the "inert" reference peak at the start of the reaction (t=0) and after time, t, respectively. $A_{EP,0}$ and $A_{EP,t}$ are the areas of the epoxy peak for the uncured and partially cured resin at a specified time respectively. The optical fibre-based sensors used for chemical monitoring in the current study are based on near-IR spectroscopy. Therefore, attention of the review is focussed only on the identification of epoxy/amine based resin systems in the near-IR range. A summary of peak assignments for epoxy resins and amine-based cross-linking agents in the near-IR range is given in Table 2.4.

Qualitative data on the rate of conversion of the reactive functional groups can also be obtained by tracking the refractive index of the resin system [85]. As the molecular weight of the resin system increases as a function of cross-linking, the optical density increases in proportion. Hence, qualitative data on the progression of the cross-linking reactions or network formation can be inferred from the refractive index of the resin system. The refractive index is a function of temperature and the wavelength of light used in the measurement. Hence, for refractive index-based process monitoring, it is necessary to monitor the temperature.

Table 2.4 Summary of peak assignments for epoxy/amine resin system in the near-IR region [4, 25, 42, 43, 78, 79].

Chemical group	Peak assignment	Wavelength (nm)	Wave number (cm^{-1})
Aliphatic primary amine	NH combination	2025	4938
	1st overtone symmetric NH stretch	1526	6553
	NH_2 stretching and bending combination bands	1923	5200
Aliphatic secondary amine	1st overtone N-H symmetric stretch	1543	6481
	NH_2 stretching and bending combination bands	1972-2000	5000-5070
Epoxy	2nd overtone of the CH stretching vibration	1159	8627
	1st overtone of CH stretch in epoxy group	1650	6060
	Epoxy ring combination 2nd overtone (epoxy ring stretching and CH bending vibration)	2207	4530
Hydroxyl	Combination of OH stretching and deformation vibrations	2090 2050	4785 4878
	1st overtone of the OH stretching fundamental	1432	6983
	Combination bands of OH	2000-2083	4800-5000
	OH overtone	1408-1429	7000-7100
	OH combination	1220	8200
CH (aromatic)	1st overtone of CH stretching vibration	1668	5995
	1st overtone of aromatic CH stretching	1672	5980
	Aromatic combination bands	2137 2165 2463	4620 4680 4060
CH (aliphatic)	CH overtones of CH_2, CH_3	1700	5882
	2nd harmonic of a CH stretch of the methyl group	1188	5232
	CH_3 combination band	2300	4350
	CH_2 combination band of methylene group	2400	4170
	Terminal methylene band due to unsaturation	2100	4760

Optical fibre-based sensor systems for monitoring the refractive index include core/cladding interactions where the matrix acts as cladding [62, 85, 86] reflections emanating from cleaved optical fibres immersed in the resin, cavities in optical fibres [87] and long-period gratings [88].

2.5.2 Cross-linking monitoring using Fresnel sensors

In this research, Fresnel sensors were used for monitoring the refractive index of the epoxy/amine resin system. These are intensity-based sensors where the reflected light from the cleaved end of a fibre varies quadratically with the index of the medium in contact [85]. The optical density of the resin increases with the cross-link density and this can be tracked via the Fresnel reflectivity at the cleaved fibre/resin interface. Such sensors [89] offer a low-cost means for tracking the progression of cross-linking reactions. A number of authors [25, 49, 90-91] have reported on the use of fibre Fresnel refractometers for cure monitoring. The Fresnel reflection 'R' emanating from the interface between a single-mode fibre core and the surrounding medium can be expressed as [25]:

$$R = \left(\frac{n_{fibre} - n_{medium}}{n_{fibre} + n_{medium}} \right)^2 \tag{2.12}$$

where n_{fibre} and n_{medium} are the refractive indices of fibre core and the medium in contact with the cleaved-end of the fibre, respectively.

Antonucci *et al.* [49] reported the simultaneous measurement of refractive index and the residual strain during non-isothermal cross-linking of an epoxy/amine resin system. A cleaved optical fibre integrating a refractometer and a fibre Bragg grating inscribed on the same fibre was used for the experiment. The cross-linking process influences the density of the material and therefore a direct relation between the extent of cross-inking and the refractive index can be obtained. On the other hand, the process-induced strain during cross-linking was measured using the fibre Bragg grating sensor.

A custom-made Teflon-coated aluminium mould was used for the experiment and the temperature was ramped from room temperature to 43 °C to 133 °C using an air circulating oven [49]. They found that the signal intensity decreased at the beginning of the cross-linking process due to the reduction in the resin viscosity. However, the signal was then progressively increased until the temperature reached around 90 °C in the cure cycle. They reported that the cross-linking reaction was almost complete at this stage.

The FBG data were used to determine the gel point during the process of cross-linking [49]. The cure-induced residual strain evolves after the onset of gel point and therefore, accurate measurement of the gel point is important for the respective resin system. They measured the gel point from the slope change of the Bragg peak wavelength during cross-linking as shown in the Figure 2.14. However, there were no details provided on the evolution of the strain during cure.

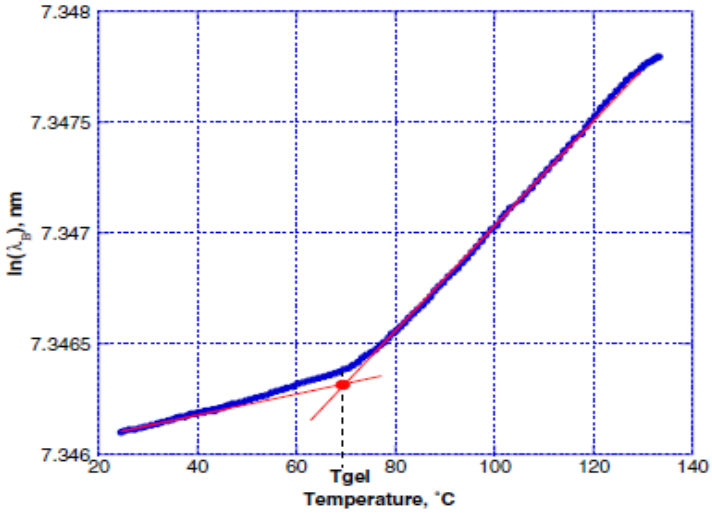

Figure 2.14 The determination of gel point from the Bragg peak wavelength shift during cross-linking [49].

The significance of the cross-linking monitoring of composites using fibre optic sensors was reviewed in this Section. Special attention was given to cure conversion monitoring using chemical and Fresnel sensors.

2.6 Overall summary of the literature

In the first part of this chapter, a review was undertaken on the cross-linking mechanism associated with the epoxy/amine resin system. The second part of this chapter reviewed the significance of process monitoring of composite structures using optical fibre-based sensors. An in-depth and critical review on EFPI and FBG sensors for monitoring the process-induced strain and temperature were presented. Optical fibre-based sensors used for monitoring of cross-linking reaction were reviewed with an emphasis on spectroscopy-based techniques.

Although optical fibre-based sensors are being used for process and structural health monitoring of composites, the majority of the sensor systems reported to-date have been single or at the most, dual measurand systems. The multi-measurand optical fibre sensor (MMS) reported in this thesis is capable of monitoring four independent measurands simultaneously: strain; temperature; relative concentration of specified functional groups in the resin system; and refractive index. The sensor design is based on the extrinsic fibre Fabry-Perot interferometer and a unique feature is that a conventional fibre-coupled near-infrared spectrometer is used to monitor four independent parameters.

3 EXPERIMENTAL

3.1 Introduction

This chapter presents the details of the materials and equipment used in this research project. The experimental procedures for the fabrication of the optical fibre sensors and test methods used for process and structural health monitoring of composite materials are described.

3.2 Materials

3.2.1 Reinforcing fibres and resin systems

The prepreg materials/reinforcing fibres and the resin system used in this study are detailed below:

(i) Unidirectional carbon/epoxy prepreg: VTM264/T700S (24K)-300-35% (Umeco, UK) prepreg material was used for manufacturing composites. The prepreg was supplied as a unidirectional tape with a 300 mm width and 0.25 mm thickness. The prepreg was stored in sealed polyethylene bags in a freezer at -18 °C in moisture-free conditions. Silica gel was placed within the polyethylene bags to absorb any moisture. Once removed from the freezer, the prepreg was allowed to thaw to room temperature before the sealed polythene bags were opened.

(ii) Woven E-glass/epoxy: Plain-weave E-glass fabric (PD-Interglas Technologies, UK) was used as the reinforcing material and Araldite LY3505/XB3403 (Huntsman

Advanced Materials, UK) was used as the resin system to manufacture woven fabric composites. LY3505 is a bisphenol-A epoxy resin and XB3403 is an aliphatic polyamine-based hardener, namely polyoxypropylene diamine. The resin and hardener were mixed in the stoichiometric ratio of 1:0.35 by weight, followed by degassing in a vacuum chamber at 70 kPa for 15 minutes.

(iii) Norland optical adhesive: NOA 68 (Norland Products Inc., USA) is a colourless single-component ultraviolet (UV) photo-curable resin. The viscosity of this resin system was 5 Pa.S at 25 °C and was used to secure/bond the optical materials during the fabrication of the sensors. The emission wavelengths of the UV light source were 300-400 nm.

3.2.2 Optical fibres

The optical fibres used in this study for fabricating the sensors are detailed below and the typical properties of the optical fibres specified by the manufacturers are summarised in Table 3.1.

(i) Extrinsic Fabry-Perot interferometric sensor for monitoring strain: 1550 nm single-mode optical fibres – SMF-28^{TM} (Corning Inc., USA) with core and cladding diameters of 8.3 and 125 ± 1 μm respectively were used.

(ii) Fibre Bragg grating sensor for monitoring strain and temperature: Photo-sensitive single-mode Germania-Boron co-doped core with acrylate-coated optical fibres – PS 1250/1500 (Fibercore, UK) with core and cladding diameters of 9 and 125 ± 1 μm respectively were used for fabricating the strain and temperature sensors. Fibre Bragg

grating inscribed on 1550 nm single-mode polyimide-coated optical fibres – SMF-28^{TM} (Alxenses, China) was also used.

(iii) Chemical sensors for monitoring the cross-linking of the LY3505/XB3403 resin system: Multi-mode step-index optical fibres (Aomolin Ltd., China) with core and cladding diameters of 105 ± 3 and 125 ± 4 μm respectively were used.

(iv) Multi-measurand sensors for monitoring strain, temperature, refractive index and cross-linking: The optical fibres described in items (i), (ii) and (iii) above were used for the fabrication of the multi-measurand sensors.

All the sensors with the exception of the polyimide-coated FBGs (Alxenses, China) were fabricated in-house.

Table 3.1 Typical properties of the optical fibres used in this research programme.

Fibre type	**SMF-28^{TM}**	**PS 1250/1500**	**Aomolin 105/125**
Source	Corning Inc., USA	Fibercore Ltd., UK	Aomolin Ltd., China
Core type	Single-mode	Single-mode	Multi-mode
Numerical Aperture	0.13	0.12 – 0.14	0.22
Core diameter (μm)	8.3	9	105 ± 3
Cladding diameter (μm)	125 ± 1	125 ± 1	125 ± 4
Coating material	Acrylate/ Polyimide	Acrylate	Acrylate

3.2.3 Vacuum bagging materials

The following materials (Amber Composites, UK) were used to vacuum bag the prepreg and woven fabric laminates prior to autoclave-based processing:

(i) Non-perforated release film: High-temperature 20 μm thick poly(ethylene/ tetrafluoroethylene) (ETFE) release-film (product code: VAClease20B1.2) was used to prevent the resin from adhering to the tooling plate and the breather cloth. This release-film is rated for operation up to 200 °C.

(ii) Breather cloth: A light-weight non-woven polyester fabric (product code: VAC B4 30) was used to permit the air and volatiles from within the vacuum bag to be extracted via the vacuum pump throughout the cure cycle.

(iii) Sealant tape: Premium grade rubber-based, 12 mm wide and 3 mm thick, (product code: VACseal G) was used as the sealant tape. This was used to form an air-tight seal between the vacuum bag and the tooling plate.

(iv) Vacuum bag film: This material was used to "bag" the laminated preform and to provide a facility to maintain the applied vacuum during the cure cycle.

(v) Polyester flash tape: A high-temperature polyester tape (product code: FT25BS) with a silicone adhesive was used to seal the edges of the vacuum bag.

3.2.4 Ancillary equipment

(i) Fibre strippers: CF-2 optical fibre stripper (Clauss, USA) was used to remove the polymeric coating on the optical fibres.

(ii) Fibre cleavers: A high precision cleaver-CT-30 (Fujikura Ltd., UK) was used to cleave the optical fibres with an accuracy of 90 ± 0.5°.

(iii) Fusion splicer: A commercially available fusion splicer-FSM-40PM (Fujikura Ltd., UK) was used to extend the length of the optical fibres via splicing and to connect it to the connectors.

(iv) Fibre connectors: Three types of connectors were used: (i) sub-miniature adaptor (SMA); (ii) fibre-optic connector/physical contact (FC/PC); and (iii) fibre-optic connector/angled physical contact (FC/APC).

(v) Capillary cleaver: A commercially-available capillary column cutter (Shortix^{TM}, SGT Singapore) was used to cleave the silica capillaries.

3.3 Instrumentation and equipment

(i) Near-infrared spectrometer: The Fourier transform near-infrared (FTNIR) spectrometer (MATRIX™-F Duplex, Bruker, UK) used in the current study was housed with six pairs of fibre-coupled input and output channels. The spectral range of the spectrometer was 4000-11000 cm^{-1}. The monitoring of the cross-linking reactions was performed at a resolution of 4 cm^{-1} (0.96 nm) over 64 scans. The reflected signals from the Fabry-Perot strain and the FBG sensors were measured at a resolution of 0.96 and 0.24 nm respectively over 16 scans. The reflected light intensity was measured using the InGaAs detector of the spectrometer.

(ii) Fibre Bragg grating interrogation unit: A multi-channel FBG interrogation unit (FiberPro IS7000) was used for monitoring the strain and temperature. The wavelength accuracy and resolution of the FiberPro were ±0.005 nm and <0.001 nm respectively over a spectral range of 1530-1570 nm.

(iii) Optical spectrum analyser: A commercial optical spectrum analyser – OSA (Anritsu MS9710B) was also used for interrogation of the reflected signal from the Fabry-Perot cavity and FBG. The signals from the sensors were acquired at a resolution of 0.07 nm with 5001 sampling points over a spectral range of 1450-1600 nm.

(iv) External light source: An amplified spontaneous emission (ASE) light source (LPB-1550-D, Lumen Photonics, UK) emitting over a spectral region of 1450-1600 nm was used as an external source to illuminate the sensors.

(v) Differential scanning calorimeter: A differential scanning calorimeter-DSC7 (Perkin Elmer, UK) was used to monitor the glass transition temperature (Tg) of the following: (i) resin systems; (ii) acrylate-coating on the optical fibres; and (iii) silica from the optical fibres. The instrument was calibrated with indium and lead using conventional procedures. The sample was placed in an aluminium pan and heated from 20-200 °C. The dynamic heating of the resin systems was carried out at a heating rate of 5 °C min^{-1} whereas the Tg of the resin systems, the acrylate coating on the optical fibres and the silica were carried out at a heating rate of 20 °C min^{-1} in a nitrogen atmosphere. An empty pan was used in the reference compartment of the DSC.

(vi) Autoclave: A conventional autoclave (99/20; Leeds and Bradford Boiler Company, UK) was used for the processing and post-processing of the composites described in this study. A commercially available software package-SV32 (Specview Ltd., UK) was used to monitor the temperature, pressure and vacuum within the autoclave during the processing of the composites.

(vii) Oven: An air-circulating oven (Memmert, UK) was used for various heating/cooling experiments throughout the study.

(viii) Microscope: A commercially available binocular microscope (Leica Wild M3C) was used throughout the study as part of the sensor fabrications.

3.4 Sensor fabrication and interrogation

The optical fibre sensors used in the current research were: (i) extrinsic Fabry-Perot interferometric sensor, (ii) fibre Bragg grating sensor, (iii) Fresnel sensor, (iv) chemical sensor and (v) multi-measurand sensor. Precision-bore round silica capillary of 128 ± 3 μm inner diameter and 300 ± 5 μm outer diameter (Vitrocom, USA) was used for: (i) the construction of the EFPI sensors; (ii) the production of the FBG-based temperature sensors; and (iii) the manufacture of the multi-measurand sensors.

3.4.1 Capillary cleaving and cleaning

The selection of an appropriate method for capillary cleaving and the resulting end-face quality is important to achieve optimum performance of the sensors. Two methods were employed to establish an appropriate cutting method for the silica capillaries:

(i) manual cutting method using a pen-cleaver; and

(ii) precision cleaving using a commercially-available capillary column cutter (Shortix^{TM}, SGT Singapore).

In the manual cutting method, the end-face quality of the capillary was poor and was operator-dependent. However, the commercially-available capillary column cutter used a diamond cutting tool to produce acceptable quality of cleaved capillary end-faces.

This method generated minimal debris and the resulting end-face quality was superior when compared to the manual cleaving method.

The capillary was supplied in lengths of 1 metre and individual lengths of approximately 40 mm were cleaved using a capillary column cutter (Shortix^{TM}, SGT Singapore). The cleaved capillary was vacuum-cleaned using a laboratory-scale vacuum cleaner (Dymax 30, Charles Austen pumps, UK) followed by cleaning in an ultrasonic water bath using isopropanol for 6 minutes. The cleaned capillary was placed vertically in a custom-made jig (see Figure 3.1) and dried at 100 °C for 15 minutes in an air-circulating oven (Memmert, UK). This was then arc-cleaned at 20 mA arc-current for 1 second using the cleaning facility of the fusion splicer. A cleaved and cleaned sacrificial optical fibre of 125 μm diameter was inserted into the capillary before the arc-cleaning process. The quality of the capillary end-faces was inspected under a binocular microscope (Leica Wild M3C).

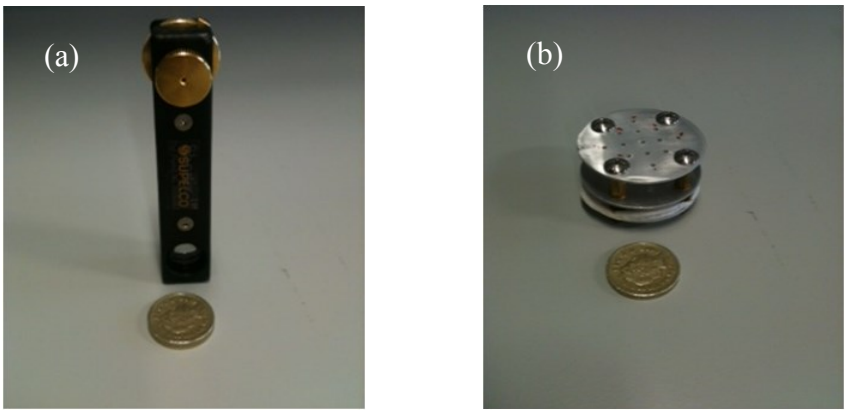

Figure 3.1 Photographs of the (a) capillary column cutter (Shortix^{TM}, SGT Singapore); and (b) custom-made jig for drying the cleaved and cleaned capillary.

3.4.2 Extrinsic Fabry-Perot interferometric sensor

The EFPI sensors were fabricated using single-mode optical fibres – SMF-28^{TM} (Corning Inc., USA). Stripped and cleaved fibre-ends were inserted into a precision-bore round silica capillary (128 ± 3 µm inner diameter and 300 ± 5 µm outer diameter) with an approximate length of 40 mm. This procedure was carried out using the microscope on the fusion splicer (BFS-60, UK). The cavity length was set by means of the manual translation facility on the fusion splicer; the cavity length was interrogated using the optical spectrum analyser (Anritsu MS9710B). The cavity length was calculated using Equation 2.5.

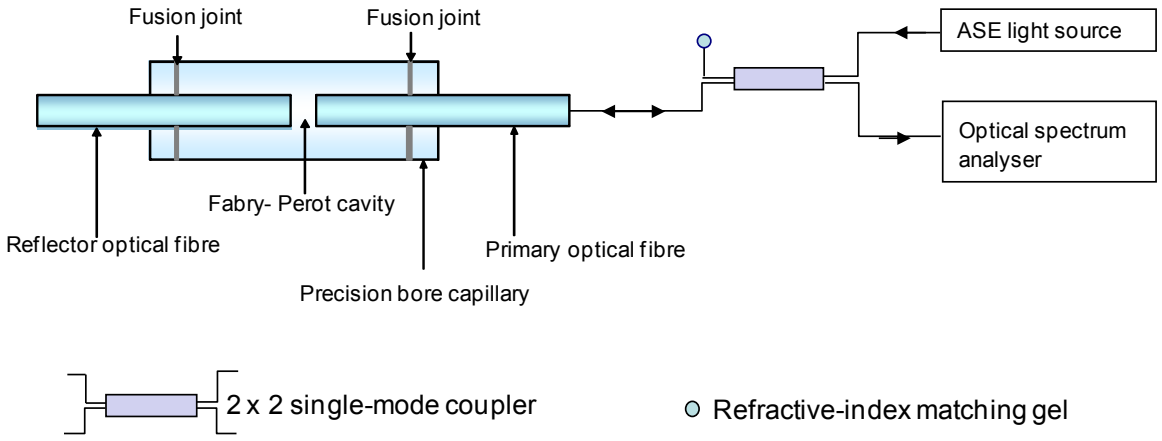

Figure 3.2 A schematic illustration of the interrogation set-up of an extrinsic Fabry-Perot interferometric sensor.

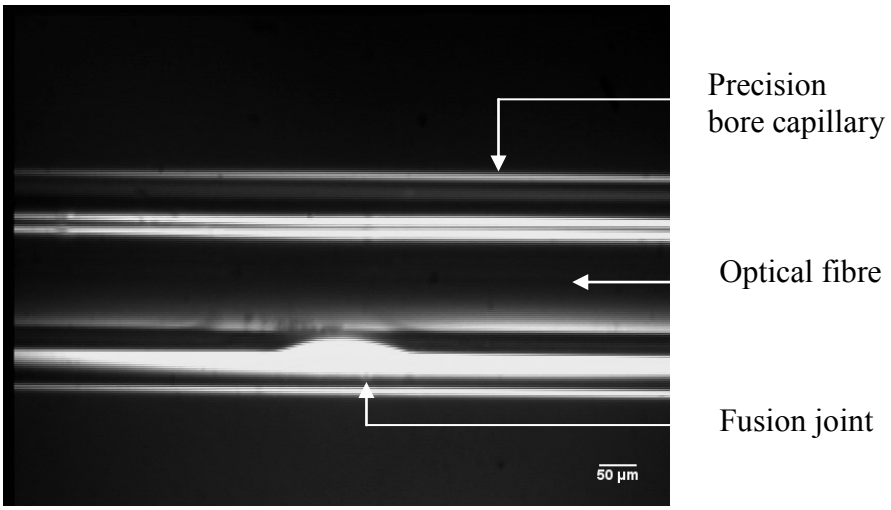

Figure 3.3 Micrograph showing the appearance of an arc-welded fusion joint between the capillary and the optical fibres located inside the capillary.

The key components of the EFPI sensors and the experimental set-up for interrogating it are shown in Figure 3.2. The cleaved optical fibres were secured within the capillary via two fusion joints using an arc discharge current of 17 mA for 3 seconds; this process was repeated five times. The gauge length of the sensors was defined as the distance between these fusion joints. The gauge length was then measured optically using a binocular microscope (Leica Wild M3C). A UV-curable epoxy resin (NOA 68) was used at both ends of the capillary to strengthen the sensor. Figure 3.3 shows a typical micrograph of a fusion joint where the inner-bore of the capillary has been fused to the outer surface of the stripped optical fibre. Each fusion joint was inspected under the binocular microscope to ensure that the fused area was symmetrical.

3.4.3 Fibre Bragg grating sensor

FBGs with a grating length of 10 mm were inscribed on photo-sensitive (GeO_2-B_2O_3 co-doped) single-mode fibres – PS 1250/1500 (Fibercore, UK). This was achieved by irradiating the fibre to an interference pattern produced by high intensity ultra-violet laser beams through a phase-mask. A 30 mm section of the acrylate-coating of the fibre was stripped using a mechanical stripper at a distance of 30 mm from the fibre-end and the stripped region was cleaned using isopropanol and lint-free tissue. This was positioned beneath a fused silica phase-mask (QPS Photronics Inc., Canada) and clamped magnetically to a 3D-translation stage. Three phase-masks designed to produce FBG reflections at 1540 nm, 1547 nm and 1552 nm were used in the current study.

A krypton fluoride (KrF) excimer laser (Braggstar 200, Coherent, UK) operating at 248 nm with a pulse repetition rate of 1000, pulse energy of 10 mJ and pulse frequency of 20 Hertz was used to fabricate the FBG sensors. The laser beam was diffracted by the phase-mask and an interference pattern was produced on the fibre core. This interference pattern was used to photo-imprint a refractive index modulation in the fibre. The FBG sensor was connected to an FBG interrogation unit (FiberPro IS7000) and the reflected light intensity was monitored using custom-written LABVIEW software.

The FBG sensor is sensitive to strain and temperature. The influence of strain (ε) and temperature (T) on a fibre Bragg grating can be calculated using Equation 2.9. In the current study, the strain was decoupled from temperature by housing the sensor in a

fusion-sealed silica capillary of 128 ± 3 µm inner diameter and 300 ± 5 µm outer diameter. Thus, the FBG is in a strain-free environment and is therefore only responsive to temperature. A Schematic illustration of the interrogation set-up for the FBG strain and temperature sensor is shown in Figure 3.4.

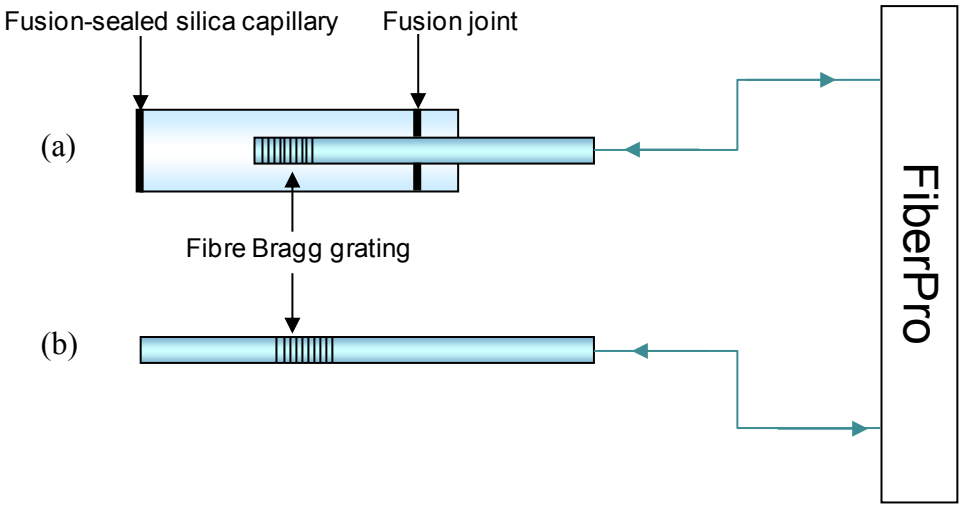

Figure 3.4 A schematic illustration of the experimental set-up and sensor configuration for the FBG: (a) temperature sensor; and (b) strain and temperature sensor.

3.4.4 Chemical sensor

The chemical sensor design consists of a gold-palladium-coated end-face of a capillary that served as a reflector for the sensing fibres and two secondary cavities. The term "secondary cavity" is used here to distinguish it from the primary cavity of the EPFI strain sensor. The function of the secondary cavities was to serve as pseudo-cuvettes to contain the resin system. The chemical sensor formed part of the sensor design for the multi-measurand sensor and further details are presented in Section 3.4.5. One face of the cleaved and cleaned capillary (as described in Section 3.4.1) was sputter-coated

(SC7640, Quorum Technologies, UK) with a gold-palladium (Au/Pd) alloy to create a reflective surface. The sputter-coating was carried out for 9 minutes using a plasma current of 20 mA and a vacuum pressure of 10 Pa. (10^{-1} mbar). This gave an approximate coating thickness of 183 nm according to Equation 3.1 [107]:

$$d = K \times I \times V \times t \tag{3.1}$$

where d is the coating thickness in Angstrom, K is 0.17 (an experimentally determined constant for a target to sample distance of 45 mm) for Au/Pd target used in an Argon environment, I is the plasma current in mA, V is the applied voltage in kV and t is the sputtering time in seconds.

During this operation, a sacrificial stripped optical fibre was threaded into the capillary to reduce the prospect of contaminating the bore of the capillary and to minimise the possibility of any deformation of the wall.

A magnified cut-out view of the chemical sensor is presented in Figure 3.5. A stripped optical fibre was inserted and secured to the capillary via a fusion joint. The arc welded fusion joints were located approximately 10 mm from the Au/Pd coated end-face of the capillary. Two cleaved multi-mode optical fibres (105/125 μm, Aomolin, China) were aligned with the gold-coated end-face of the capillary using a 3D micro-translation stage (Newport, UK) and bonded onto the supporting fibre using a UV-curable adhesive (NOA 68, Norland Products Inc. USA).

With reference to the lower section of Figure 3.5, the solid arrow-heads represent the incident light rays striking the reflective coating, and the open arrow-heads depict the reflected rays. Within specified incident angles, the light can be coupled back into the multi-mode optical fibre with a radius 'r'. In the current case, the lengths of the two secondary cavity 'd' were approximately 500 µm. When the chemical sensor was immersed in the resin system, the secondary cavities were filled. On illuminating the multi-mode fibres, the radiation was transmitted through the resin system and subsequently reflected off the reflective coating on the end-face of the capillary. The reflected light was coupled back into the multi-mode optical fibres, after travelling an effective path length of '2d'. The light was then directed via a 2 × 2 coupler to the detector on the FTNIR spectrometer enabling spectra to be obtained during the cross-linking process.

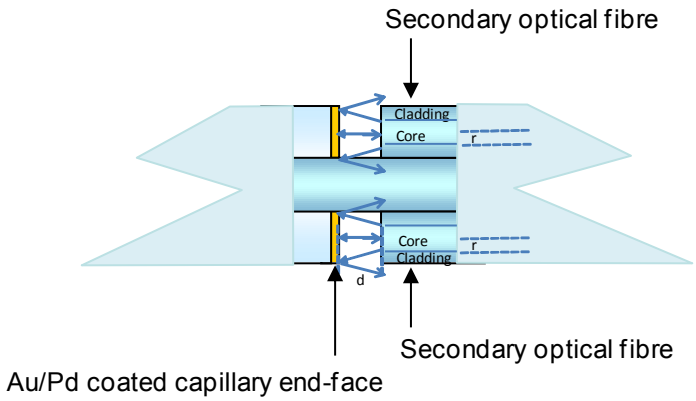

Figure 3.5 A schematic illustration of the transmission/reflection sensor design.

3.4.5 Multi-measurand sensor

A schematic illustration of the multi-measurand sensor (MMS) design is presented in Figure 3.6 and descriptions of the coded items are described below.

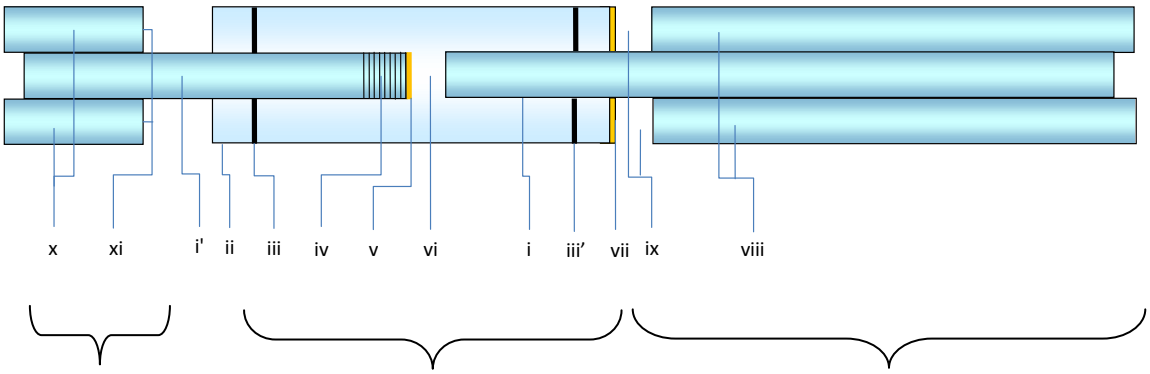

Figure 3.6 A schematic illustration of the multi-measurand fibre-optic sensor design.

The coded items are as follows: i - cleaved single-mode optical fibre (SMF-28^{TM}); i' - photo-sensitive single-mode optical fibres (PS1250/1500); ii - precision-bore capillary tube; iii and iii' fusion joints; iv – fibre Bragg grating inscribed in close proximity to the cleaved single-mode optical fibre; v - reflective coating on the single-mode photo-sensitive optical fibres; vi - air-gap constituting the Fabry-Perot cavity; vii - reflective coating on the end-face of the capillary tube; viii - secondary multi-mode optical fibre secured on the SMF-28^{TM} optical fibre; ix – secondary cavity between the reflective end-face on the capillary and the cleaved end-faces of a pair of multi-mode optical fibres. This cavity serves as a reservoir for the resin system to enable transmission/reflection near-infrared spectroscopy; x – a pair of cleaved multi-mode optical fibres that serve as a Fresnel reflection sensor to monitor the refractive index; and xi – Fresnel reflection sensors to monitor the refractive index of the resin system. Sections A, B and C represent the EFPI/FBG, secondary cavity for

transmission/reflection spectroscopy and Fresnel reflection sensors to monitor the refractive index respectively.

With reference to Figure 3.6, section [A] representing the combined EFPI/FBG strain/temperature sensor configuration where item [i] is a cleaved single-mode SMF-28^{TM} optical fibre (Corning Inc, USA). Item [i'] is a cleaved photosensitive single-mode optical fibre (PS1250/1500, Fibercore, UK), with an outer diameter of 125 ± 1 μm.

Component [ii] is a precision-bore capillary (Vitrocom, UK) with inner and outer diameters are 128 ± 3 and 300 ± 5 μm respectively. A capillary of approximately 40 mm length was cleaved using a capillary column cutter (Shortix^{TM}, SGT Singapore). The cleaved capillary was cleaned as described in Section 3.4.1. One face of the cleaved and arc-cleaned capillary end-face was sputter-coated (SC7640, Quorum Technologies, UK) with an Au/Pd alloy to create a reflective surface. The sputter-coating was carried out for 9 minutes using a plasma current of 20 mA and a vacuum of 10 Pa. (10^{-1} mbar) to achieve a coating thickness of approximately 183 nm.

A Bragg grating [iv] was inscribed on a stripped and cleaned portion of the photo-sensitive Ge-B co-doped optical fibre (PS1250/1500, Fibercore Ltd, UK) using a 1540 nm phase mask in conjunction with a KrF excimer laser (Braggstar, Coherent, UK) operating at 248 nm with a pulse energy of 10 mJ. The peak reflectivity of the Bragg grating was >90 % centred at 1539.84 nm. The fibre was cleaved in close proximity to

the distal-end of the Bragg and the cleaved-end was sputter-coated [v] with Au/Pd under identical conditions that were used for coating the capillary.

3.4.5.1 Assembling the multi-measurand sensor

With reference to Figure 3.6, the cleaved fibres (SMF-28^{TM}) [i] and the gold-coated fibre (PS1250/1500) with the inscribed FBG [i'] were mounted on the fusion splicer (BFS-60, UK) and threaded carefully into the capillary [ii]. The cavity length between the cleaved end-faces was monitored using an FBG interrogation system (FiberPro IS7000). Once the desired cavity length was attained, the optical fibres were secured to the capillary via two fusion joints [iii and iii'] using an arc discharge current of 17 mA for 3 seconds; this process was repeated five times. The gauge length (distance between the fusion joints) was measured and the general profiles of the fusion joints were inspected using a binocular microscope (Leica Wild M3C).

In Figure 3.6, section B representing the secondary cavity that was created to enable transmission/reflection spectroscopy. The secondary cavity [ix] was created by securing two cleaved multi-mode optical fibres [viii] (105/125 μm, Aomolin, China) on fibre [i]; the cavity length was 500 μm. The multi-mode optical fibres were bonded to fibre [i] using a UV-curable adhesive (NOA 68, Norland Products Inc. USA). The cleaved ends of the multi-mode fibres were aligned with the gold-coated end-face of the capillary using a 3D micro-translation stage (Newport, UK). This secondary cavity served as the reservoir for the resin thus permitting transmission/reflection spectroscopy to be conducted via the multi-mode optical fibres.

With reference to Figure 3.6, Section C illustrates the situation where two additional cleaved multi-mode optical fibres [x] were surface-bonded on fibre [i'] approximately 50 mm from the end-face of the capillary. This was done to prevent reflections from the end-face of the capillary from coupling back into the fibres. These fibres served to monitor the Fresnel reflectivity [xi] at the cleaved end-faces as a function of the optical density of the resin system.

The primary EFPI-FBG sensor, as described previously in Section 3.4.5, with a cavity length of approximately 91 μm was fabricated prior to the construction of the secondary sensors, namely the chemical and Fresnel reflection sensors. The arc welded fusion joints were located approximately 10 mm from the Au/Pd coated end-face of the capillary. The gauge length of the sensor was measured at 28.68 mm. The fusion jointing processes did not degrade the reflectivity of the coating on the capillary.

A schematic illustration of the multi-measurand sensor interrogation scheme is presented in Figure 3.7. MMS was interrogated using the FTNIR spectrometer as described in Section 3.3. An ASE light source (LPB-1550-D, Lumen Photonics, UK) emitting over a spectral region of 1450-1600 nm was used to illuminate the primary Fabry-Perot cavity and the FBG sensor. The reflected signals from the Fabry-Perot cavity and FBG were measured at a resolution of 4 cm^{-1} (0.96 nm) and 1 cm^{-1} (0.24 nm) respectively over 16 scans.

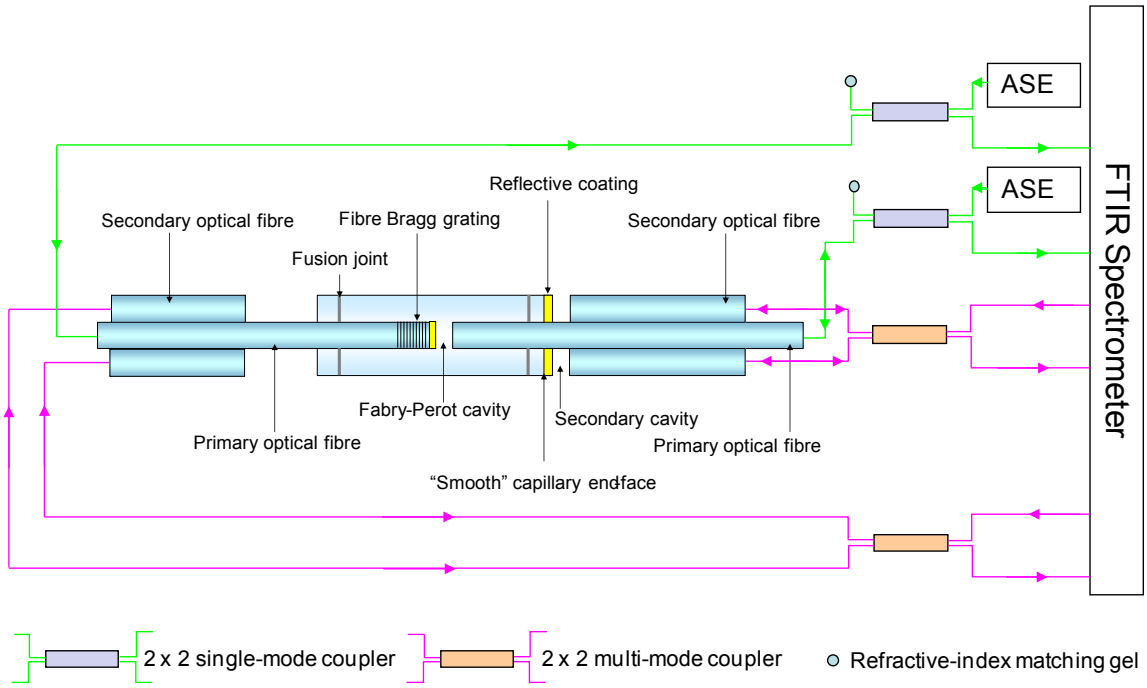

Figure 3.7 A schematic illustration of the experimental set-up for interrogating the multi-measurand sensor.

With reference to Figure 3.7, the secondary cavities (chemical sensors) and the Fresnel sensors were illuminated using the internal light source of the FTNIR spectrometer. The spectral range of the spectrometer was 4000 - 11000 cm^{-1}. The monitoring of the cross-linking reactions was performed at a resolution of 4 cm^{-1} (0.96 nm) over 64 scans.

3.5 Optimisation of the MMS design

A series of experiments were carried out as part of the development and optimisation of the multi-measurand sensor design. The experimental details are described below:

3.5.1 FTNIR-based interrogation and data acquisition parameters for the Fabry-Perot sensor

The optimum resolution and the number of scans for measuring the Fabry-Perot cavity length was determined using FTNIR spectroscopy. An EFPI sensor of cavity length 85.69 μm was secured on to a Teflon-coated flat aluminium plate using polyester flash tape. The internal light source of the FTNIR spectrometer was used to illuminate the sensor. The interference fringes from the EFPI sensors were interrogated at 2 cm^{-1} resolution over 64, 128, 192 and 512 scans. The experimental set-up is shown in Figure 3.8.

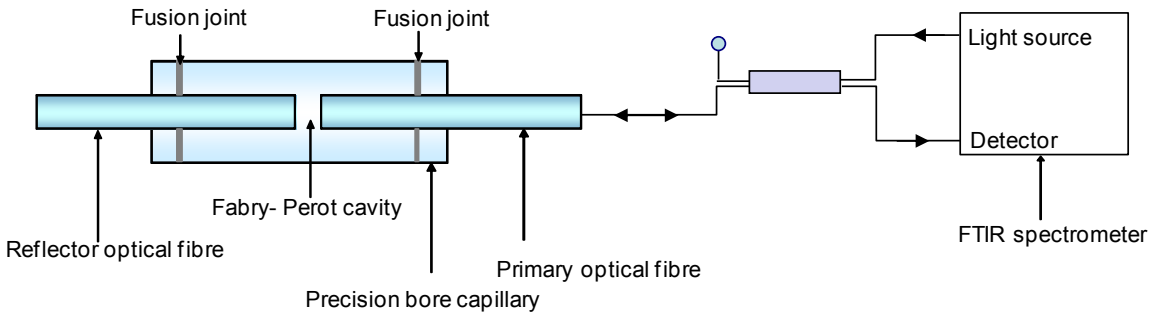

Figure 3.8 A schematic illustration of the experimental set-up for optimising the data acquisition parameters for the EFPI sensor.

3.5.2 EFPI/FBG cavity length measurement using FTNIR spectrometer

The deconvolution or separation of the EFPI and FBG signals was important for the multi-measurand sensor design to prevent any cross-coupling. An EFPI sensor and an integrated EFPI/FBG sensor were used in this experiment. Single-mode optical fibres –

SMF-28^{TM} were used for the fabrication of EFPI sensor whereas photo-sensitive (GeO_2-B_2O_3 co-doped) single-mode fibres – PS 1250/1500 were used for the fabrication of the integrated EFPI/FBG sensor. The cavity length of each sensor was varied from 20 to 260 µm at 20 µm intervals using the manual translation facility of the fusion splicer (BFS-60, UK). The ASE light source was used to illuminate the sensors and the reflected signals were measured at a resolution of 1 cm^{-1} (0.24 nm) over 16 scans using the FTNIR spectrometer. The experimental set-up is shown in Figures 3.9 (a and b).

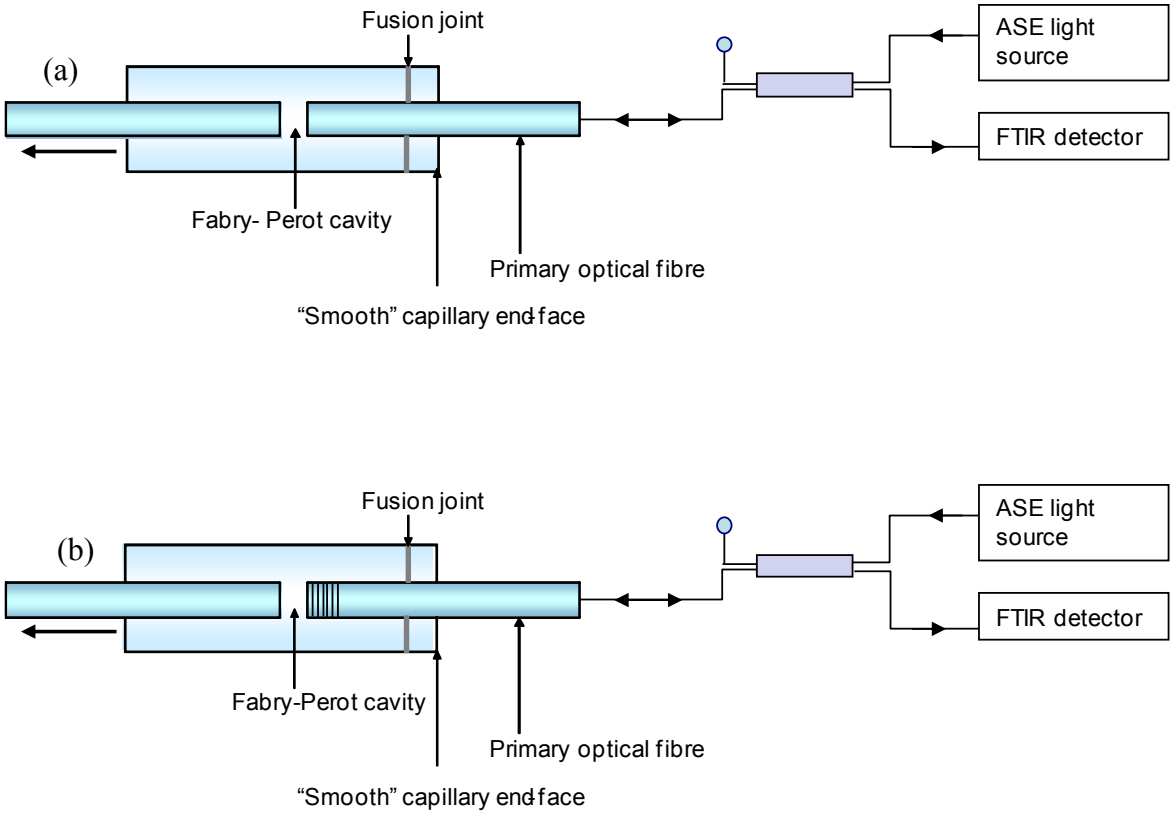

Figures 3.9 (a and b) Schematic illustrations of the experimental set-up for measuring the cavity length of (a) the EFPI sensor and (b) the integrated EFPI/FBG sensor.

3.5.3 Annealing the gold/palladium coatings

3.5.3.1 Annealing the Au/Pd coated end-face of cleaved fibre

The effect of annealing the sputter-coated gold/palladium-coatings on the cleaved-end of the photo-sensitive optical fibre – PS 1250/1500 was studied. This was carried out by monitoring the intensity of the reflected light from the coated fibre-end when light from an ASE source, emitting over a spectral region of 1450-1600 nm, was coupled into the fibre. The reflected light intensity was measured using the InGaAs detector of the fibre-coupled FTNIR spectrometer.

Three Au/Pd-coated optical fibres were housed in individual silica capillaries using the fusion splicer (BFS-60, UK). These were secured on to a Teflon-coated aluminium flat plate in a stress-free condition and placed in an air circulating oven (Memmert, UK). The annealing of the coated fibre-end was carried out from 30 °C to 180 ^{o}C with 30 minutes dwell time over four heating/cooling cycles. The experimental set-up is shown in Figure 3.10.

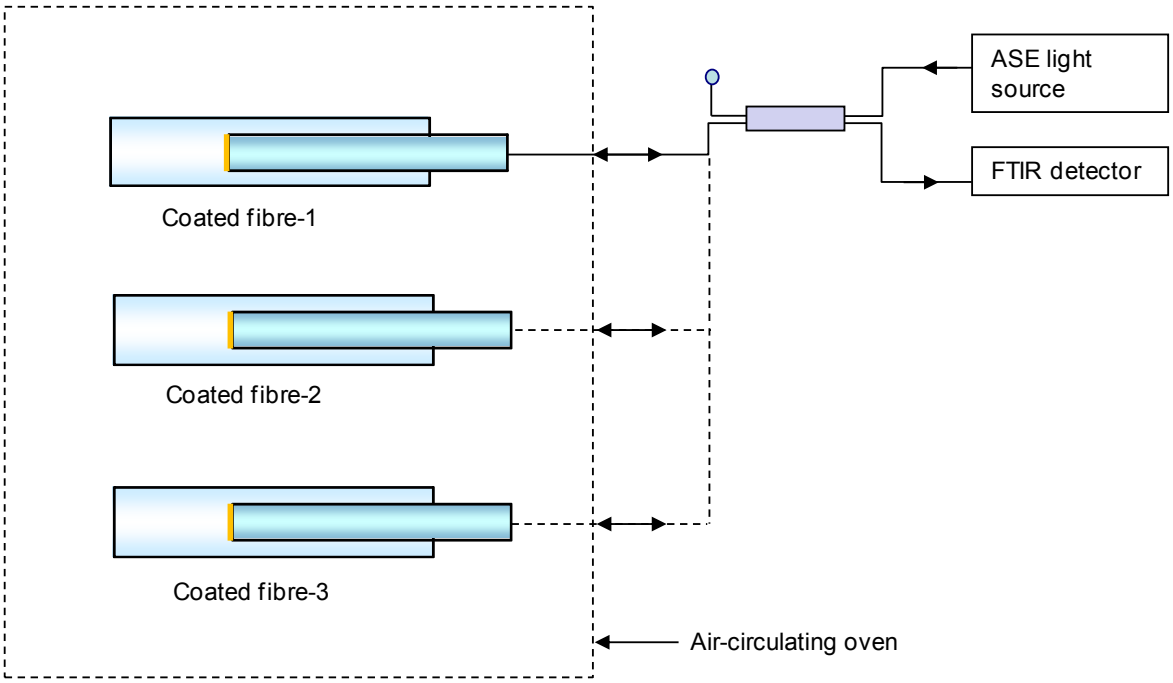

Figure 3.10 A schematic illustration of the experimental set-up for interrogating the annealing of the gold-palladium coatings in an air-circulating oven. The sensors were connected and disconnected each time during the temperature dwell periods.

3.5.3.2 Annealing the Au/Pd coated end-face of a fibre with an FBG integrated within an EFPI sensor

The effect of subjecting the Au/Pd coating to a series of heating and cooling cycles on the cavity length of the EFPI sensors and the output of the FBG sensors were studied. A schematic illustration of the sensor and interrogation configurations for this series of experiments is shown in Figure 3.11. A reference EFPI sensor (without the Au/Pd coating) and a coated EFPI sensor (with one of the fibres within the capillary being coated) with cavity lengths of 100 µm and 102 µm respectively were used to study the effect of annealing the reflective coating within the Fabry-Perot cavity. A reference

FBG sensor (without the Au/Pd coating on the cleaved-end of the fibre) and an FBG sensor where the end of the cleaved optical fibre was coated, with peak FBG reflection wavelengths of 1552.3 nm and 1552.5 nm, were used to study the effect of temperature cycling (and annealing) on the output of the FBGs. The sensors were heated from 30 to 180 °C with 30 minute dwells at 30, 90, 120, 150 and 180 °C in an air-circulating oven. A K-type thermocouple was located in close proximity to the EFPI sensors to monitor the temperature. The EFPI cavity lengths and FBG peak wavelengths were measured during the isothermal dwells. The sensors were interrogated using the FTNIR spectrometer and the FiberPro interrogation unit operating at a wavelength resolution of 0.96 nm and 1 pm respectively. The ASE light source was switched-off when connected to FiberPro and vice-versa to prevent any cross-coupling of the signals. The experiments were repeated three times for each sensor using the two interrogation units. The absolute cavity length was calculated by determining the wavelengths corresponding to the adjacent maxima of the bright fringes.

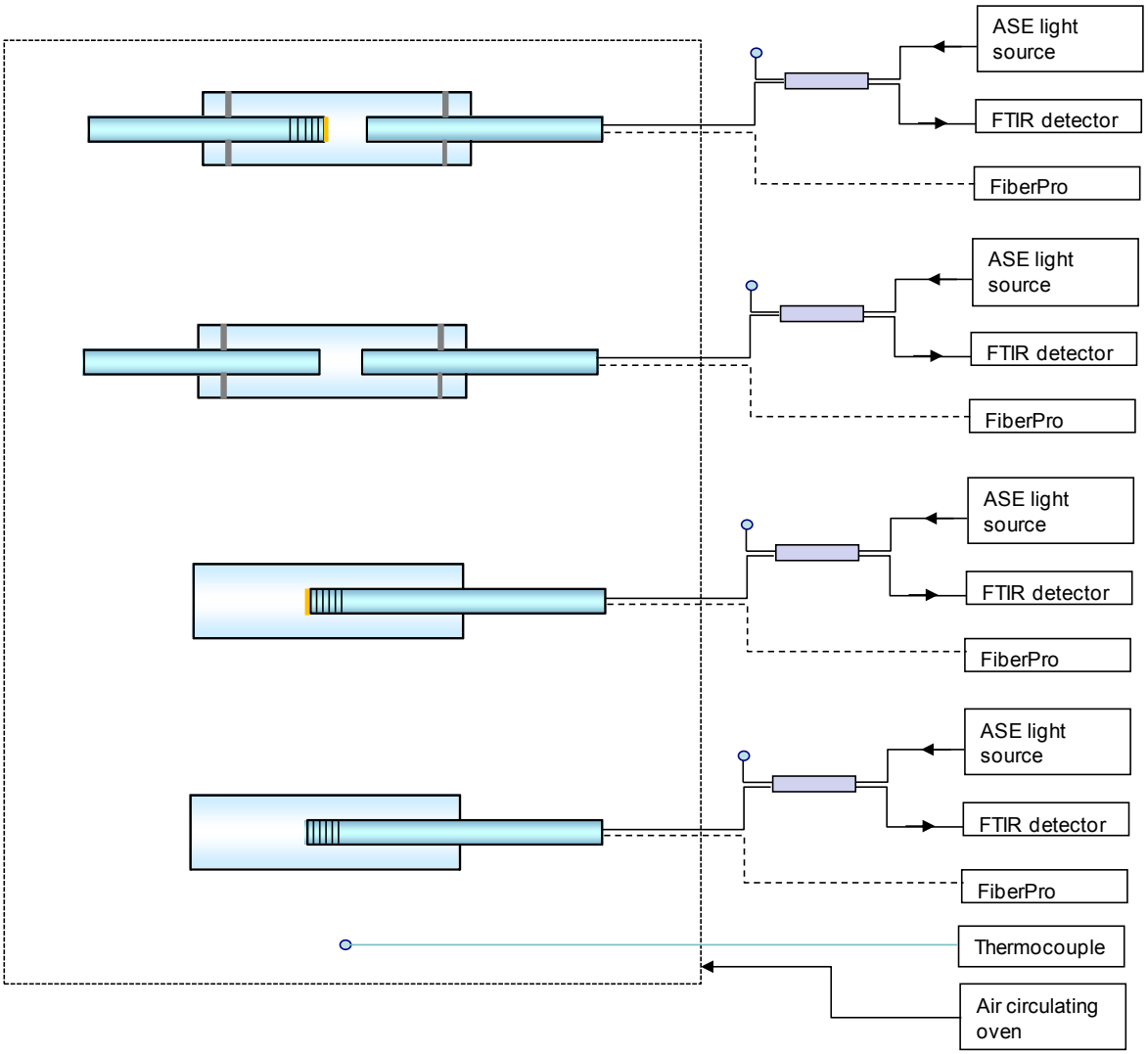

Figure 3.11 A schematic illustration of the experimental set-up for measuring the effect of annealing the reflective coating on the Fabry-Perot cavity lengths and the output of the FBG sensors.

3.5.4 Plasma exposure on the FBG sensor

The effect of exposing the FBG sensor to the plasma during the sputter-coating process was studied. An FBG sensor of peak wavelength 1552.09 nm was exposed to the plasma of the sputter-coater (SC7640, Quorum Technologies, UK). The sputter-coater

was operated for nine minutes using a current of 20 mA with a vacuum of 10 Pa. (10^{-1} mbar). The sensor was rotated by 180 ° (opposite face) using a fibre chuck holder and coating was re-applied for another 9 minutes. The Au/Pd-coating of the FBG was then removed using isopropanol and lint-free tissue. The FBG was interrogated using the FiberPro IS7000. The FBG peak at each stage was measured and compared.

3.5.5 Effect of the clamping stress on the response of the FBG sensor

An FBG with a peak wavelength of 1552.30 nm was fabricated and the effect of the clamping stress exerted by the magnetic clamps of the micro-translation stage on the FBG peak was studied. FBG interrogation unit (FiberPro IS7000) was used to interrogate the sensor and the experiment was repeated five times. The FBG spectra were obtained under the following conditions:

- with clamps and phase-mask resting on the fibre;
- with clamps but phase-mask lifted;
- with and without clamping stresses; and
- without stress on a flat aluminium plate.

3.5.6 Secondary fibre alignment on the translation stage

An experiment was carried out to check the alignment of the EFPI sensor and the secondary fibres on a 3D-translation stage before the fabrication of the chemical sensor. Two cleaved ends of the single-mode fibres – SMF-28^{TM} were aligned with the gold-coated end-face of the capillary using a 3D micro-translation stage (Newport, UK). The ASE light source was used to illuminate the fibre and an optical spectrum analyser with

a resolution of 0.07 nm was used to measure the reflected signals. Secondary fibres were secured onto the 3D-translation stage using polyester flash tape. These were initially positioned to butt-stage with the gold-coated end-face of the capillary and the cavity length varied from 100 to 500 μm in 100 μm steps. The cavity length for each set-gap was calculated.

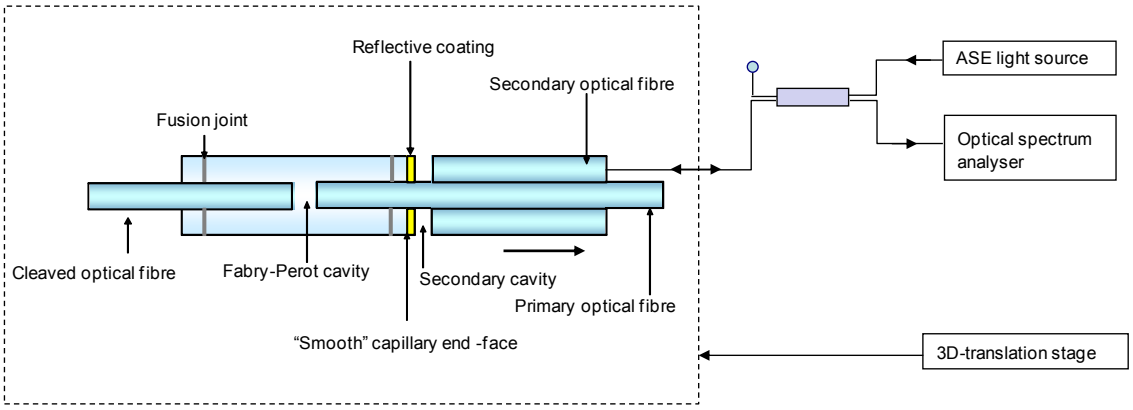

Figure 3.12 A schematic illustration of the experimental set-up for checking the alignment of the secondary optical fibres using a 3D micro-translation stage.

3.6 Production of composites

Two types of composites with embedded optical fibre sensors were prepared in this study:

(a) Unidirectional carbon fibre reinforced polymer composites (CFRP): Unidirectional carbon/epoxy prepreg plies – VTM264/T700S (Umeco, UK) were cut to dimensions of 300 × 300 mm. An eight-ply unidirectional laminate sequence $[0]_8$ was employed.

(b) Woven E-glass reinforced fabric laminates: Eight-ply plain-weave E-glass fabric (PD-Interglas Technologies, UK) were cut to dimensions of 130 × 200 mm. A commercially-available thermosetting epoxy/amine resin system LY3505/XB3403 (Huntsman Advanced Materials, UK) was used to impregnate the laminates.

3.6.1 Hand lay-up and embedding of optical fibre sensors

The prepreg reel was taken out of the freezer and allowed to thaw to room temperature for 24 hours before commencing the lay-up process. The required numbers of prepreg plies were cut using a fresh portion of a razor blade. The plies were aligned in the required orientation and stacked using a custom-made vacuum assisted jig as shown in Figure 3.13a. In the case of fabric laminates, the fabric layers were impregnated and laminated manually. A hand-roller was used to consolidate each ply carefully and to expel the entrapped air from between them.

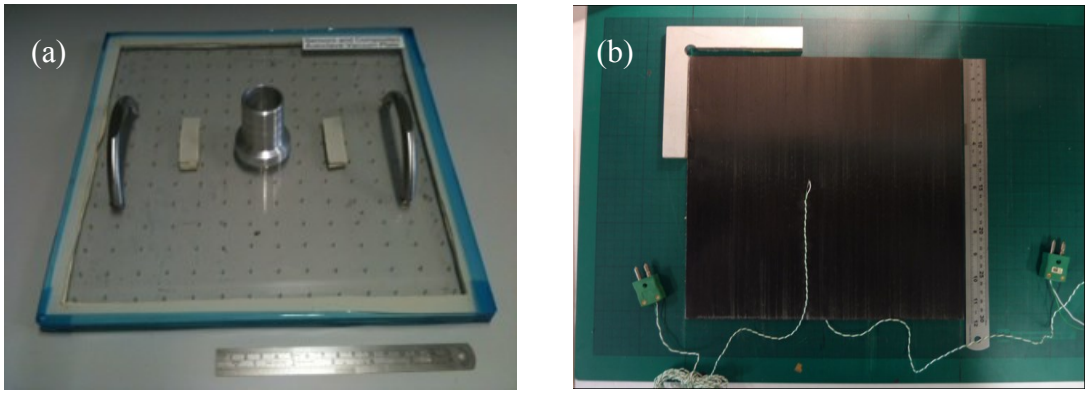

Figure 3.13 Photographs showing: (a) the custom-made vacuum assisted jig for the alignment of the prepregs; and (b) a laminated 8-ply unidirectional carbon fibre prepreg.

The optical fibre sensors were aligned with the fibre direction in the CFRP laminates as shown in Figure 3.14. Polytetrafluoroethylene (PTFE) tubing was used to protect the optical fibres at the entry and exit points of the laminate. The ends of the PTFE tubes were sealed with a UV-curable epoxy resin to prevent the resin from wicking into the PTFE tube during processing. Conventional thermocouples (type-K, chromel-alumel) were also embedded in the laminate at approximately 20-30 mm from the edge.

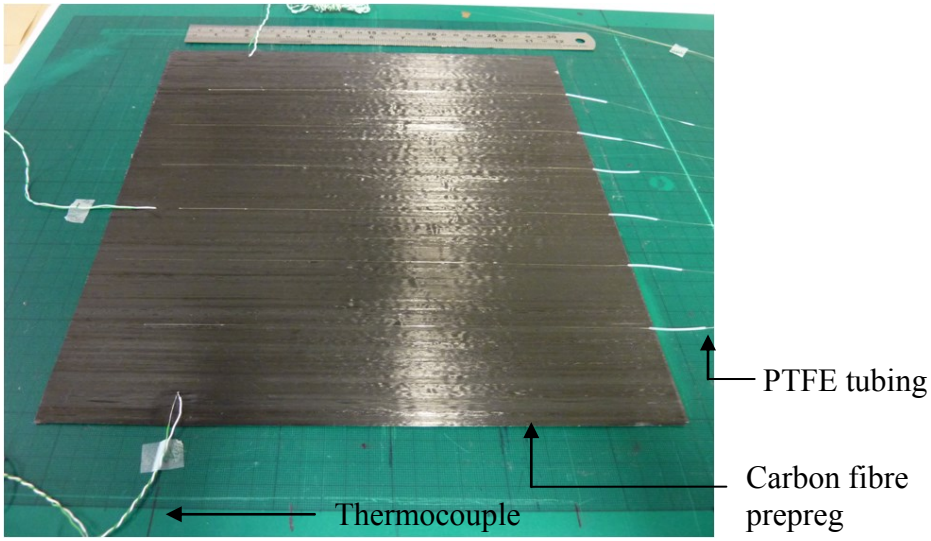

Figure 3.14 Photograph showing the positioning of the optical fibre sensors in alignment with the reinforcing fibre direction in the mid-plane (ply 4) of an eight-ply CFRP laminate.

3.6.2 Vacuum bagging

The laminated prepreg was placed on to a carbon composite tooling plate of dimension: 1500 mm x 600 mm x 3.5 mm and vacuum-bagged using the materials described in Section 3.2.3. A schematic illustration of the various components of the vacuum bagged

assembly is shown in Figure 3.15. A photograph of the vacuum bagging assembly consisting of an eight-ply laminated carbon fibre prepreg is shown in Figure 3.16.

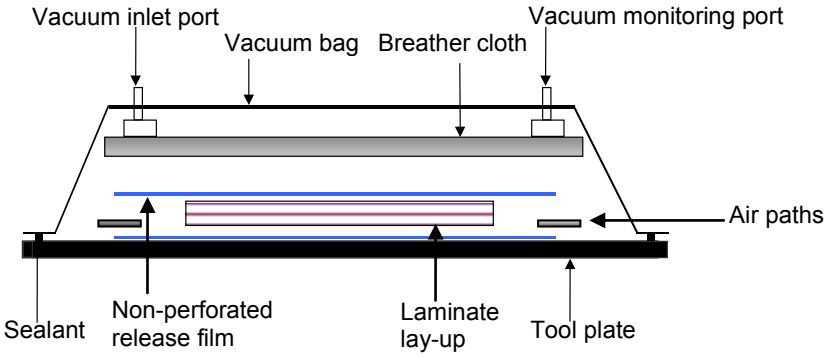

Figure 3.15 A schematic illustration of the vacuum bagging arrangement for autoclave-processing of the fabric laminate.

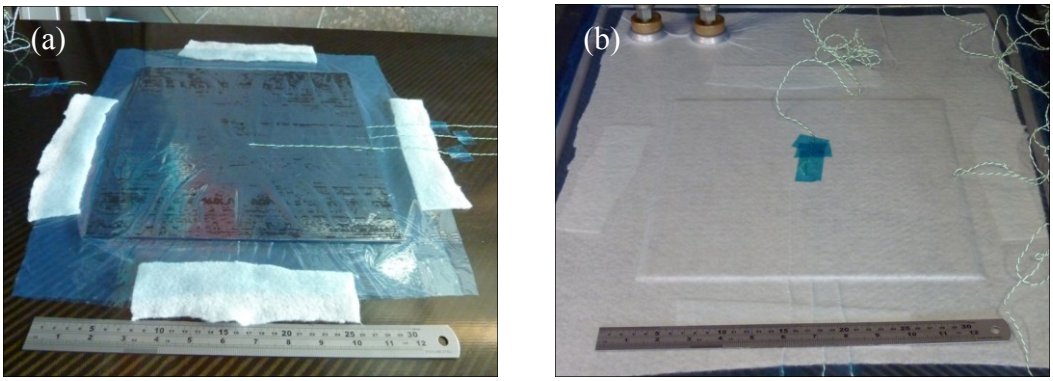

Figure 3.16 Vacuum bagging assembly of an eight-ply CFRP composite laminate.

3.6.3 Autoclave-based processing

All the laminates prepared in this study were processed using an autoclave (LBBC, UK). The laminate was subjected to a vacuum of 0.1 MPa for 30 minutes prior to initiating the cross-linking cycle. The processing schedule used was as follows. The vacuum bagged assembly was heated from ambient to 120 °C at 2 °C per minute. The

pressure inside the autoclave was increased from 0.007 MPa to 0.48 MPa at 0.02 MPa/minute. The vacuum-bagged assembly was held at 120 °C for one hour and then cooled to ambient. The vacuum was maintained throughout the cure cycle and the pressure was maintained until the end of the isothermal temperature dwell. The temperature on the surface of the vacuum bag was also measured using an independent thermocouple.

3.7 Process monitoring of the laminate preforms

The experimental details of the autoclave-based process monitoring of CFRP and woven glass fabric laminates are described in the following section.

3.7.1 Temperature monitoring within the CFRP laminate during processing

The evolution of the temperature during the cross-linking of an eight-ply unidirectional CFRP laminate of dimension 300 × 300 mm was monitored using six K-type thermocouples. Thermocouples-1, 2 and 3 were embedded in the laminate and located as follows: Thermocouple-1 in the mid-plane in between the 4^{th} and 5^{th} plies, thermocouple 2 under the 1^{st} ply and thermocouple 3 on top of the 8^{th} ply as shown in Figure 3.17. The thermocouples were positioned at distances of 150 mm (middle), 130 mm (bottom) and 170 mm (top) from the edge. The other three thermocouples were placed on the vacuum bag, under the vacuum bag and on the tool plate respectively. The laminate was vacuum-bagged and cured in an autoclave at 120 °C for 1 hour as per the cure cycle described in Section 3.6.3.

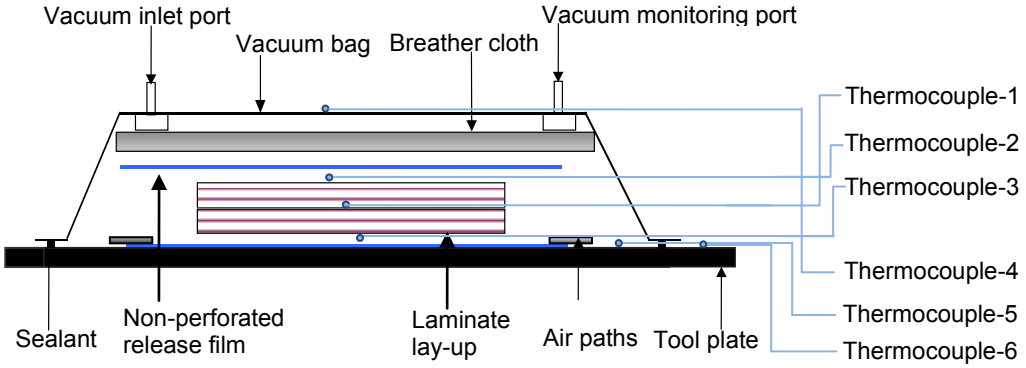

Figure 3.17 A schematic illustration of the location of the thermocouples in an eight-ply unidirectional CFRP laminate.

3.7.2 Process monitoring of CFPR laminate using multiplexed FBGs

The development of strain and temperature during the processing of an eight-ply UD CFRP laminate was monitored using embedded multiplexed FBGs. FBGs with peak wavelengths of 1539.80, 1546.78 and 1552.22 nm were inscribed on a single photo-sensitive optical fibre – PS 1250/1500. The gratings were spaced equally at a distance of 55 mm from the stripped region of the fibre and the total length of the sensor was approximately 60 cm. Six such sensors (comprising of three gratings each) were prepared and annealed at 150 °C for 12 hours in an air-circulating oven before embedding.

The sensors were embedded between the 4^{th} and 5^{th} plies of an eight-ply unidirectional CFRP laminate. A schematic illustration of the location of the sensors is shown in Figure 3.18. With reference to Figure 3.18, the experimental set-up consists of a total of 15 FBG strain sensors and 3 FBG temperature sensors. Three thermocouples were

embedded in the laminate in close proximity to the FBG temperature sensors. An independent thermocouple was also placed outside the vacuum bag. The laminate was vacuum-bagged and cured in an autoclave at 120 °C for 1 hour. The signals from FBG temperature and strain sensors were acquired simultaneously using the multi-channel FBG interrogation unit (FiberPro IS7000).

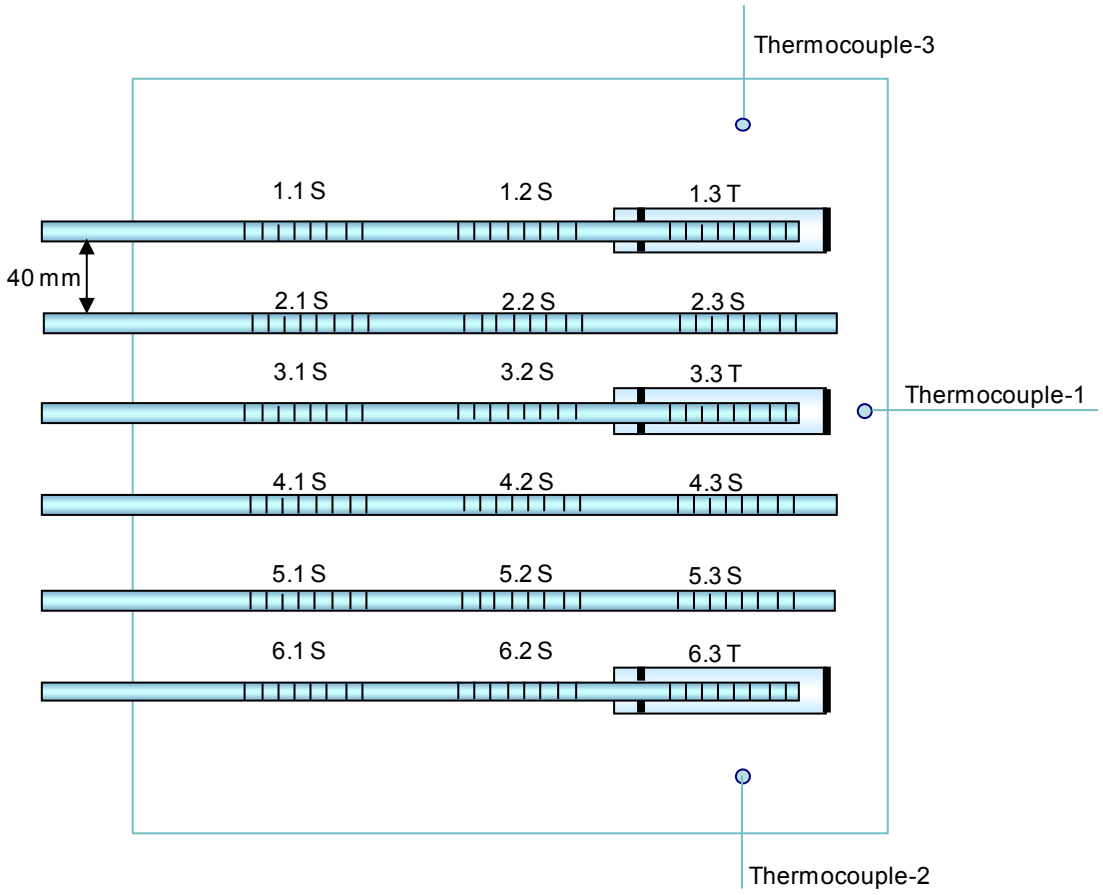

Figure 3.18 A schematic illustration of the locations of the multiplexed FBG sensors in an eight-ply unidirectional CFRP laminate. 'S' and 'T' denote strain and temperature sensors respectively.

3.7.3 Process monitoring of CFRP laminate using FBGs and Fresnel sensors

The process monitoring of an eight-ply unidirectional CFRP laminate was carried out using FBG and Fresnel sensors. The development of strain and temperature within the laminate during processing was monitored using the embedded FBG sensors whereas the cure progression was monitored using embedded Fresnel sensors.

FBGs with peak wavelengths of 1539.90 nm were inscribed on photo-sensitive optical fibre – PS 1250/1500. The sensors were annealed at 150 °C for 12 hours in an air-circulating oven. The Fresnel sensors were manufactured using SMF-28^{TM} fibre. The cleaved ends of the fibres were cleaned with isopropanol and examined under optical microscope to ensure a clean surface and normal cleave angle.

The sensors were positioned in between the 1st and 2nd plies, 4th and 5th plies, and 7th and 8th plies as shown in Figure 3.19. FBG strain and temperature sensors were interrogated using the multi-channel FBG interrogation unit (FiberPro IS7000). A temperature-controlled laser-diode (LDC 3900, ILX lightwave) operating at 1550 nm was used as the light source for the Fresnel sensors. A fibre circulator was used to transmit/receive the light. An InGaAs photodiode – PDC 10CS (Thorlabs, UK) detector was used to monitor the optical signal via the Fresnel reflection from the cleaved end of the fibre. An optical channel selector (Anritsu MN9674A) was used to enable automatic switching between the sensors.

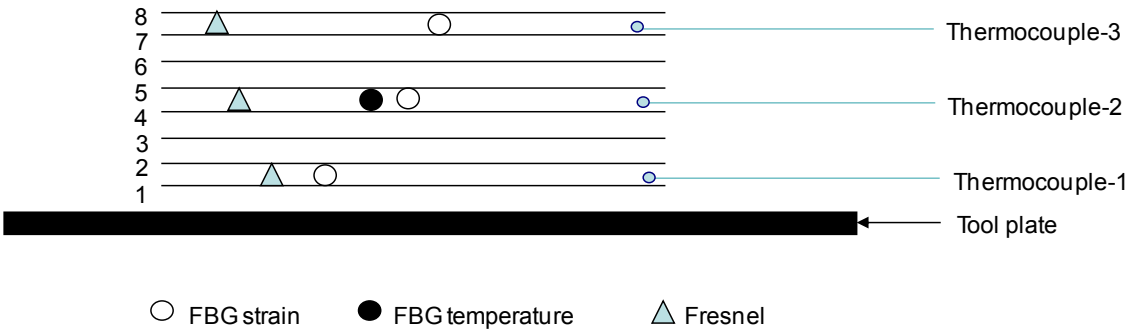

Figure 3.19 A schematic illustration of the locations of FBG and Fresnel sensors in an eight-ply unidirectional CFRP laminate.

The influence of vacuum, temperature and pressure cycles on the cured CFRP laminate was studied using FBG sensors. The laminate was placed in the vacuum-bag assembly inside the autoclave. The following experiments were carried out to study the post-processing of the composite:

(i) Vacuum cycle: The laminate was subjected to three sets of vacuum/vent cycles. A dwell time of 20 minutes was given to each vacuum/vent stage and the FBG spectra were recorded using the FBG interrogation unit (FiberPro IS7000).

(ii) Temperature cycle: The laminate was reheated and cooled from room temperature to 120 °C. A temperature dwell of 30 minutes was given at 120 °C and then cooled-back to room temperature. The vacuum was not applied and the pressure inside the autoclave was maintained at 0.007 MPa throughout the experiment. The strain was monitored *in-situ* using the FBG sensors.

(iii) Pressure cycle: Pressure inside the autoclave was increased from 0.007 MPa to 0.48 MPa. A pressure dwell of 30 minutes was given and then brought back to 0.007 MPa. Vacuum was not applied and the temperature inside the autoclave was set at 25 °C

during this cycle. FBG sensors were monitored continuously using the FBG interrogation unit (FiberPro IS7000).

(iv) Normal cure cycle: A normal cure cycle (120 °C for 1 hour) as described in Section 3.6.3 was carried out on the cured composite. The strain in the composite was monitored continuously using FBG sensors.

3.7.4 Process monitoring of fabric laminate using the MMS

The details of the resin system used to impregnate the E-glass fabric was presented in Section 3.2.1. The multi-measurand sensor was embedded in-between the fourth and fifth plies of the eight-ply E-glass plain-weave fabric laminate. An independent FBG (strain and temperature) sensor was also embedded alongside the MMS to enable comparison between the sensors. These sensors were annealed at 150 °C for 12 hours in an air circulating oven before embedding. Conventional K-type thermocouples were also embedded in-between 4^{th} and 5^{th} plies of the laminate at approximately 20-30 mm from the edge. A schematic illustration of the location of the various sensors is shown in Figure 3.20.

The laminated fabric with the embedded sensors was placed on a carbon composite tooling plate and vacuum-bagged in the autoclave using conventional procedures. The laminate was cured at 120 °C for 1 hour as per the cure cycle described in Section 3.6.3. The primary EFPI-FBG sensor of the MMS was illuminated using an ASE light source, and connected to the FTNIR spectrometer via 2 × 2 single-mode couplers. The secondary sensors, namely, the chemical and Fresnel reflection sensors were

illuminated using the FTNIR light source and connected to the spectrometer via 2 × 2 multi-mode couplers. The independent FBG (strain and temperature) sensor was interrogated using an FBG interrogation unit (FiberPro IS7000) and the strain and temperature data were acquired simultaneously using this unit.

The cured fabric composite was subjected to temperature cycles to study the development of strain during post-processing. The laminate was reheated and cooled three times without pressure or vacuum in the autoclave. The development of strain was monitored in-situ using MMS-EFPI sensor and independent FBG strain sensor.

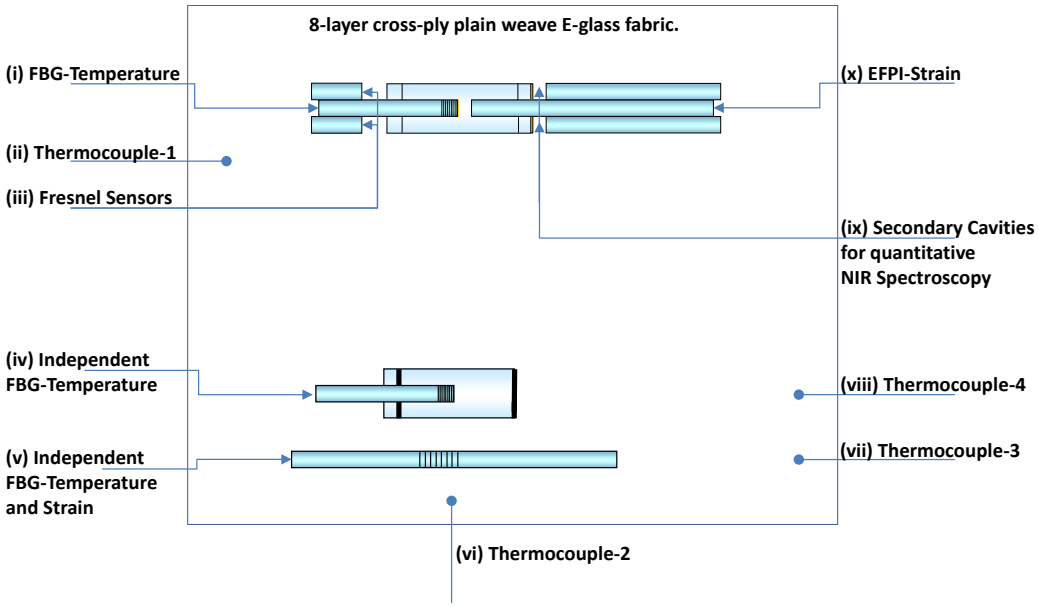

Figure 3.20 A schematic illustration of the location of the MMS (EFPI, FBG-temperature, chemical and Fresnel reflection sensors) between the fourth and fifth plies of an eight-ply fabric laminate of dimension: 130×200 mm. The locations of the independent FBG-temperature, FBG-strain/temperature and conventional thermocouples are also indicated.

3.7.4.1 Validation of chemical sensor via cuvette-based experiments

A demountable cuvette (Starna®, UK) with a 1 mm path length was used to obtain data simultaneously from a conventional FTNIR transmission experiment and that obtained from a MMS chemical sensing element during the cross-linking of the epoxy/amine resin system. The chemical sensing element (secondary cavity) of the MMS, as illustrated in Figure 3.5, was secured in the demountable cuvette. The mixed resin system was injected via a syringe into the Starna® demountable cuvette. The FTNIR spectrometer was used to acquire spectra at a resolution of 0.96 nm over 64 scans. The cross-linking experiments were conducted at 50, 60 and 70 °C and repeated two times. The cuvette containing the resin system was housed in a CUV-TLC-50F temperature-regulated cuvette holder (Ocean Optics Inc). The cuvette holder contained four optical ports with two of these accommodating an SMA connector each with integrated collimating lens. With reference to the FTNIR spectroscopy transmission experiments, two low-OH optical fibre probes (Ocean Optics Inc.) were used to connect two of the optical ports positioned at 180º to the light source and detector of the spectrometer respectively.

3.7.5 Strain anomalies of acrylate-coated photo-sensitive fibres

Anomalies in the output of the FBG sensors were observed when acrylate-coated photo-sensitive fibres were embedded in eight-ply unidirectional CFRP prepregs and woven fabric laminates. Therefore, a study was undertaken using FBGs inscribed on polyimide-coated fibres (SMF-28™ Alxenses, China). Stripped FBGs were also used where the acrylate-coating of the photo-sensitive fibres were removed along the whole

length of the optical fibre using a mechanical stripper. These fibres were cleaned using isopropanol before embedding. All the sensors were annealed at 150 °C for 12 hours in an air-circulating oven prior to embedding.

3.7.5.1 Unidirectional CFRP laminate

Two unidirectional CFRP laminates of dimension: 300 × 300 mm were prepared. Two acrylate-coated and fully-stripped FBGs were embedded in the first laminate whereas two acrylate- and polyimide-coated FBGs were embedded in the second laminate. A FBG temperature sensor was used to decouple strain from temperature. The sensors were positioned between the 4^{th} and 5^{th} plies of an eight-ply unidirectional CFRP laminate. The locations of the sensors are shown in Figure 3.21 (a and b). The laminate was vacuum-bagged and subsequently cured in the autoclave at 120 °C for 1 hour as per the cure cycle described in Section 3.6.3. The sensors were interrogated using the FBG interrogation unit. The cured composites were also subjected to temperature cycles without vacuum or pressure in the autoclave.

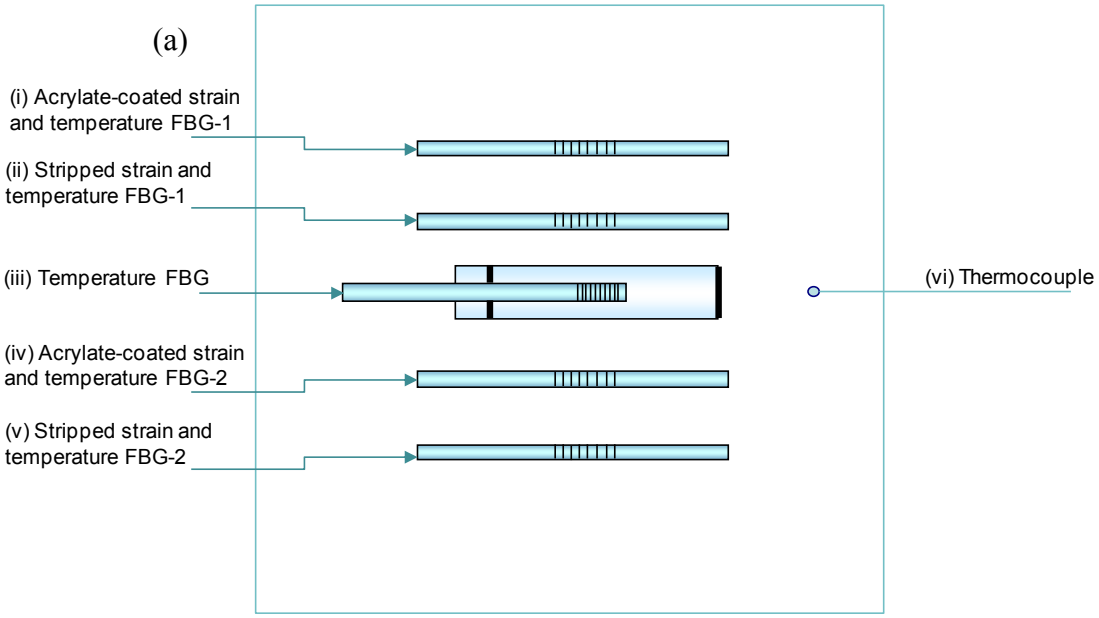

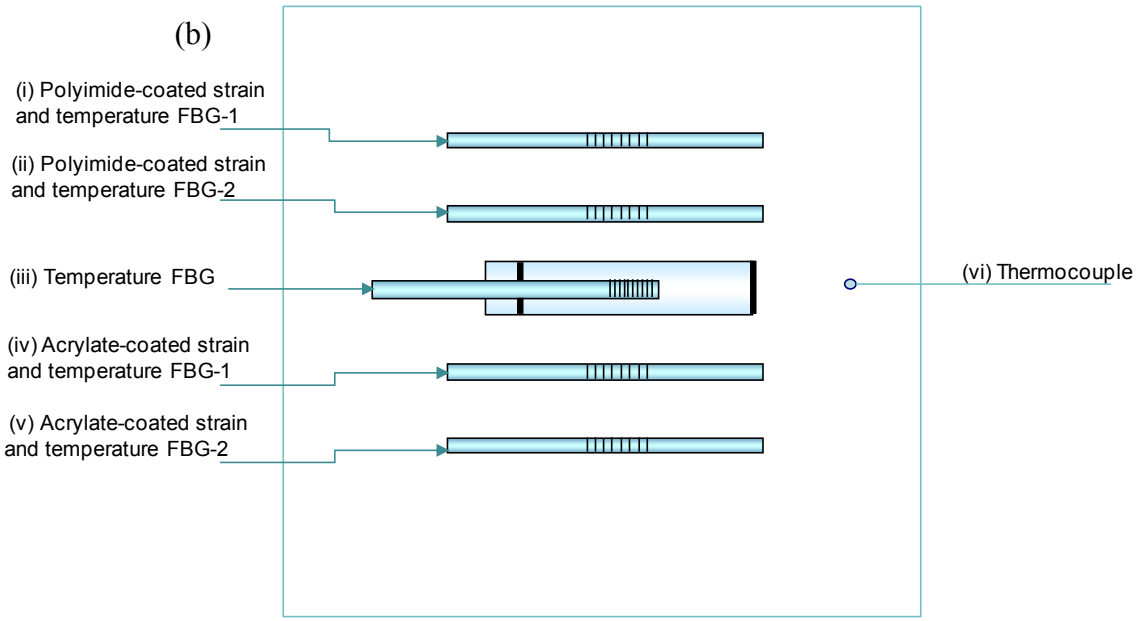

Figure 3.21 Schematic illustrations of the locations of the sensors in the eight-ply CFRP (a) laminate-1 and (b) laminate-2. This experiment was carried out to study the effect of the coating materials (acrylate and polyimide) on the response of the FBG sensor during autoclave-based processing.

3.7.5.2 Woven E-glass fabric laminate

Woven E-glass fabric laminate of dimension: 130 × 200 mm were prepared and impregnated with the LY3505/XB3403 resin system as described in Section 3.2.1. One acrylate-coated FBG, two FBGs where the acrylate coating was removed along the whole length of the optical fibres FBGs, one polyimide-coated FBG and an FBG temperature sensor were embedded in between the 4^{th} and 5^{th} plies of an eight-ply laminate. The locations of the sensors are shown in Figure 3.22. The laminate was vacuum-bagged using conventional procedures and cured in the autoclave at 120 °C for 1 hour. The signals from the sensors were acquired continuously using the multi-channel FBG interrogation unit.

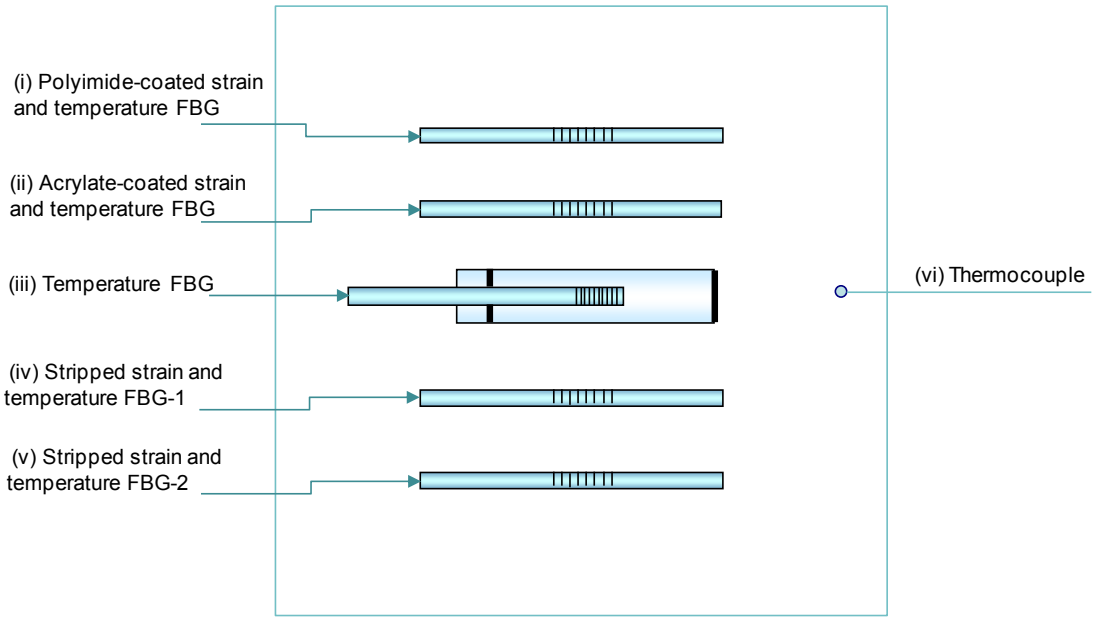

Figure 3.22 A schematic illustration of the locations of the sensors in the eight-ply woven fabric laminate. This experiment was carried out to study the effect of the acrylate and polyimide coating on the response of the FBG sensors.

4 RESULTS AND DISCUSSION

The results of the experiments described in Chapter 3 are presented and discussed in this chapter. This chapter is divided into the following sub-sections:

(i) optimisation of the multi-measurand sensor;

(ii) process monitoring of CFRP laminate using embedded multiplexed FBG sensors;

(iii) process monitoring of CFRP laminate using embedded FBG and Fresnel sensors;

(iv) process monitoring of E-glass fabric laminate using embedded multi-measurand sensor; and

(v) strain anomalies of acrylate-coated photo-sensitive fibres during the process monitoring of carbon and E-glass fabric laminates.

4.1 Quality of the cleaved capillary for MMS fabrication

Unlike the fabrication of conventional EFPI sensors, in the case of the multi-measurand sensor, it was necessary to pay special attention to the cleaved capillary, as one end-face was destined to be used as reflective surface for the chemical sensor. The processing routines used (ultrasonic and arc-cleaning) on the cleaved capillary were found to be satisfactory in obtaining repeatable quality and consistency with regard to the reflectivity of the end-face of the capillary.

The quality of the capillary end-faces was inspected under a binocular microscope (Leica Wild M3C). Typical micrographs of the end-faces before and after post-processing are shown in Figures 4.1 and 4.2 respectively. Figures 4.2 (a and b) show the end-face of an as-cleaved capillary where some surface irregularities can be seen; on inspecting Figures 4.2 (a and b), it can be concluded that some of the surface irregularities have been made less prominent by the fusion-arc cleaning process.

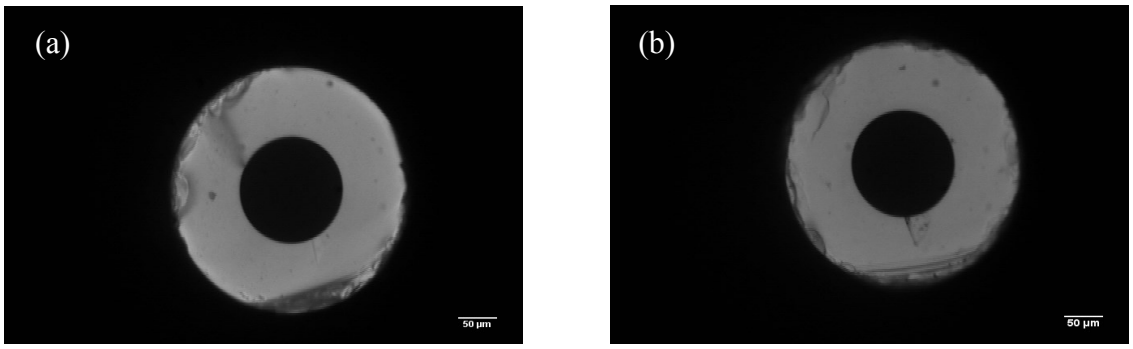

Figures 4.1 (a and b) Micrographs showing the poor end-faces of the capillary produced using the manual-cleaving method.

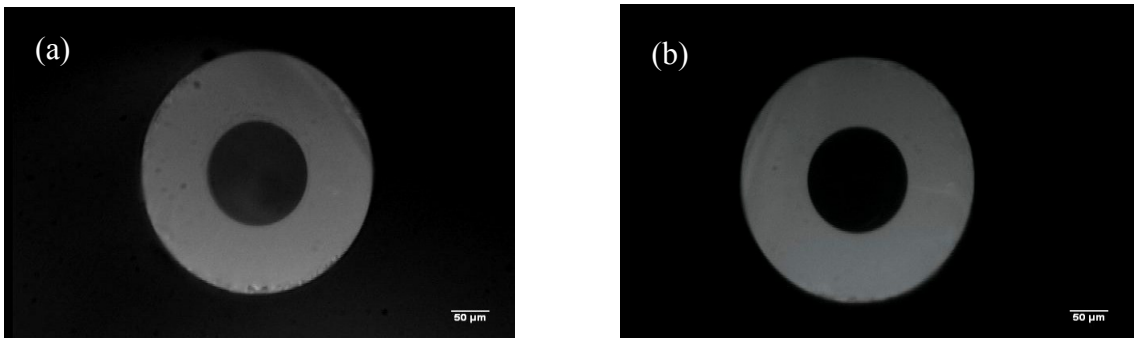

Figures 4.2 (a and b) Micrographs of "acceptable" capillary end-faces after post-processing. The capillaries were cleaved using a commercially-available Shortix^{TM} cutter. (a) Before electric arc-cleaning and (b) after electric arc-cleaning.

The arc-cleaning post-processing procedure was adopted for manufacturing the sensors that involved the capillary in their construction (EFPI, MMS and FBG-temperature).

4.2 Optimisation of the MMS design

4.2.1 FTNIR-based interrogation and data acquisition parameters for the Fabry-Perot sensor

In the initial phase of this research, the feasibility of using the internal light source of the FTNIR to illuminate the sensor was investigated. An EFPI sensor with a fixed cavity length of 85.69 μm was used and the sensor was interrogated at 2 cm^{-1} resolution over 64, 128, 192 and 512 numbers of scans.

The interference fringes obtained at 2 cm^{-1} resolution are shown in Figure 4.3. With reference to Figures 4.3, the quality of the interference fringes was found to be noisy when the EFPI sensor was illuminated using the internal light source of the FTNIR spectrometer. Therefore, an amplified spontaneous emission (ASE) light source was used to illuminate the primary EFPI cavity. This was necessary because the coupling of the light from the internal light source of the FTNIR spectrometer to the single-mode fibre was inadequate; the FTNIR spectrometer was designed to operate with SMA-terminated multi-mode optical fibres.

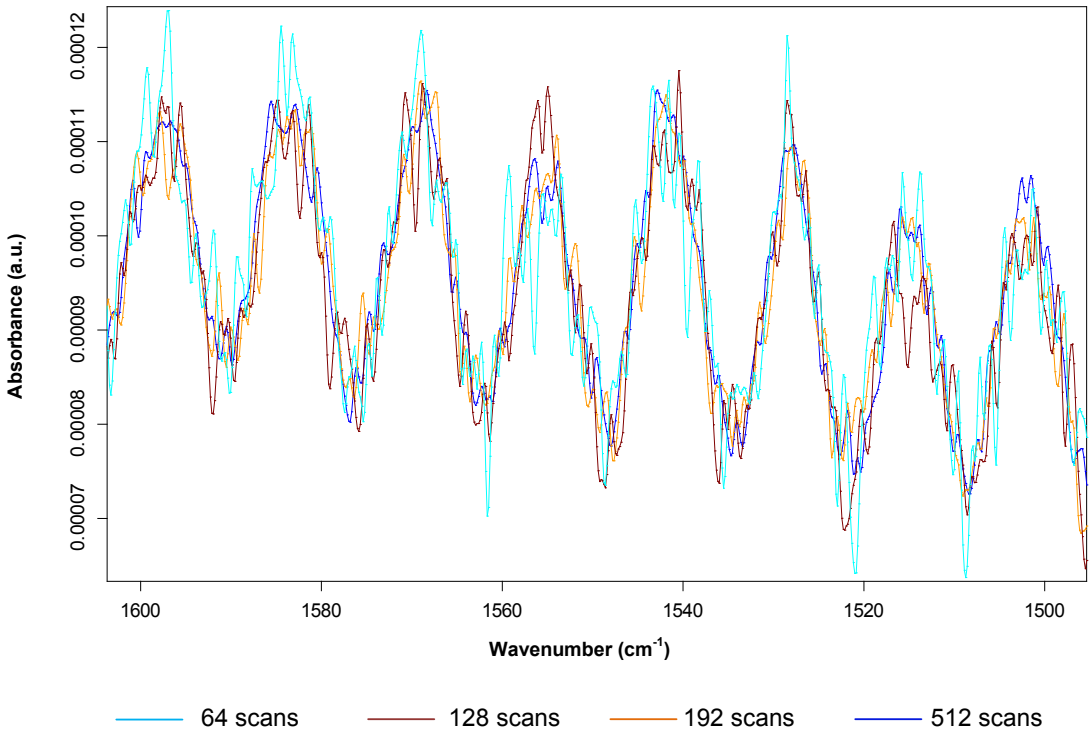

Figure 4.3 Illustration of the quality of the interference fringes obtained from an EFPI sensor that was interrogated using the FTNIR spectrometer at a resolution of 2 cm^{-1} over specified number of scans.

Figure 4.4 shows the interference fringes that were obtained using the external ASE light source. The EFPI cavity length was 100 µm and it was interrogated using a resolution of 1 cm^{-1} over 16 scans.

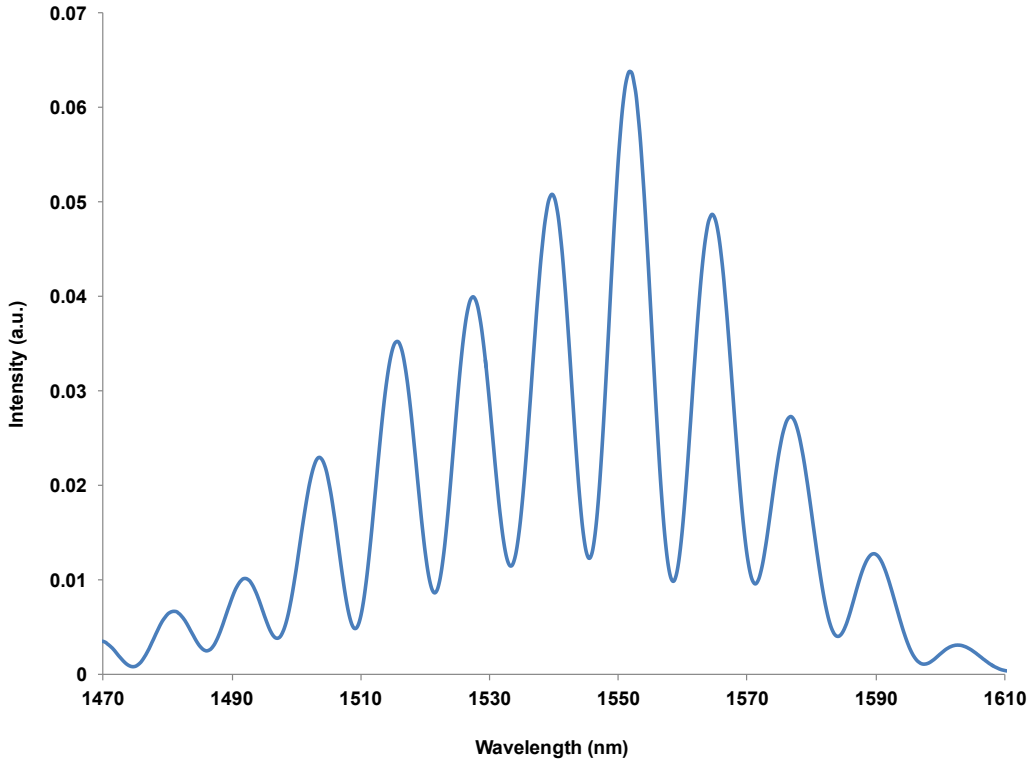

Figure 4.4 Typical interference fringes obtained from an EFPI sensor with a cavity length of 100 μm that was illuminated using an ASE light source and interrogated using the FTNIR spectrometer.

On the basis of the quality of the interference fringes in Figure 4.4, all subsequent MMS were illuminated using the ASE light source and interrogated via the FTNIR spectrometer at a resolution of 1 cm^{-1} and 16 scans.

4.2.2 EFPI/FBG cavity length measurement using the FTNIR spectrometer

The cross-coupling of the signals from the output of the integrated EFPI/FBG sensor was studied. With reference to Figure 4.5, the cross-coupling of the EFPI (interference fringes) and FBG (Bragg reflection) signals is readily apparent. Therefore, special

attention was given to the deconvolution/separation of the EFPI and FBG signals when the multi-measurand sensor was designed. With reference to Figure 3.6, in the MMS design, the FBG was inscribed in close proximity to the cleaved-end of the reflector fibre, and the end-face of the fibre was sputter-coated with Au/Pd. The sensor design and the interrogation scheme illustrated in Figures 3.6 and 3.7 negated the cross-coupling of the reflected light from the EFPI and the FBG signals. This is an advancement of the sensor design used by Liu *et al.* [56] for interrogating an integrated EFPI and FBG sensor. The cavity lengths of the EFPI and the integrated EFPI/FBG sensors were calculated using the Equation 2.5 and the data are presented in Figure 4.6.

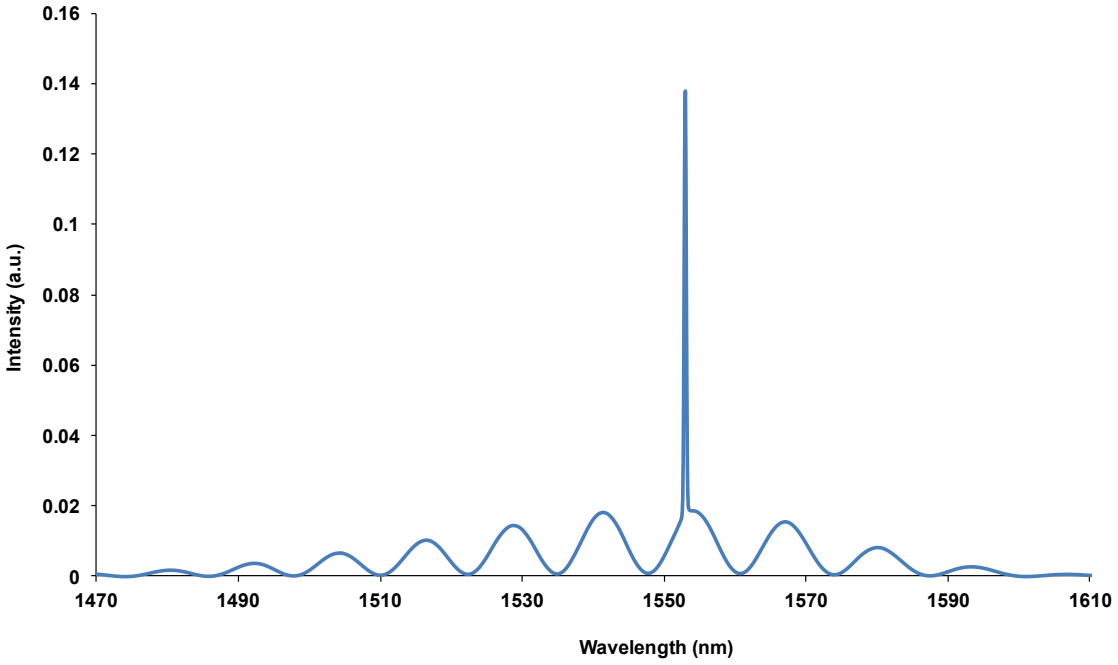

Figure 4.5 Typical output from an integrated EFPI/FBG sensor showing the overlapped interference fringes from the EFPI sensor and the FBG reflection peak. The EFPI cavity length was 100 μm and the integrated EFPI/FBG sensor was interrogated using the FTNIR spectrometer.

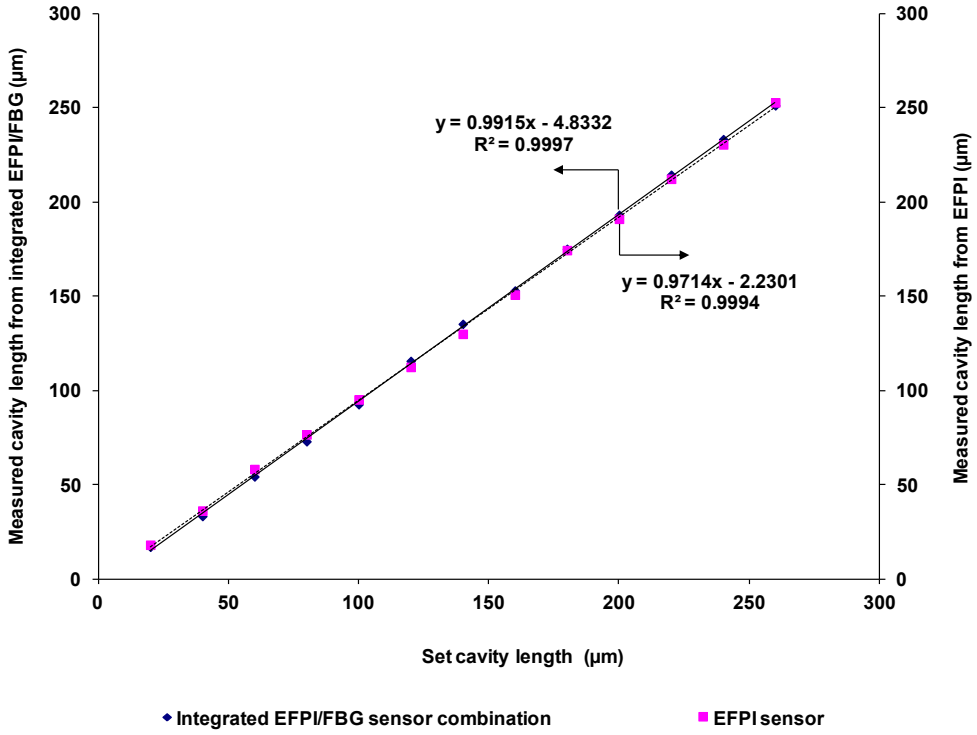

Figure 4.6 Measured versus the set cavity lengths for the EFPI and the integrated EFPI/FBG sensors. The cavity length of the EFPI was varied from 20 to 260 µm.

From Figure 4.6, the variations in the two datasets may be attributed to: (i) the errors in the set cavity lengths (the position accuracy of the BFS-60 fusion splicer was ± 0.1 µm; (ii) the presence of the superimposed Bragg reflection peak on the EFPI interference fringes. These issues were not investigated any further because the focus of the current study was to design the integrated EFPI/FBG sensor such that the output signals from the two devices are physically de-coupled. This was achieved by the interrogation method used for the two sensor systems as shown previously in Figure 3.7.

.

4.2.3 Annealing the Au/Pd coatings

With reference to the integrated EFPI/FBG sensor configuration illustrated in Figure 3.6, the rationale for the reflective coating on the optical fibre with the FBG was to prevent cross-talk between the two sensor signals. However, this dictated the need to ensure that the presence of the reflective coating did not generate any unintentional influence or artifact on the performance of the FBG and the EFPI sensors. Three issues were investigated: (i) the correlation between the reflectivity of the coating on the cleaved optical fibres and temperature cycling; (ii) the effect of the reflective coating on the response of the EFPI output; and (iii) the effect of temperature cycle on the output of the FBG. The information derived here will also apply when considering the mode of operation of the secondary cavity that was created between the coated end-face of the capillary and the cleaved secondary optical fibres (this is discussed in Section 3.4.5).

4.2.3.1 Annealing the Au/Pd coated end-face of cleaved fibre

The effect of the reflectivity of the coating on the cleaved end-face of an optical fibre was investigated from ambient to 180 °C over four heat/cool cycles. The effect of this heating/cooling cycle on the reflectivity of the Au/Pd coated fibres is shown in Figure 4.7. The reflectivity measurements were carried out using the ASE light source and detector on the FTNIR spectrometer where the area under the reflected spectrum between 1450-1600 nm was calculated for the specified temperature cycles. On inspecting Figure 4.7, it can be seen that the reflectivity of cleaved optical fibres increased by approximately 1900% after applying the Au/Pd coating.

After the first heat/cool cycle, the average reflectivity of the coated fibres was increased by approximately 45% when compared to the reflectivity at 30 °C. A possible reason for the observed increase in the reflectivity is the consolidation [106] and/or annealing of the Au/Pd particles in the sputter-coated film. Previous reports on annealing of thin gold films evince that irreversible morphological changes are mainly due to grain mobility and coalescence accompanied by improved adherence to glass substrates [108].

Subjecting the gold films to thermal cycles showed that the first thermal cycle produced permanent modifications to the microstructure [108]. This was said to lead to improved structural stability with repeated thermal cycling. In the current study, the variation in the reflected intensities of the coated fibres after the second, third and fourth temperature cycles from 30 to 180 °C was less than 3%, indicating a stabilisation of the reflectivity of the coating.

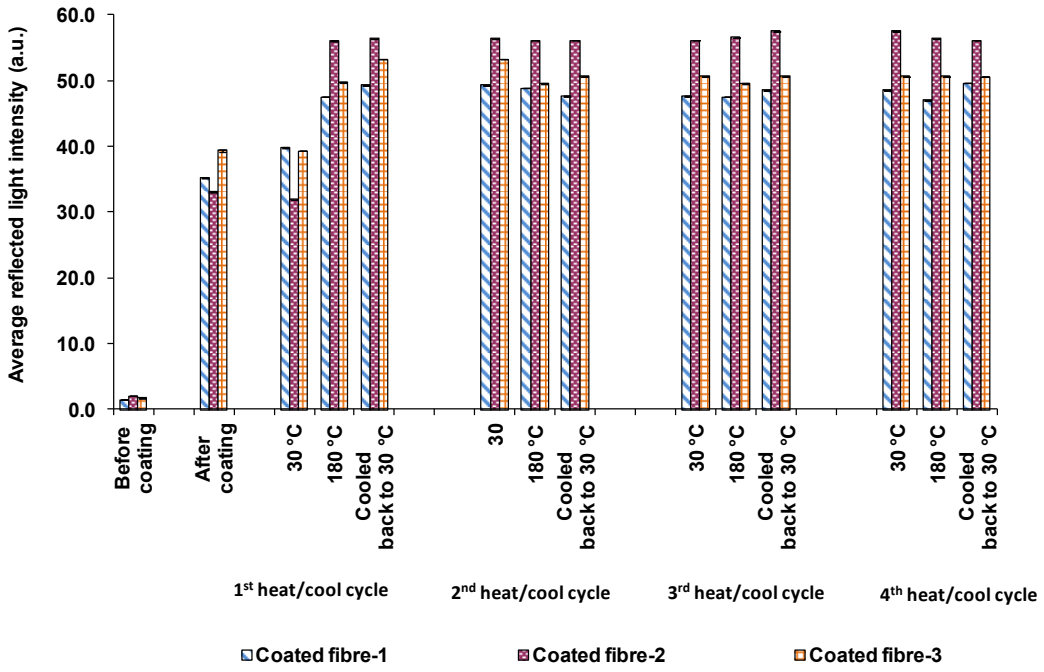

Figure 4.7 Reflectivity of the Au/Pd coating on the cleaved optical fibres as a function of four heating/cooling cycles from 30-180 °C.

4.2.3.2 Annealing the Au/Pd coated end-face of a fibre with an FBG integrated within an EFPI sensor

The effect of the reflective Au/Pd coating on the response of the EFPI output and the temperature sensitivity of the FBG sensors were studied with two interrogation units (FiberPro and FTNIR spectrometer). In general, the temperature sensitivity of the EFPI sensor is relatively low due to: (i) the low thermal expansion of fused silica and the cleaved optical fibres in the capillary (0.55×10^{-6} $^{o}C^{-1}$) [8]; and (ii) the fact that the free-ends of the silica fibres and the capillary undergo thermal expansions in opposite directions [5]. This cancels the effect of thermal expansion of the two components on

the cavity length when the sensor is not embedded in the composite. Given the higher resolution of the FiberPro interrogation unit (1 pm compared to 0.24 nm for the FTNIR spectrometer), the thermally-induced changes in the cavity length of the EFPI can be measured more accurately. The data generated via the FiberPro interrogation unit and the FTNIR are presented in Figures 4.8 and 4.9 respectively where the insensitivity of the reference and coated-EFPI sensors when heated in air is apparent. The standard deviation of the cavity lengths for the reference and coated EFPI sensors over the three heat/cool cycles was found to be less than 0.2 μm and 0.3 μm respectively. The maximum percentage change in the cavity length at 30 ^{o}C for subsequent thermal cycles for the reference and coated EFPIs was less than 0.2% and 0.5% respectively. The cavity lengths of the reference and Au/Pd coated EFPI sensors measured using FiberPro and FTNIR spectrometer over three heating/cooling cycles are summarised in Table 4.1. Assuming the thermal expansion of the capillary and the fibre to be the same, in practice, the cavity length of the reference EFPI sensor may show a small temperature sensitivity when it is heated in air due to one or more of the following reasons: (i) differences (if any) in the thermal expansion of fibre and fused silica capillary; (ii) distortion or deviation from geometrical symmetry in the fusion welds between the fibres and capillary and; (iii) the uniformity (physical and optical) of the sputter-coating and the subsequent annealing and consolidation of Au/Pd coating morphology.

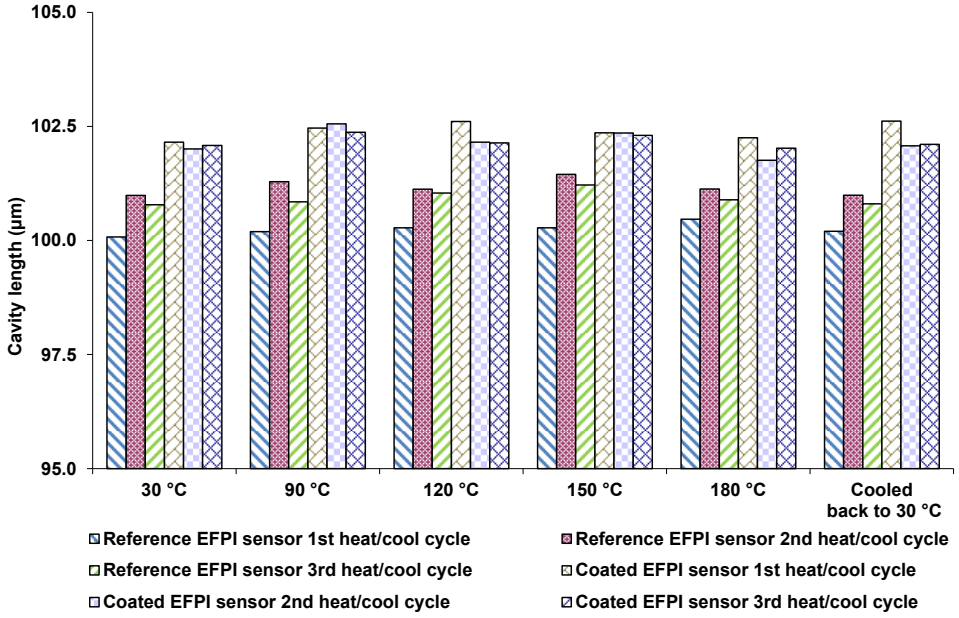

Figure 4.8 Summary of the cavity lengths of the reference and Au/Pd coated EFPI sensors measured using the FiberPro interrogation unit over three heating/cooling cycles.

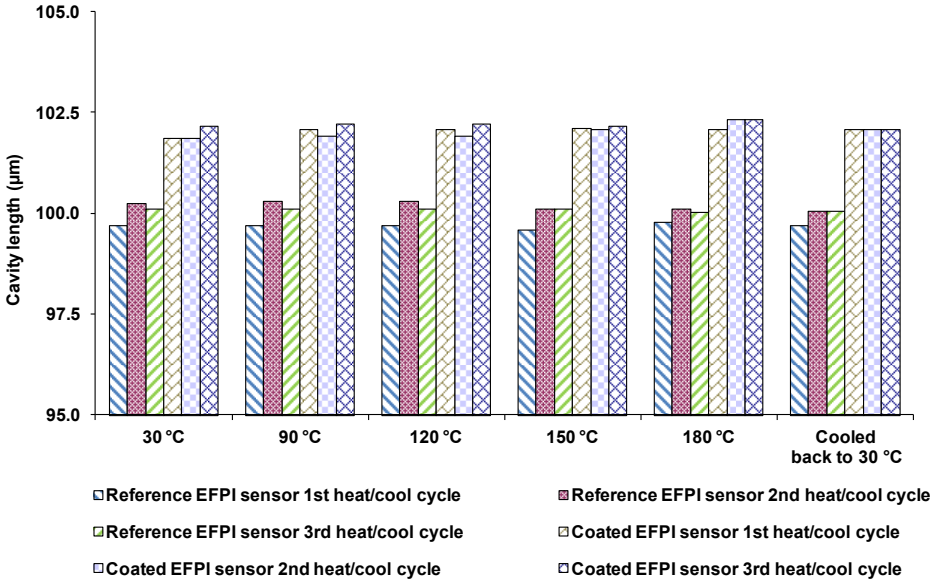

Figure 4.9 Summary of the cavity lengths of the reference and Au/Pd coated EFPI sensors measured using the FTNIR spectrometer over three heating/cooling cycles.

Table 4.1 Summary of the cavity lengths of the reference and Au/Pd coated EFPI sensors measured using FiberPro and FTNIR spectrometer over three heating/cooling cycles.

FiberPro	**Reference EFPI sensor**			**Coated EFPI sensor**		
	1st heat/cool cycle	2nd heat/cool cycle	3rd heat/cool cycle	1st heat/cool cycle	2nd heat/cool cycle	3rd heat/cool cycle
30 °C	100.08	100.99	100.79	102.15	102.01	102.08
90 °C	100.19	101.29	100.85	102.46	102.55	102.37
120 °C	100.28	101.12	101.04	102.61	102.16	102.14
150 °C	100.28	101.45	101.22	102.36	102.36	102.30
180 °C	100.46	101.13	100.89	102.25	101.76	102.02
Cooled back to 30 °C	100.20	100.99	100.80	102.62	102.08	102.11
Average	***100.25***	***101.16***	***100.93***	***102.41***	***102.15***	***102.17***
Standard deviation	***0.13***	***0.18***	***0.17***	***0.19***	***0.28***	***0.14***
Percentage change	***0.12***	***0.00***	***0.02***	***0.45***	***0.07***	***0.02***

FTNIR	**Reference EFPI sensor**			**Coated EFPI sensor**		
	1st heat/cool cycle	2nd heat/cool cycle	3rd heat/cool cycle	1st heat/cool cycle	2nd heat/cool cycle	3rd heat/cool cycle
30 °C	99.71	100.24	100.10	101.86	101.86	102.16
90 °C	99.71	100.30	100.10	102.09	101.92	102.22
120 °C	99.70	100.30	100.10	102.09	101.92	102.22
150 °C	99.59	100.10	100.10	102.10	102.09	102.16
180 °C	99.78	100.10	100.01	102.09	102.33	102.33
Cooled back to 30 °C	99.71	100.05	100.05	102.09	102.09	102.09
Average	***99.70***	***100.18***	***100.08***	***102.05***	***102.03***	***102.20***
Standard deviation	***0.06***	***0.11***	***0.04***	***0.10***	***0.17***	***0.08***
Percentage change	***0.00***	***0.19***	***0.05***	***0.23***	***0.23***	***0.07***

The reflection peak for the reference and the coated FBGs measured using FiberPro showed a negative shift of 0.06 nm and 0.03 nm respectively after annealing and cooling to room temperature (30 °C).

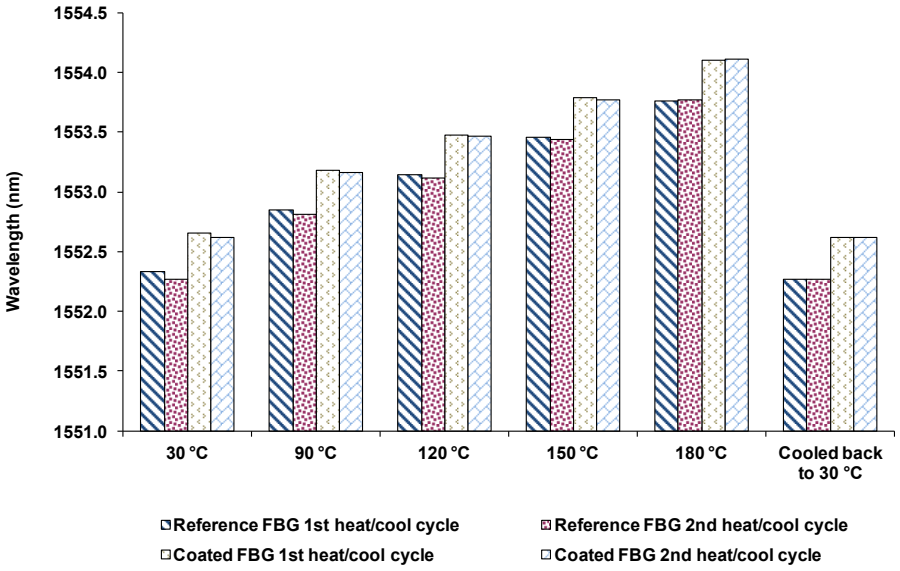

Figure 4.10 Summary of the peak shift of the reference and Au/Pd coated FBG sensors measured using the FiberPro over two heating/cooling cycles.

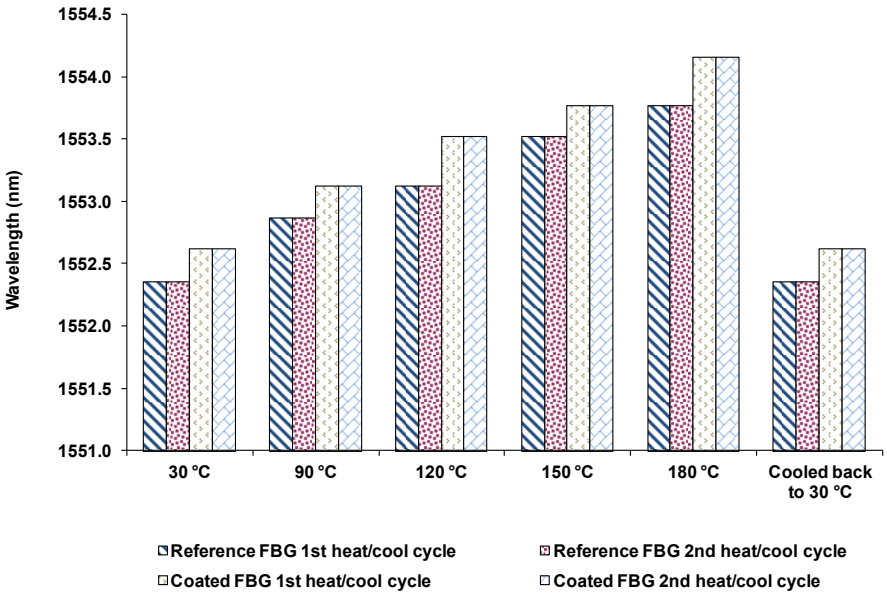

Figure 4.11 Summary of the peak shift of the reference and Au/Pd coated FBG sensors measured using the FTNIR spectrometer over two heating/cooling cycles.

Thermal annealing of type-I Ge-B co-doped fibre gratings is said to lead to a negative shift in the Bragg wavelength accompanied by a drop in the reflectivity. This has been attributed to the decay of the grating structure [57]. The temperature sensitivities of FBGs at a peak wavelength of 1552.3 nm determined using FiberPro during the 1st and 2nd heat/cool cycles for both the reference and coated FBGs were in the range of 9.7-9.9 pm $^{o}C^{-1}$ respectively by considering a linear fit. The data reported in the literature for the temperature sensitivity of type-I Ge-B co-doped optical fibre grating was in the range of 9.19-10.69 pm $^{o}C^{-1}$ [53, 57]. It is reasonable to expect such small discrepancies owing to the differences in the FBG peak wavelengths and non-linearity of peak wavelength versus temperature over a wide temperature range. Accepting the lower wavelength resolution of the FTNIR spectrometer, the corresponding temperature sensitivity for the coated and reference FBG sensors measured via the FTNIR spectrometer were in the range of 9.5-10.2 pm $^{o}C^{-1}$.

4.2.4 Plasma exposure on the FBG sensor

The spectra of the FBG sensor before and after exposure to the plasma of the sputter-coating are shown in Figure 4.12. The FBG sensor was subjected to sputter-coating for nine minutes with the aid of a fibre chuck holder. After the first coating operation, the procedure was repeated after the relative orientation of the optical fibre was rotated by 180°. The coating was then removed manually and the above-mentioned procedure was repeated four times. The effect of the coating on the Bragg reflection peak was in the range 0.03-0.05 nm. Typical Bragg reflection peaks before and after exposure is shown in Figure 4.12. The manual cleaning of the Au/Pd coating did not cause any shifts in

the Bragg peak reflections. It can be concluded that the sputter-coating process, to create the reflective coating on the cleaved fibre end-face, did not cause any distortions on the Bragg signal.

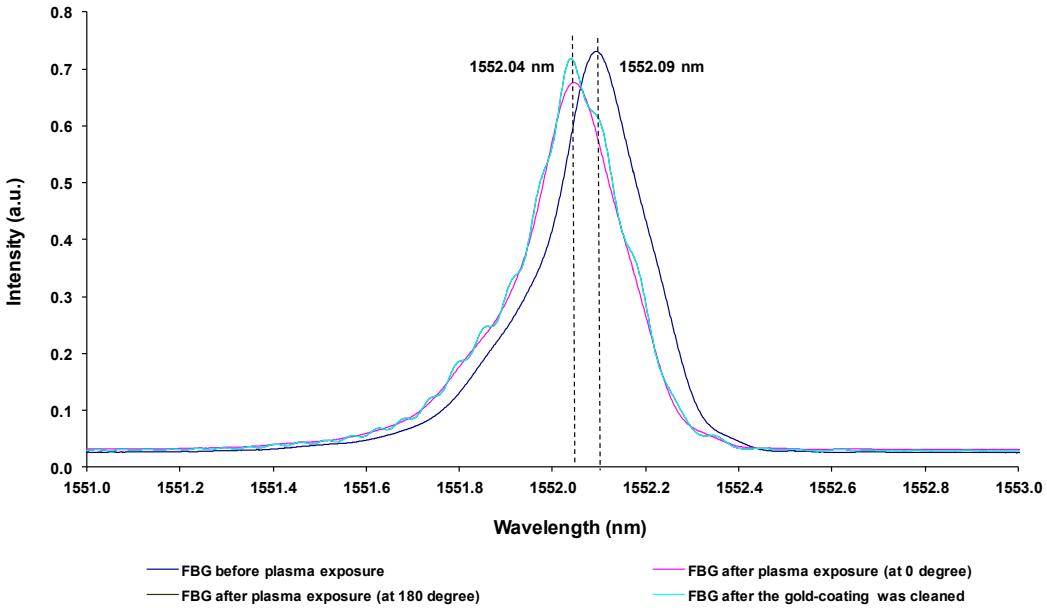

Figure 4.12 FBG peak wavelengths before and after exposed to the plasma of the sputter-coater.

4.2.5 Effect of the clamping stress on the response of the FBG sensor

The effect of the clamping stress exerted by the magnetic clamps of the micro-translation stage during the fabrication of FBG sensor is shown in Figure 4.13. From Figure 4.13, a negative peak shift of 0.07 nm was observed when the magnetic clamps were removed after the fabrication of the sensor. This was expected, as an appropriate clamping stress is required to establish good contact and alignment of the optical fibre

with the phase-mask during the fabrication of the sensor. Placing the Bragg grating sensor on a flat aluminium plate did not indicate any shift in the Bragg reflection peak. The experiments were repeated a further four times and the mean FBG peak wavelength is summarised in Table 4.2.

Table 4.2 Summary of the FBG peak wavelengths with and without clamping stress exerted by the micro-translation stage during the fabrication of the sensor.

	Mean peak wavelength (nm)	Standard deviation
FBG with clamping stress	1552.15	0.0235
FBG without clamping stress	1552.07	0.0055
FBG without stress on a flat-aluminium plate	1552.07	0

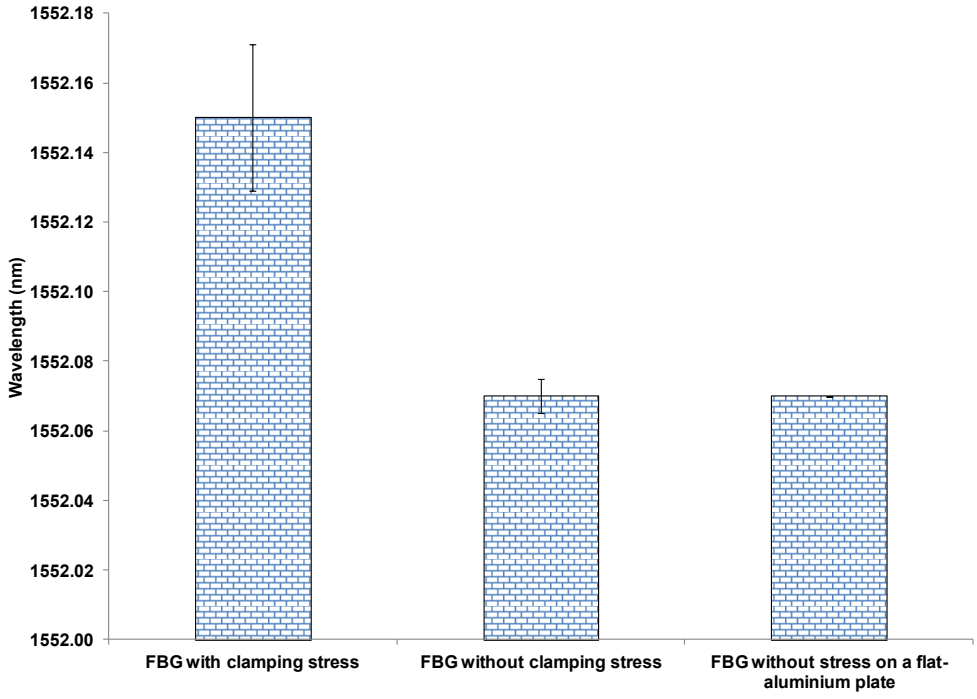

Figure 4.13 FBG peak wavelength shift with and without the clamping stress exerted by the magnetic clamps of the translation stage during the fabrication of the sensor.

4.2.6 Secondary fibre alignment on the translation stage

The alignment of the secondary fibres with the Au/Pd coated end-face of the EFPI sensor was checked before the fabrication of the chemical sensor. The cavity length between the Au/Pd coated end-face of the capillary and the cleaved end-faces of the secondary fibres were varied in increments of 100 µm to a maximum of 500 µm and the interference fringes were interrogated using the OSA. The interference fringes obtained at defined cavity lengths are shown in Figure 4.14. With reference to Figure 4.14, the quality of the interference fringes up to a distance of 500 µm is readily apparent and this confirms the acceptable alignment of the secondary fibres.

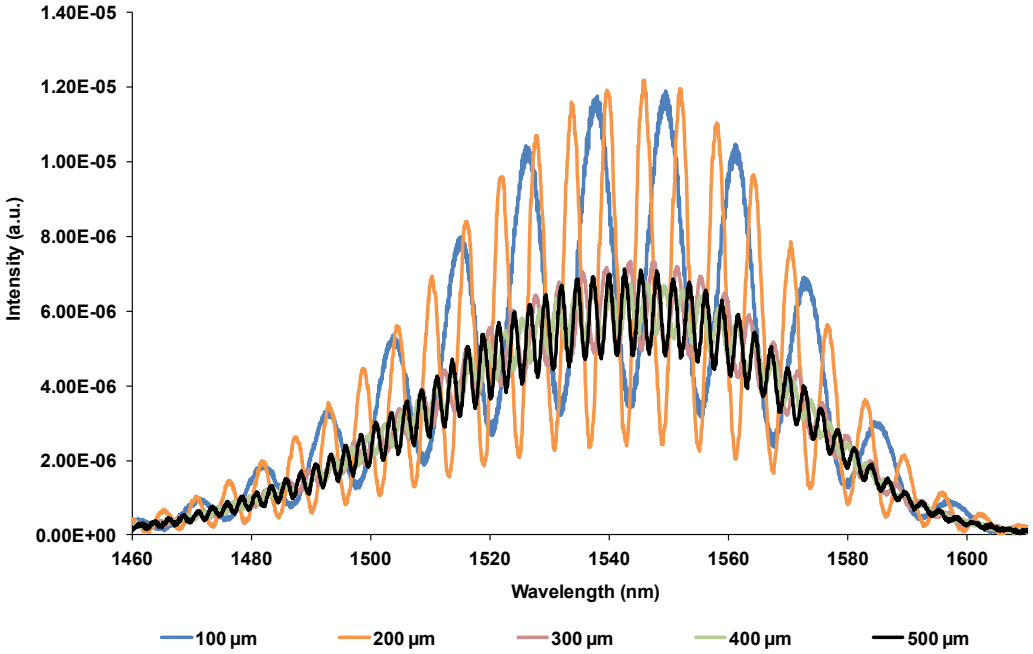

Figure 4.14 The quality of the interference fringes obtained at different set cavity lengths between the Au/Pd coated end-face of the capillary and the cleaved secondary fibres.

4.3 Process monitoring of composite laminates

4.3.1 Verification of temperature within the CFRP laminate

Figure 4.15 shows the autoclave temperature obtained via the in-built thermocouple, the temperatures measured by six independent thermocouples and the pressure cycle as a function of the processing time. Thermocouples-1, 2 and 3 were embedded in the mid-plane of an eight-ply CFRP laminate; the other three thermocouples (4-6) were placed on the vacuum bag, under the vacuum bag and on the tooling plate, respectively. It is apparent that the temperature profiles obtained from the embedded thermocouples are similar. However, a thermal lag is observed between the embedded thermocouples and that recorded by the in-built thermocouple in the autoclave. The rate of heating experienced by the laminate is approximately 1 °C/minute whereas that recorded by the autoclave is 2 °C/minute. An enlarged view of the temperature and pressure profile of the laminate during the heating phase is shown in Figure 4.16. With reference to Figure 4.16, as expected, the temperature profile of the surface-mounted thermocouples showed a faster response than the embedded thermocouples. The set isothermal temperature in the autoclave is attained after 54 minutes whereas the embedded thermocouples indicate that the desired temperature is achieved after 117 minutes. Moreover, the maximum temperature recorded by the embedded thermocouple in the middle of the laminate is 122 °C; this is most likely due to the exotherm as a consequence of the cross-linking reactions of the resin system. The cure schedule is programmed on the basis of the temperature obtained from the thermocouples that were embedded in the preform and not that recorded by the autoclave. Inspecting the data

from the embedded thermocouples, it is seen that the laminate was above the desired isothermal temperature for 60 minutes. After this period, the pressure was released from 0.48 to 0.007 MPa and the heating was terminated. The composite was then allowed to cool to 30 °C.

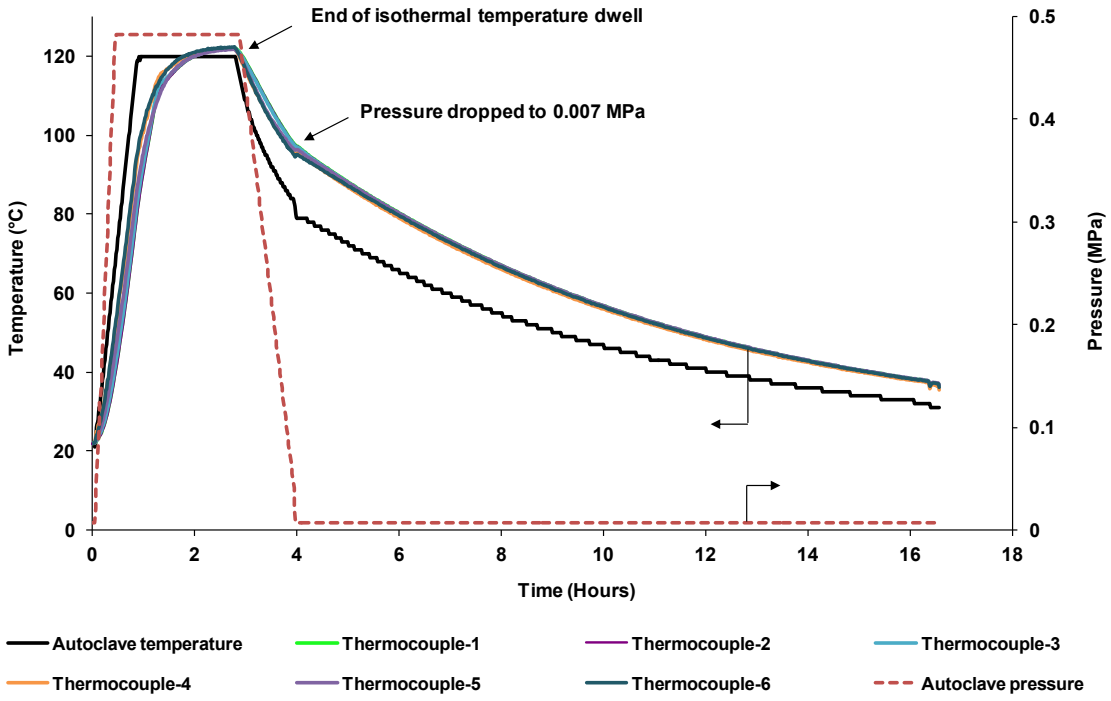

Figure 4.15 Temperature and pressure profile during the autoclave-based processing of the eight-ply unidirectional CFRP laminate. Thermocouples 1-3 were embedded in the mid-plane of the laminate; thermocouples 4-6 were placed on the vacuum bag, under the vacuum bag and on the tooling plate, respectively.

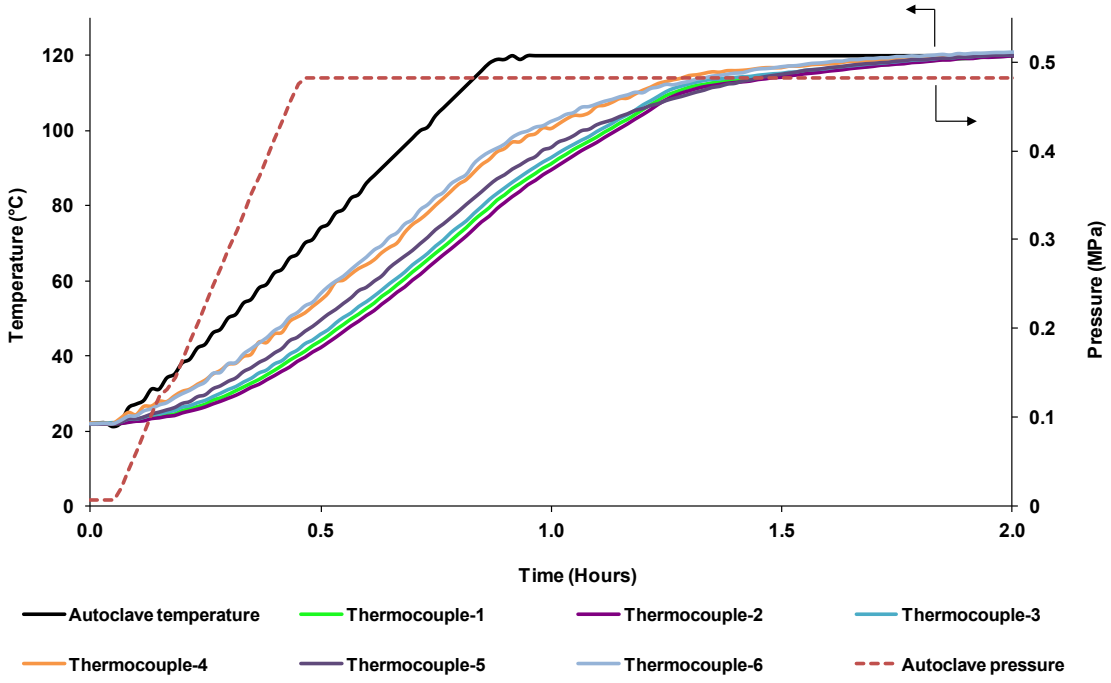

Figure 4.16 Temperature and pressure profile of the eight-ply unidirectional CFRP laminate during the heating phase of the cross-linking cycle. Thermocouples 1-3 were embedded in the mid-plane of the laminate; thermocouples 4-6 were placed on the vacuum bag, under the vacuum bag and on the tooling plate, respectively.

From Figure 4.16, the maximum deviation between the embedded thermocouples during the heating phase was ± 2 °C. It can be concluded that the data from the embedded thermocouples provide a better means of tracking the temperature within the preform during processing.

4.4 Process monitoring of a CFRP laminate using multiplexed FBG sensors

4.4.1 FBG sensors during embedding and after curing in a CFRP laminate

Prior to embedding the FBGs in the CFRP laminate, the annealing of the sensors was considered. Six independent optical fibres with three wavelength-specific Bragg gratings each were used in this experiment. The relative positions of the strain and temperature sensors were shown previously in Figure 3.18. The sensors were annealed in an air-circulating oven at 150 °C for 12 hours. A typical spectrum obtained from one of the optical fibres with three multiplexed FBG sensors before and after annealing is shown in Figure 4.17a. The FBG peak wavelengths measured at room temperature after annealing showed a negative deviation ranging from 0.07 to 0.12 nm. This is consistent with the results presented and discussed in Section 4.2.3.2. After the annealing procedure, the sensors were embedded in the mid-plane of an eight-ply unidirectional CFRP laminate (See Section 3.7.2). A typical spectrum of one of the optical fibres with three FBGs at different stages of processing is shown in Figure 4.17b. A summary of the output of fifteen strain sensors and three temperature sensors at different stages of processing are presented in Table 4.3 and Figures 4.18 to 4.21. A total of five measurements were taken at each stage of processing. The FBG peak wavelength at a single stage of operation did not change for the repeat measurements and therefore, standard deviations cannot be reported.

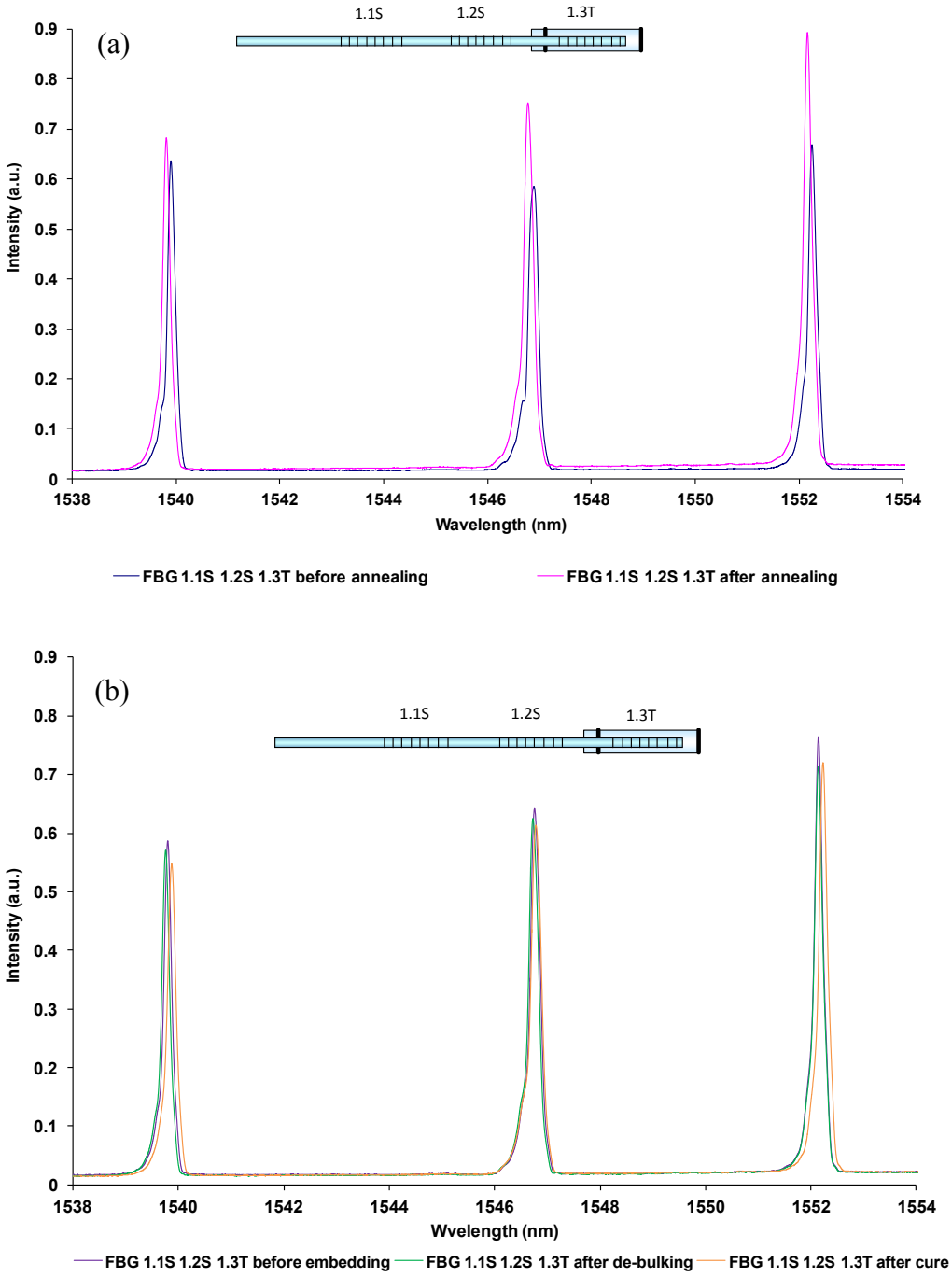

Figures 4.17 (a and b) Multiplexed FBG spectrum (a) before and after annealing, and (b) at different stages of processing. 'S' and 'T' denote strain and temperature sensors respectively.

Table 4.3 Summary of the FBG peak wavelength shifts during different stages of processing. 'S' and 'T' in the sensor type denote strain and temperature sensors, respectively.

Sensor number	Sensor type	Before annealing (nm) (A)	After annealing (nm) (B)	*Difference (B) - (A) (nm)*	Before embedding (nm) (C)	After de-bulking (nm) (D)	*Difference (D) - (C) (nm)*	After curing (nm)
1	FBG 1.1S	1539.89	1539.80	*-0.09*	1539.78	1539.74	*-0.04*	1539.86
2	FBG 2.1S	1539.91	1539.82	*-0.09*	1539.79	1539.78	*-0.01*	1539.82
3	FBG 3.1S	1539.90	1539.81	*-0.09*	1539.76	1539.73	*-0.03*	1539.78
4	FBG 4.1S	1539.86	1539.76	*-0.10*	1539.73	1539.75	*0.02*	1539.90
5	FBG 5.1S	1539.96	1539.84	*-0.12*	1539.82	1539.85	*0.03*	1540.00
6	FBG 6.1S	1539.95	1539.83	*-0.12*	1539.92	1539.98	*0.06*	1540.17
7	FBG 1.2S	1546.89	1546.78	*-0.11*	1546.74	1546.72	*-0.02*	1546.77
8	FBG 2.2S	1546.88	1546.77	*-0.11*	1546.74	1546.73	*-0.01*	1546.85
9	FBG 3.2S	1546.88	1546.76	*-0.12*	1546.73	1546.71	*-0.02*	1546.73
10	FBG 4.2S	1546.87	1546.77	*-0.10*	1546.75	1546.78	*0.03*	1546.91
11	FBG 5.2S	1546.92	1546.82	*-0.10*	1546.80	1546.82	*0.03*	1546.92
12	FBG 6.2S	1546.88	1546.78	*-0.11*	1546.83	1546.90	*0.07*	1547.00
13	FBG 2.3S	1552.16	1552.08	*-0.08*	1552.05	1552.02	*-0.03*	1552.21
14	FBG 4.3S	1552.26	1552.19	*-0.07*	1552.16	1552.16	*0.00*	1552.32
15	FBG 5.3S	1552.23	1552.15	*-0.08*	1552.11	1552.11	*0.00*	1552.25
16	FBG 1.3T	1552.24	1552.16	*-0.08*	1552.13	1552.14	*0.01*	1552.23
17	FBG 3.3T	1552.30	1552.23	*-0.07*	1552.19	1552.19	*0.00*	1552.24
18	FBG 6.3T	1552.20	1552.12	*-0.08*	1552.08	1552.08	*0.00*	1552.13

It is also apparent from Table 4.3 that vacuum bagging and vacuum de-bulking had negligible effect on the output of the FBG sensors.

As seen in Table 4.3, the peak wavelengths of FBG strain sensors 1-3 showed a negative deviation whereas 4-6 showed a positive deviation before and after embedding. The observed variation from -0.01 nm to 0.07 nm suggests that the embedded sensors were not loaded uniformly. This wavelength variation translates to a strain range of -50 to 60 με. This may be attributed to one or more of the following: (i) the location of the vacuum inlet port where sensors 1-3 were in close proximity; (ii) the difference in the compaction of the laminates in relation to the vacuum port; and (iii) variability in the reinforcing fibre volume fraction, in the vicinity of the embedded optical fibres, and its ease of embedment between the two plies. The data presented in Table 4.3 are shown graphically in Figures 4.19 to 4.22. The variation in the distribution of strain within a laminate, using multiple gratings, was also reported by Liu *et al.* [61].

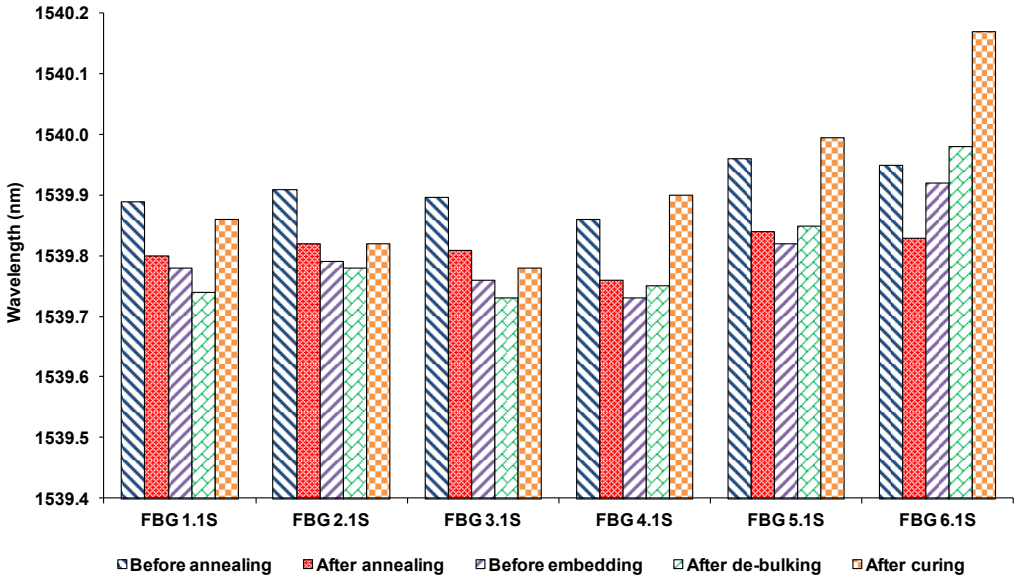

Figure 4.18 Peak wavelength shifts of 1539.80 nm FBG strain sensors during different stages of processing of the CFRP laminate. 'S' denotes strain sensors.

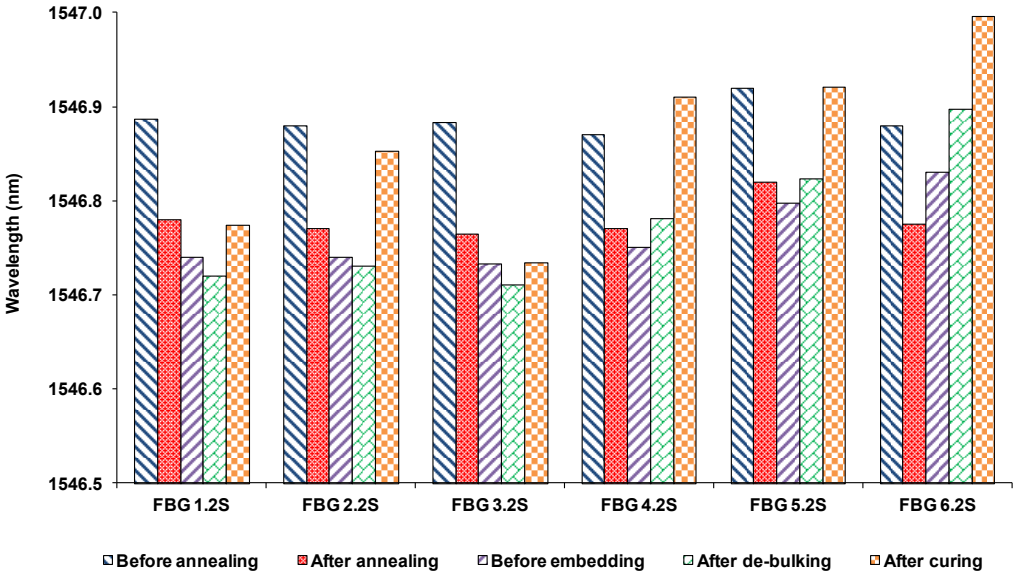

Figure 4.19 Peak wavelength shifts of 1546.80 nm FBG strain sensors during different stages of processing of the CFRP laminate. 'S' denotes strain sensors.

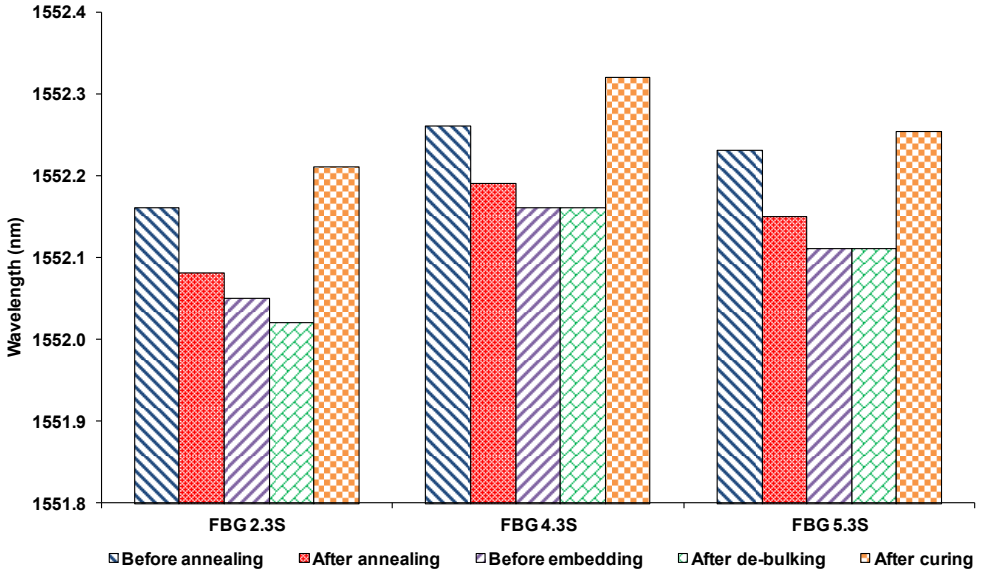

Figure 4.20 Peak wavelength shifts of 1552.20 nm FBG strain sensors during different stages of processing of the CFRP laminate. 'S' denotes strain sensors.

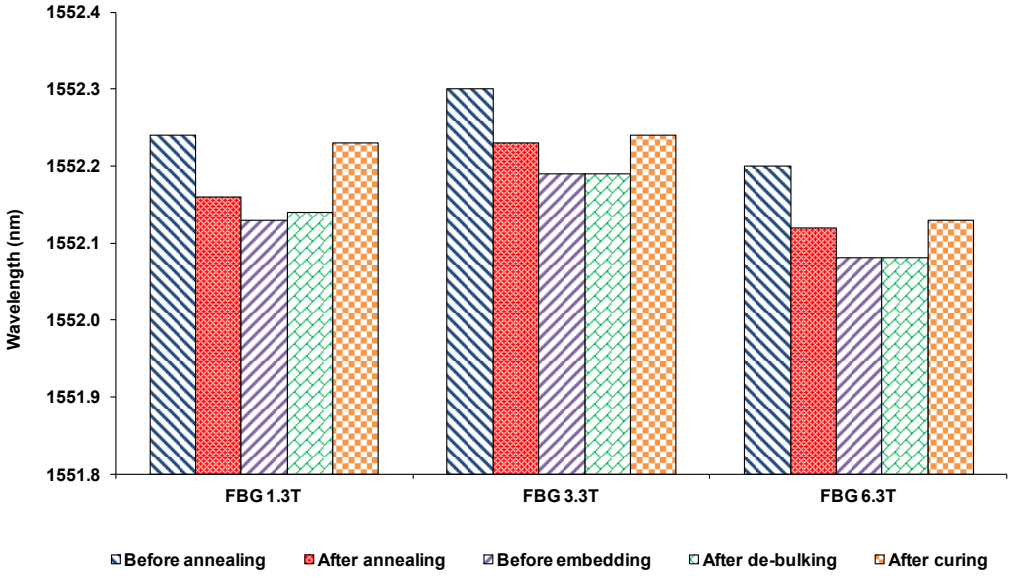

Figure 4.21 Peak wavelength shifts of 1552.20 nm FBG temperature sensors during different stages of processing of the CFRP laminate. 'T' denotes temperature sensors.

4.4.2 Real-time process monitoring of a CFRP laminate

The temperature and pressure during the processing of the eight-ply unidirectional CFRP laminate is shown in Figure 4.22. With reference to Figure 4.22, the embedded thermocouples indicate that the desired temperature (120 °C) is achieved after 108 minutes. The maximum temperature recorded by the embedded thermocouple at the middle of the laminate is 122 °C. The laminate was above the desired isothermal dwell period for 60 minutes; after this, the pressure was released to 0.007 MPa and the heating was terminated. The composite was then allowed to cool to 30 °C prior to removal from the autoclave.

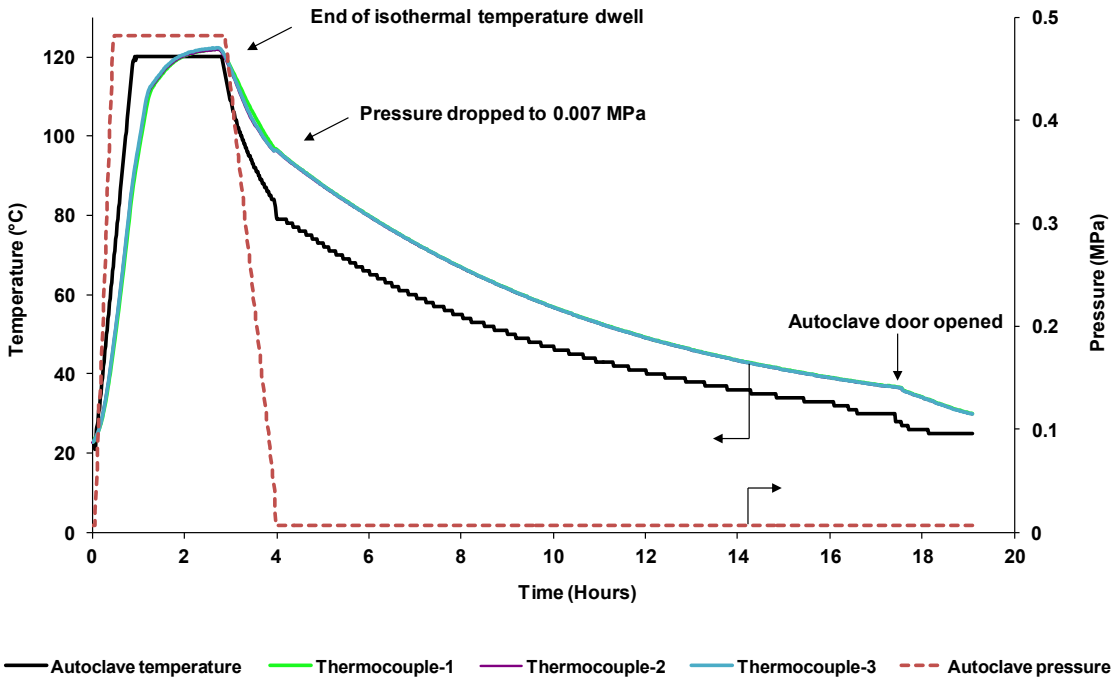

Figure 4.22 Temperature and pressure during the processing of the eight-ply unidirectional CFRP laminate with embedded multiplexed FBG sensors.

The influence of strain and temperature on the FBG sensors was calculated using Equation 2.9. The strain was de-coupled from temperature using the capillary-sealed FBG temperature sensors. The evolution of the strain measured using fifteen FBG strain sensors during the processing of the unidirectional CFRP laminate is presented in Figure 4.23. The development of strain in the laminate during heating from ambient to 120 °C is shown in Figure 4.24.

Due to embedding and vacuum de-bulking, an initial strain was recorded by the sensors at the start of processing. The strain measured at different stages of processing are summarised in Table 4.4.

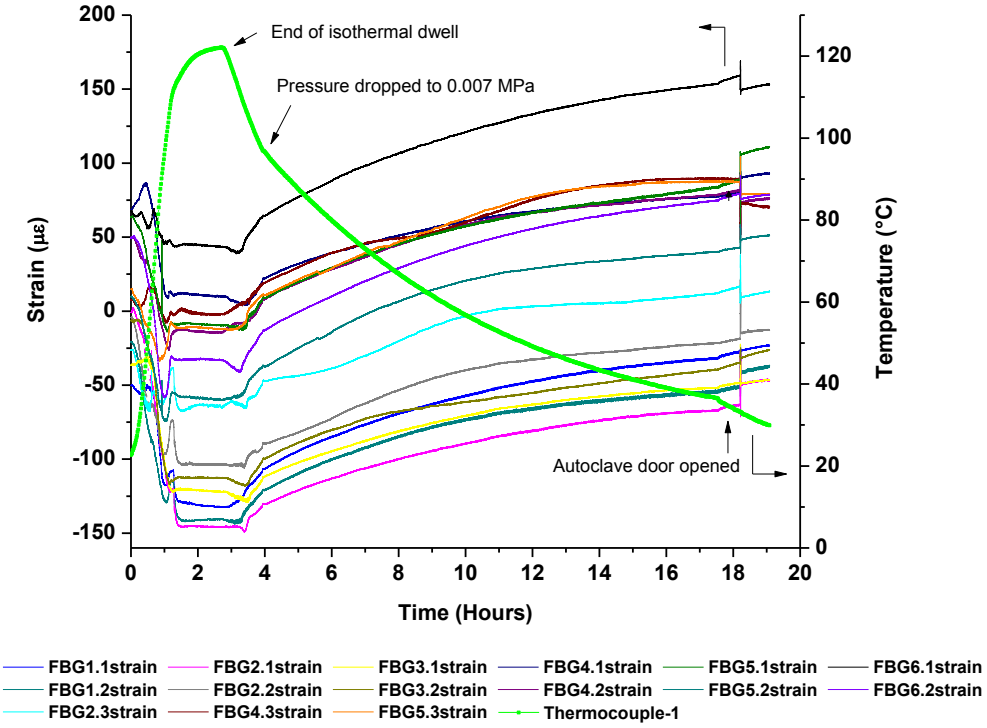

Figure 4.23 The evolution of strain during the processing of the eight-ply unidirectional CFRP laminate.

With reference to Figure 4.24, the graph has been divided into zones (a), (b), (c), (d) and (e). In zone (a), the variation of the strain recorded by each sensor is different and this may have been due to the "nesting" of the sensors within the preform during the vacuum bagging, and when the temperature was increased. During this period, the viscosity of the resin decreases, thus possibly permitting some movement of the optical fibres. In zone (b), the temperature within the preform was increased from 30 to 70 °C. Eight of the fifteen sensors recorded a compressive strain, three showed the development of tensile strain, one showed minimal change and the remaining had components of tensile and compressive strain. This demonstrates that it is difficult to

control the relative orientation of the sensors within the preform during processing. However, this variation may also have been due to localised variations in the fibre volume fraction and heat transfer characteristics within the locality of the sensors. Cross-linking of the resin is unlikely to have been a contributing factor because the DSC data, discussed later in Figure 4.26 shows the onset of the cross-linking commences at approximately 110 °C. Zone (c) represents the temperature range from 70 to 100 °C. The major feature observed in zone (c) for all the sensors was the development of a decrease in the strain values followed by equilibrium up to the end of zone (c). The temperature data recorded by the thermocouple also shows a change in the slope in zone (c). It is speculated that this may be part responsible for the levelling off of the strain data. In zone (d), a positive slope is recorded by the majority of the sensors followed by a levelling off period and some of the sensors showed a decrease in strain. Once again, a temperature profile measured by the thermocouple showed a change in slope. Zone (e) represents the region leading up to the isothermal dwell.

A Further study was undertaken to understand the reasons for the observed decrease in the strain recorded by the FBGs in zone (c). As mentioned previously, the temperature was increasing and therefore, the expectation was that the FBG should record a positive strain. It is proposed that the decrease in the strain recorded by the FBG may have been caused by exceeding the glass transition temperature (Tg) of the acrylate-coating on the optical fibre. In another words, as the Tg is approached, the stiffness of the coating will decrease. This in turn, will lead to a loss of coupling or strain transfer from the matrix to the optical fibre through the acrylate coating. In order to verify this hypothesis, the

acrylate coating was extracted from the optical fibre and the Tg was evaluated using a differential scanning calorimeter.

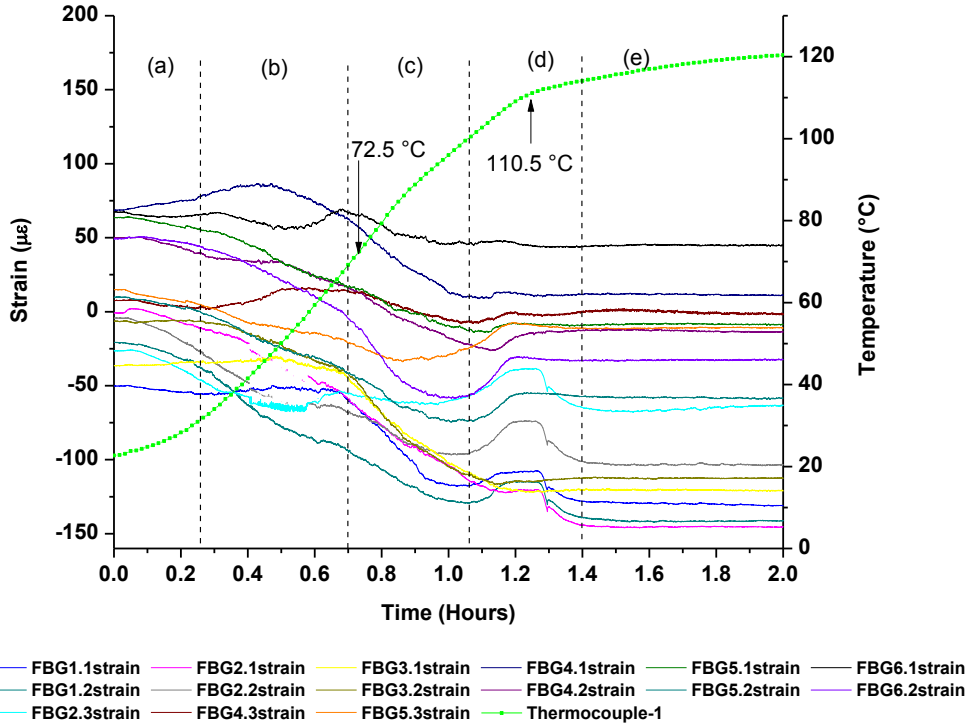

Figure 4.24 The evolution of strain recorded by the FBGs at the mid-ply of an eight-ply CFRP laminate during heating from ambient to 120 °C.

A typical thermogram of the acrylate coating measured via the DSC is presented in Figure 4.25. The sample was heated from 30-200 °C at a heating rate of 20 °C min^{-1}. The average Tg of the acrylate coating was found to be 78.6 ± 0.9 °C. This represents an average of four experiments. Since the heating rate in the autoclave was 2 °C/minute, further DSC experiments were carried out at heating rates corresponding to 5 and 10 °C min^{-1}. The average Tg values at these heating rates were approximately 58.10 and 72.80

°C respectively. Therefore, it concluded that the decrease in strain data in zone (c) is primarily caused by the Tg of the acrylate coating being exceeded. Further studies were undertaken to investigate the strain anomalies of acrylate-coated FBG sensors and this is discussed in Section 4.7.

A thermogram of the VTM 264 resin system is shown in Figure 4.26 where it is seen that the onset of cross-linking commences at 110 °C with a peak at 125.3 °C. Therefore, the cross-linking of the resin system may not have contributed to the observed decrease in the Bragg data shown in Figure 4.24 in zone (c).

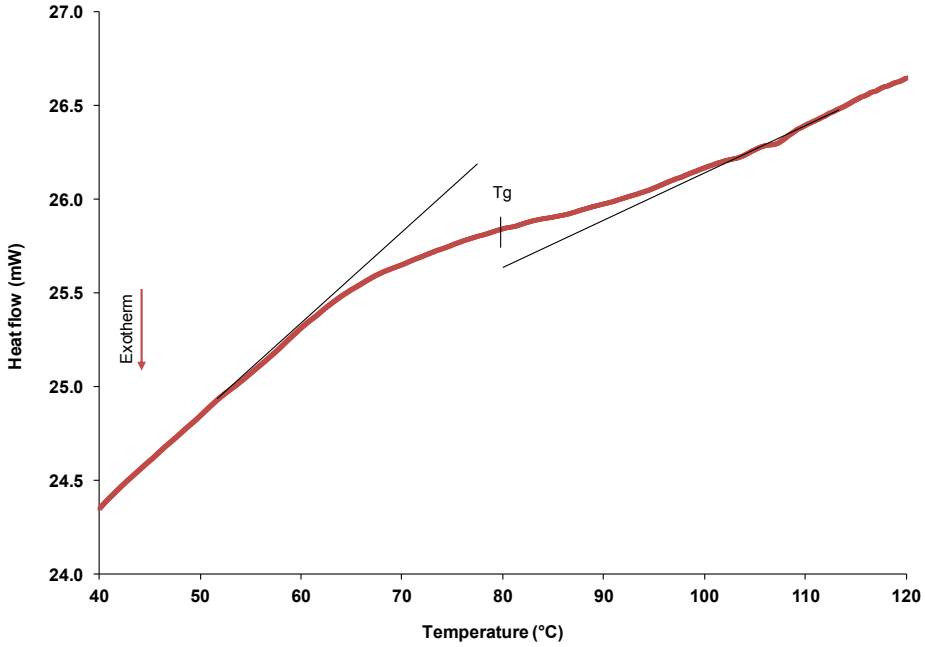

Figure 4.25 A typical thermogram of the acrylate coating on the optical fibre measured via DSC.

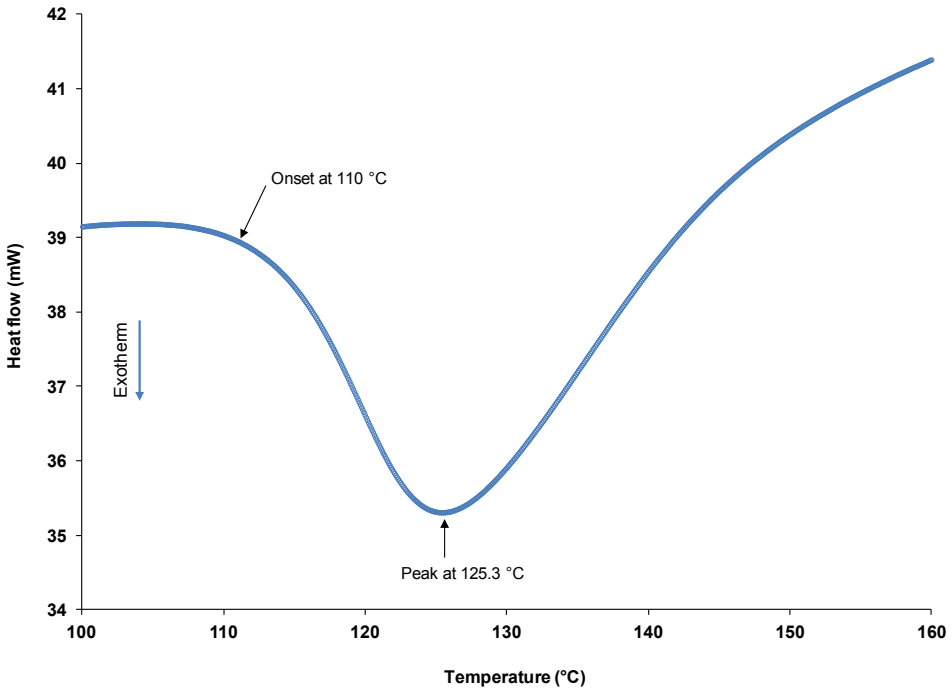

Figure 4.26 DSC thermogram of the VTM 264 resin system obtained by a dynamic heating experiment at 5 °C min^{-1}.

Considering Figure 4.23, as expected, an increase in the FBG strain was observed during the cooling phase. This was mainly due to the combined effects of thermally-induced contraction, the thermal expansion mismatch between the unidirectional carbon fibres and the epoxy resin, laminate/tool interactions. The residual fabrication strain recorded at 30 °C is summarised in Table 4.4. From Table 4.4, it is apparent that the final residual strain values at different locations in the mid-plane of an eight-ply CFRP laminate are different. Possible reasons for this variability in the FBG strain data within the mid-ply of a UD composite was discussed previously. A summary of the residual strain data reported by other researchers are presented in Appendix B. The residual strain range reported was in the range -300 to 313 με [8, 26, 45, 46, 50, 53, 55].

Table 4.4 Summary of the measured strain values at various stages of processing of the CFRP laminate in the autoclave.

Sensor number	Sensor type	Before embedding (με)	After de-bulking (με)	Maximum at zone (c) at 72.5 °C (με)	Maximum at zone (d) at 110.5 °C (με)	End of isothermal dwell at 120 °C (με)	Residual strain at 30 °C (με)
1	FBG 1.1S	0.00	-50.35	-66.44	-108.16	-132.12	-23.14
2	FBG 2.1S	0.00	-0.98	-66.03	-120.90	-145.66	-46.79
3	FBG 3.1S	0.00	-36.56	-52.70	-122.17	-122.15	-46.56
4	FBG 4.1S	0.00	68.60	56.64	11.31	9.76	92.91
5	FBG 5.1S	0.00	63.58	14.49	-8.36	-9.85	111.07
6	FBG 6.1S	0.00	67.15	64.59	45.21	43.05	153.19
7	FBG 1.2S	0.00	-20.94	-98.38	-114.95	-140.85	-36.73
8	FBG 2.2S	0.00	-4.19	-70.61	-73.84	-103.47	-12.86
9	FBG 3.2S	0.00	-6.56	-49.44	-114.35	-112.81	-26.19
10	FBG 4.2S	0.00	49.97	12.48	-14.97	-12.68	76.25
11	FBG 5.2S	0.00	9.87	-46.04	-54.85	-59.45	51.23
12	FBG 6.2S	0.00	49.32	-12.15	-30.91	-34.27	78.82
13	FBG 2.3S	0.00	-26.43	-56.90	-38.63	-63.32	13.39
14	FBG 4.3S	0.00	7.52	12.81	-1.64	-1.47	70.29
15	FBG 5.3S	0.00	14.87	-23.62	-8.26	-12.48	78.64

This therefore highlights the difficulty in comparing strain data from other published sources. Moreover, this study has demonstrated that even if due care and attention is paid to the embedment process and the alignment of the optical fibres within the preform, it is difficult to control the subsequent movement or strain field (reinforcing

fibre distribution) within the vicinity of the sensor. This study has also enabled the decoupling of strain and temperature data by using multiple FBG temperature sensors.

The responses of the embedded FBG temperature sensors that were housed within the capillary and three K-type thermocouples are presented in Figure 4.27. Good correlation is observed between the two independent devices for monitoring the temperature.

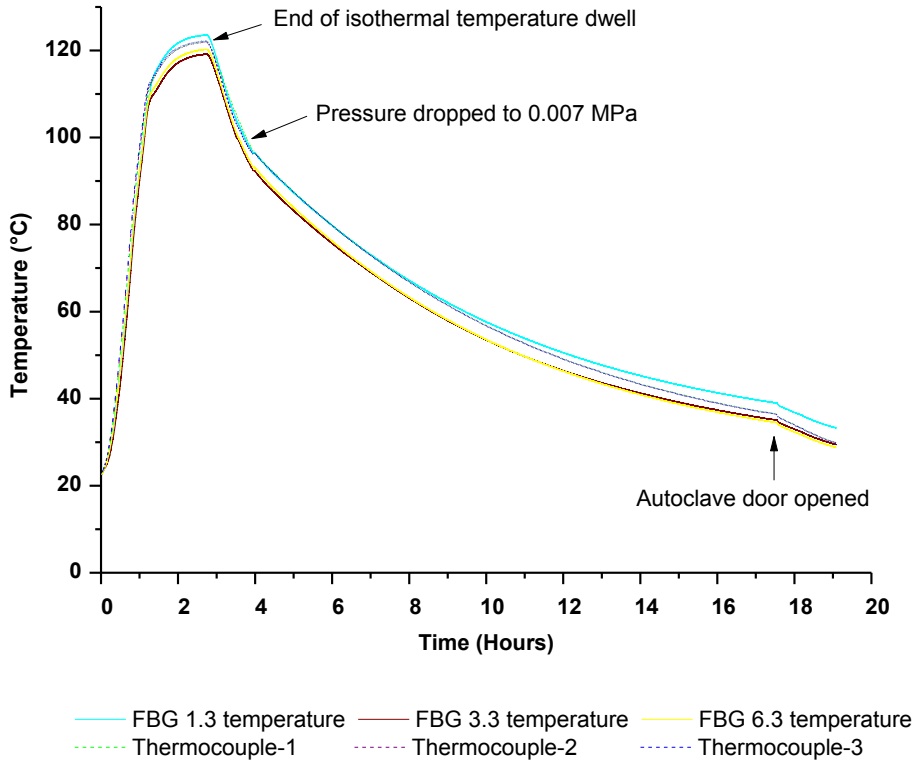

Figure 4.27 Responses of the embedded FBG temperature sensors and thermocouples during the processing of the eight-ply unidirectional CFRP laminate.

4.5 Process monitoring of CFRP laminate using FBGs and Fresnel sensors

In the previous section, the strain and temperature profile in the mid-ply of a unidirectional eight ply laminate was discussed. The current section is concerned with the deployment of FBG and Fresnel sensors in a different CFRP laminate, in between plies 1-2, 4-5 and 7-8. These sensors, in relation to their spatial position within the preform can be compared with sensors FBG 3.2S and FBG 4.2S in Section 4.4.

4.5.1 Temperature and pressure in the autoclave

The temperature and pressure within the laminate during the cross-linking cycle is presented in Figure 4.28.

With reference to Figure 4.28, the embedded thermocouples indicate that the laminate achieved the desired temperature after 120 minutes. The maximum temperature recorded by the embedded thermocouple at the middle of the laminate is 121.5 °C. The laminate was above the desired isothermal dwell period for 60 minutes; after this, the pressure was released to 0.007 MPa and the heating was terminated. The composite was then allowed to cool to 30 °C. The temperature profiles of the thermocouples positioned between the 1st and 2nd plies, 4th and 5th plies, and 7th and 8th plies were found to be similar.

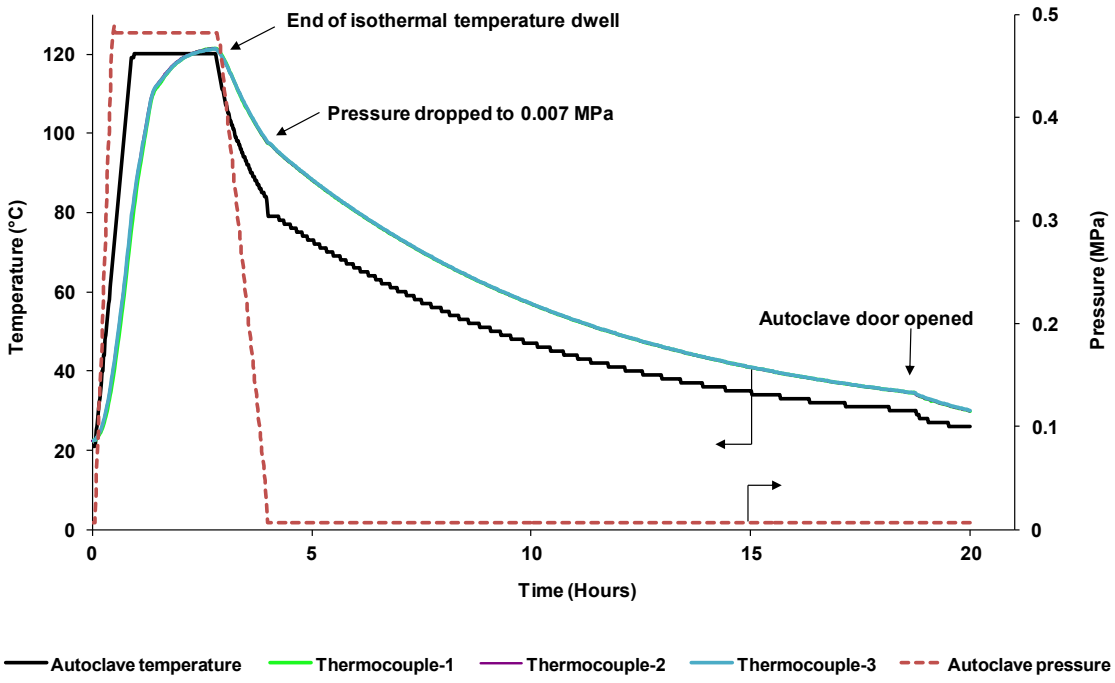

Figure 4.28 Temperature and pressure during the processing of the eight-ply unidirectional CFRP laminate with embedded FBG and Fresnel sensors.

4.5.2 Strain and temperature monitoring using embedded FBG sensors

The evolution of strain and temperature was monitored during the processing of the laminate. FBG strain and temperature sensors embedded in between the 1st and 2nd plies (bottom), 4th and 5th plies (middle), and 7th and 8th plies (top) were used for this purpose. The experimental details were presented in Section 3.7.3. The development of strain at the bottom, middle and top plies of the unidirectional CFRP laminate during the cross-linking process is presented in Figure 4.29.

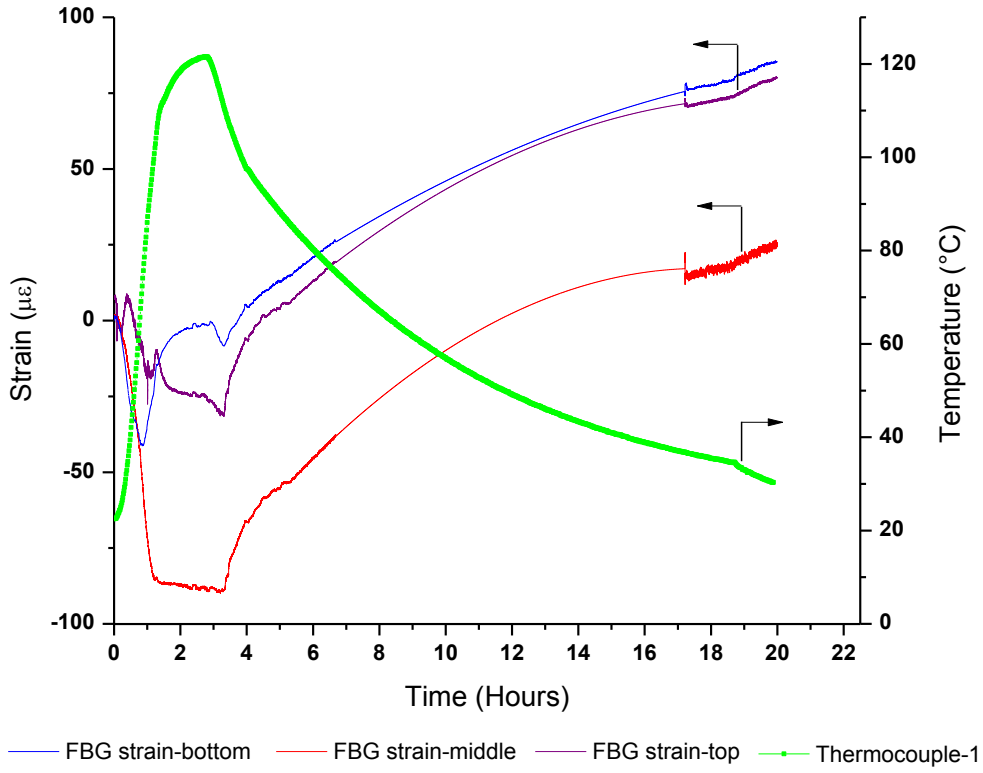

Figure 4.29 The development of strain recorded by the FBG sensors in between plies 1-2 (bottom), 4-5 (middle) and 7-8 (top) during the processing of the eight-ply unidirectional CFRP laminate.

A small initial strain was recorded by the sensors at the start of the cross-linking cycle due to the effect of embedding and vacuum de-bulking. The evolution of strain during the heating phase of the cross-linking cycle is shown in Figure 4.30.

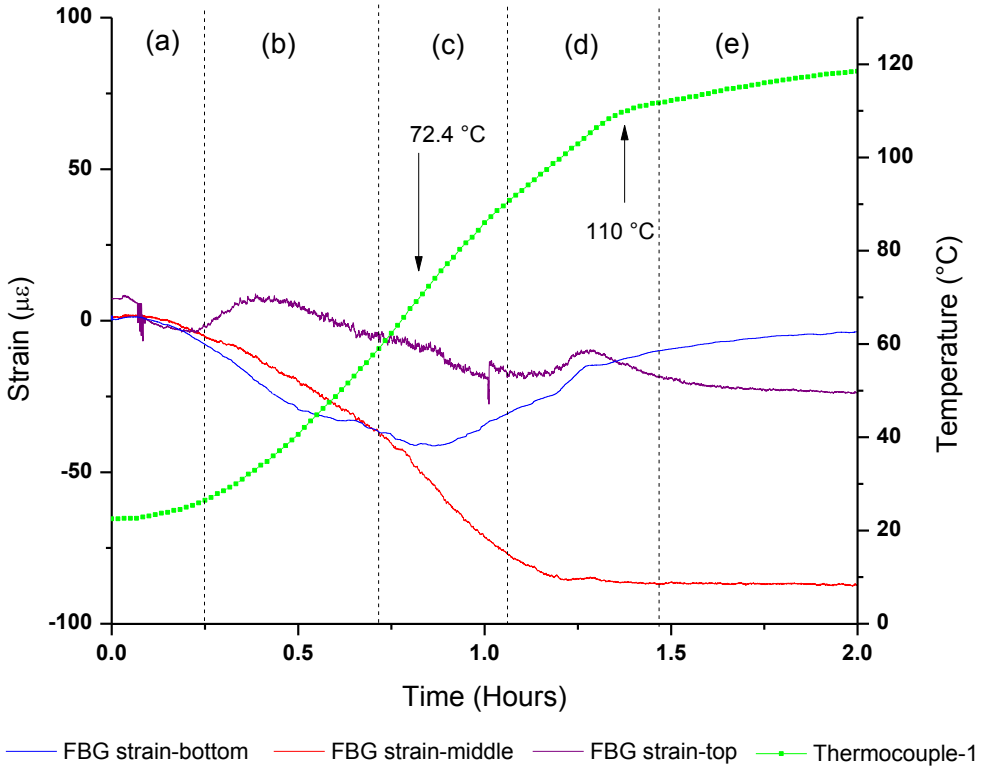

Figure 4.30 The evolution of strain recorded by the FBG sensors during the heating phase from ambient to the isothermal dwell.

The strains recorded by the three FBGs in zone (a) seem to be similar. However, a notable feature here and on comparing the data presented in Figure 4.24, is that significantly lower scatters in the data are observed. In zone (b), the sensor that was located between plies 1-2 recorded a positive strain initially but then started to decrease after attaining 36 °C. On the other hand, sensors positioned between plies 4-5 and 7-8 showed a compressive strain. This decrease is observed to continue in zone (c), similar to that observed in Figure 4.24 and the reasons for this was attributed to the Tg of the acrylate coating being exceeded. In the case of zones (d) and (e), the general trend in the

data shown in Figure 4.30 are similar to that presented in Figure 4.24. The residual fabrication strain recorded at 30 °C is summarised in Table 4.5.

Table 4.5 Summary of the strain recorded by FBG sensors at various stages of processing of the CFRP laminate.

Sensor number	Sensor type	Before embedding (με)	After de-bulking (με)	Start of isothermal dwell at 120 °C (με)	End of isothermal dwell at 120 °C (με)	Residual strain at 30 °C (με)
1	FBG strain-bottom	0.00	1.66	-2.57	-2.16	85.59
2	FBG strain-middle	0.00	1.66	-87.55	-88.97	25.07
3	FBG strain-top	0.00	7.24	-24.13	-25.88	80.16

The responses of the embedded FBG temperature sensor and the K-type thermocouple are presented in Figure 4.31. As observed previously in Figure 4.27, good correlation is observed between the FBG temperature sensor and the thermocouple.

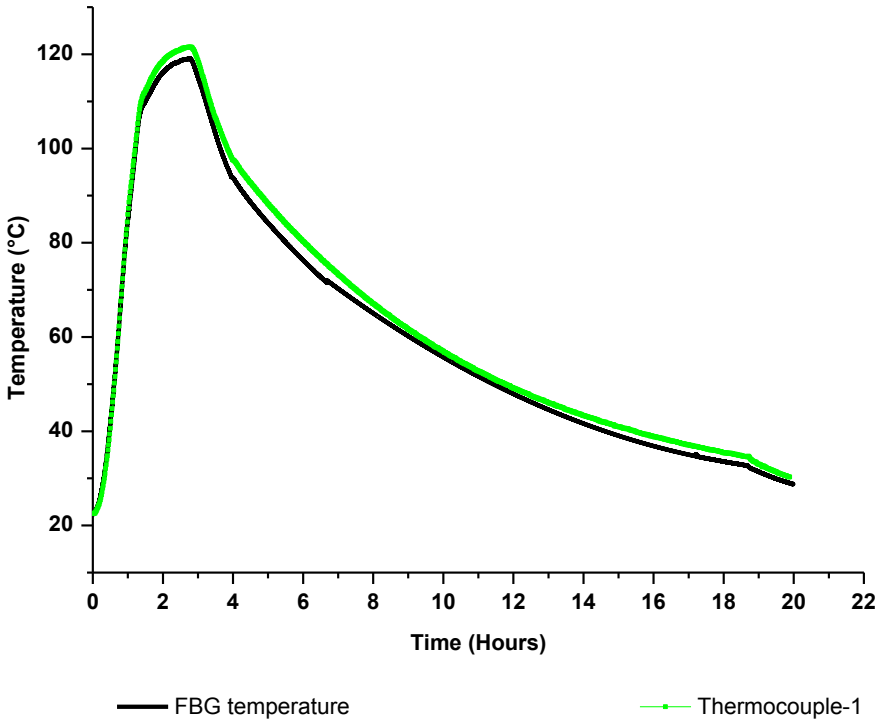

Figure 4.31 Temperature recorded by the FBG temperature sensor and the thermocouple during the processing of the CFRP laminate.

4.5.3 Process monitoring using embedded Fresnel sensors

These experiments involving the Fresnel sensors were necessary to gain experience and validate the subsequent research that was undertaken to develop and deploy the MMS.

The responses of the three Fresnel sensors embedded between plies 1-2 (bottom), 4-5 (middle) and 7-8 (top) are shown in Figure 4.32. The variations in the optical density of the medium in contact with the sensing-ends are inferred through the variations in the Fresnel signal. However, mechanically-induced perturbations along the embedded length during vacuum bagging can also cause changes in Fresnel signal. Table 4.6

shows the variations in Fresnel signal during various stages of processing. With reference to the embedded sensors in the top and middle plies, the Fresnel reflection reduced by approximately 94% by the start of the cross-linking cycle as compared to that in air. The Fresnel sensor embedded in the bottom ply showed approximately 48% reduction. The drop in the Fresnel reflection occurs mainly due to diminished index contrast between the core and the resin system. In comparison to the sensor signals from the top and the middle plies at the beginning of the heating phase, the signal from the bottom ply indicates that the matrix material is not fully in contact across the core.

Table 4.6 Fresnel signals obtained from the sensors at different stages of processing of the CFRP laminate.

Sensor type	**Fresnel reflection (V)**						
	At core/air	**After embedding**	**After de-bulking**	**At the start of curing**	**At the start of isothermal dwell**	**At the end of isothermal dwell**	**After cooled back to 30 °C**
Fresnel-bottom	0.2887	0.1528	0.1512	0.1508	0.0172	0.0171	0.0194
Fresnel-middle	0.2931	0.2927	0.0186	0.0185	0.0171	0.0170	0.0184
Fresnel-top	0.3121	0.0077	0.0191	0.0188	0.0181	0.0179	0.0193

The temperature inside the autoclave reached the isothermal regime after 58 minutes of heating when the temperature within the plies was 86 ^{o}C. From Figure 4.32, the resin viscosity decreased until 65 minutes when the temperature in the laminate was 93 ^{o}C. This phase corresponds to the consolidation via the flow of the resin under the influence of vacuum and autoclave pressure. This phase eventually determines the compaction and spatial distribution of the fibre within the laminate. The fluctuating response of the

Fresnel sensors during this period is apparent from Figures 4.32 (a and b). The subsequent cross-linking process causes matrix densification and thereby increasing the refractive index rapidly. At around 95 minutes, the slopes of refractive index as a function of time decreased significantly indicating the onset of vitrification. The temperatures within the plies attained isothermal regime after 120 minutes. The isothermal and isobaric conditions co-exist for 60 minutes after which the pressure inside the autoclave was released.

The expanded graph shown in Figure 4.32 (b) shows: (i) the noisy nature of the signal, possibly due to incomplete contact between the matrix and the cleaved optical fibre end-face; (ii) presence of micro-bubbles; and (iii) vibrations caused by the oscillating pressure within the autoclave. Due to an experimental error, the commencement of the data logging between plies 1-2 was not synchronised with the other two.

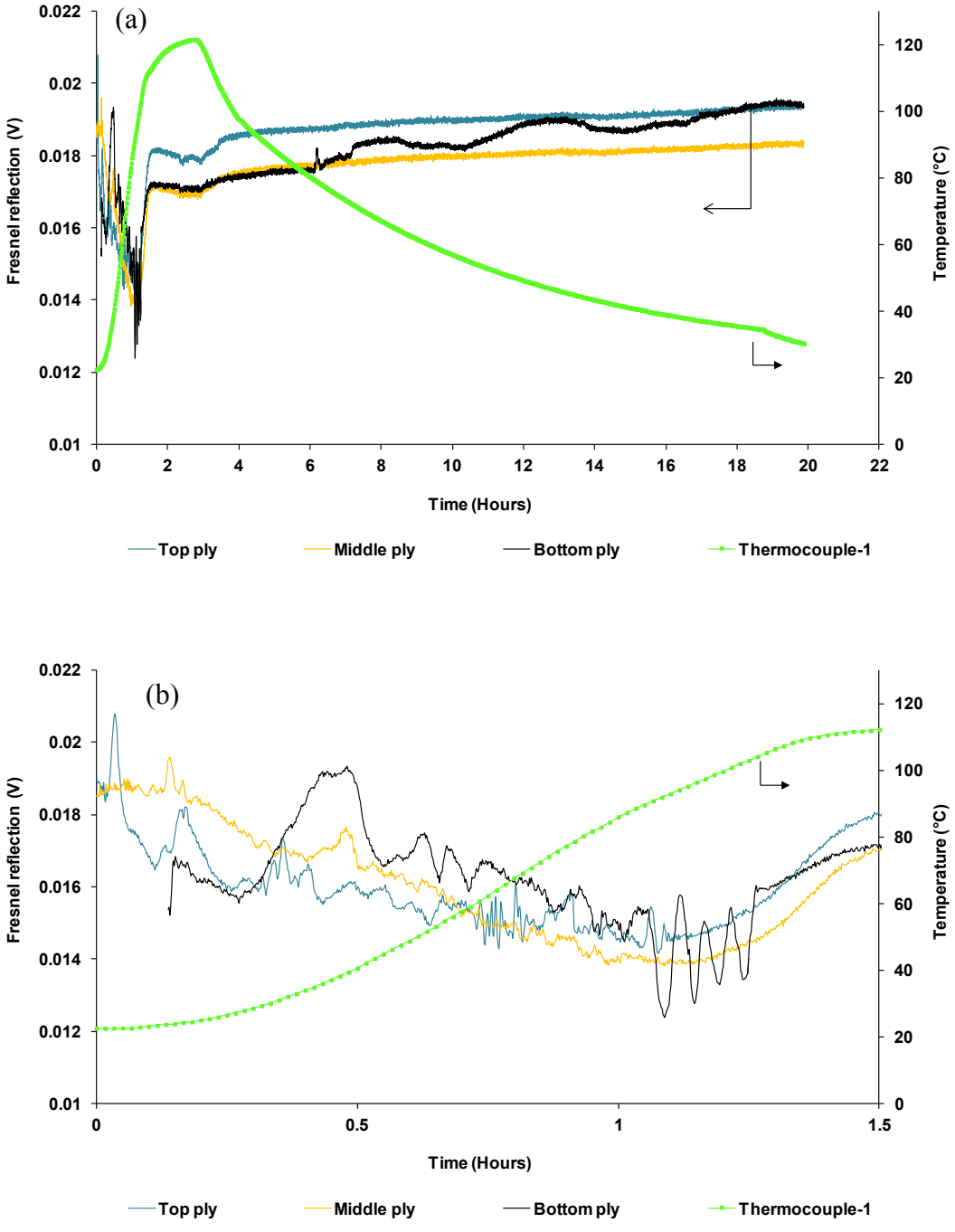

Figure 4.32 (a and b) Responses of the Fresnel sensors (a) during the processing of the eight-ply CFRP laminate and (b) enlarged version of (a) showing the initial heating.

It is worthy of note that the evolution of refractive index is influenced by the processing parameters. Therefore, the Fresnel reflection as detected by the sensors is not entirely representative of the cross-linking process but a result of the processing parameters. Accepting the variability in the Fresnel data, the responses of the sensors located at the bottom and middle plies were similar during the isothermal dwell period. However, the sensors showed variations in the Fresnel reflections during the cooling phase. As expected, during the cooling phase, an increase in the optical density was observed. The sensor in the top and bottom plies showed relatively high Fresnel reflection compared to the middle ply when the laminate was cooled down to 30 °C.

The feasibility of monitoring strain and temperature using embedded FBG sensors was demonstrated again. In addition, the deployment of Fresnel sensors for inferring the evolution of the refractive index during processing was demonstrated.

4.5.4 Post-processing of the CFRP laminate (with the embedded Bragg and Fresnel sensors)

The laminate with the embedded sensors that was used in Section 4.5 was used here to investigate the effect of vacuum, temperature, pressure and the normal autoclave cure cycle on the output of the FBG sensors.

4.5.4.1 Vacuum cycle

The effect of vacuum/vent cycles on the CFRP composite was studied. The composite was subjected to vacuum/venting three times and the output of the FBG sensors were recorded as shown in Figure 4.33. The peak wavelength of the FBG sensors before and after embedding during the cross-linking of the laminate was also cross-plotted. It is apparent from Figure 4.33 that there is a negligible effect of the vacuum on the output from the sensors during the processing and post-processing.

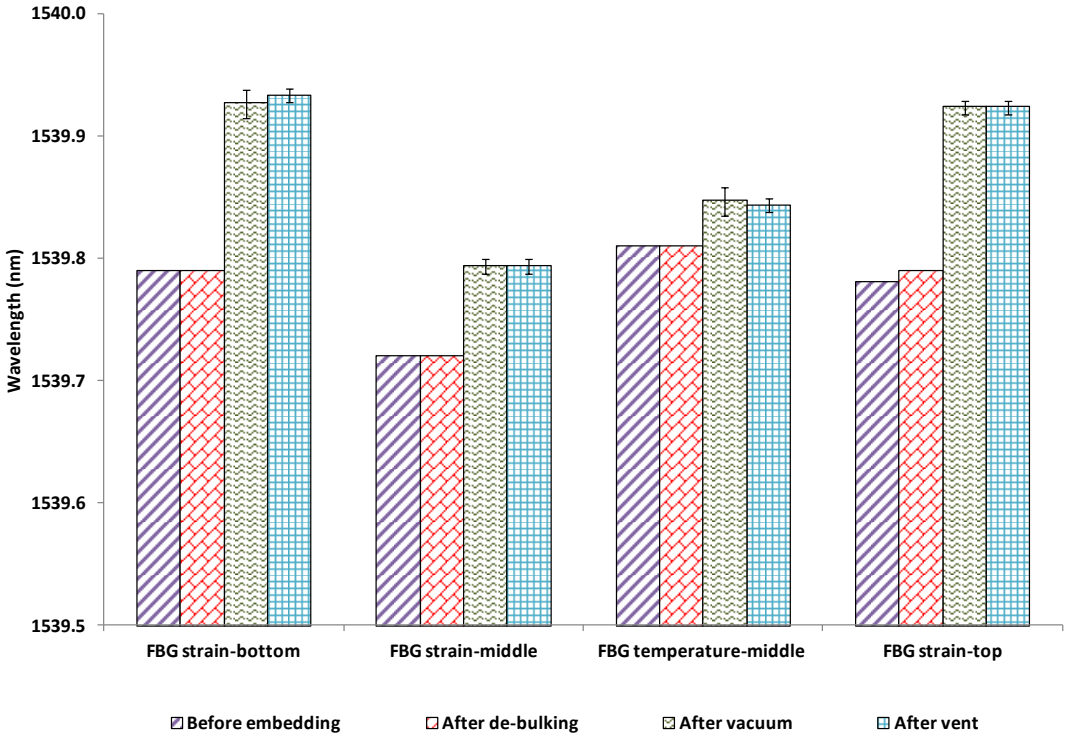

Figure 4.33 Responses of the FBG sensors during the autoclave vacuum/vent cycles of the CFRP composite.

4.5.4.2 Temperature cycle

The development of strain recorded by the FBG sensors during the post-cure temperature cycle of the CFRP composite is shown in Figure 4.34. The maximum temperature recorded by the embedded thermocouple at the middle of the laminate is 107.6 °C. The laminate was held at this temperature for 30 minutes without the use of pressure and vacuum. After this, the heating was terminated and the composite was allowed to cool to 30 °C.

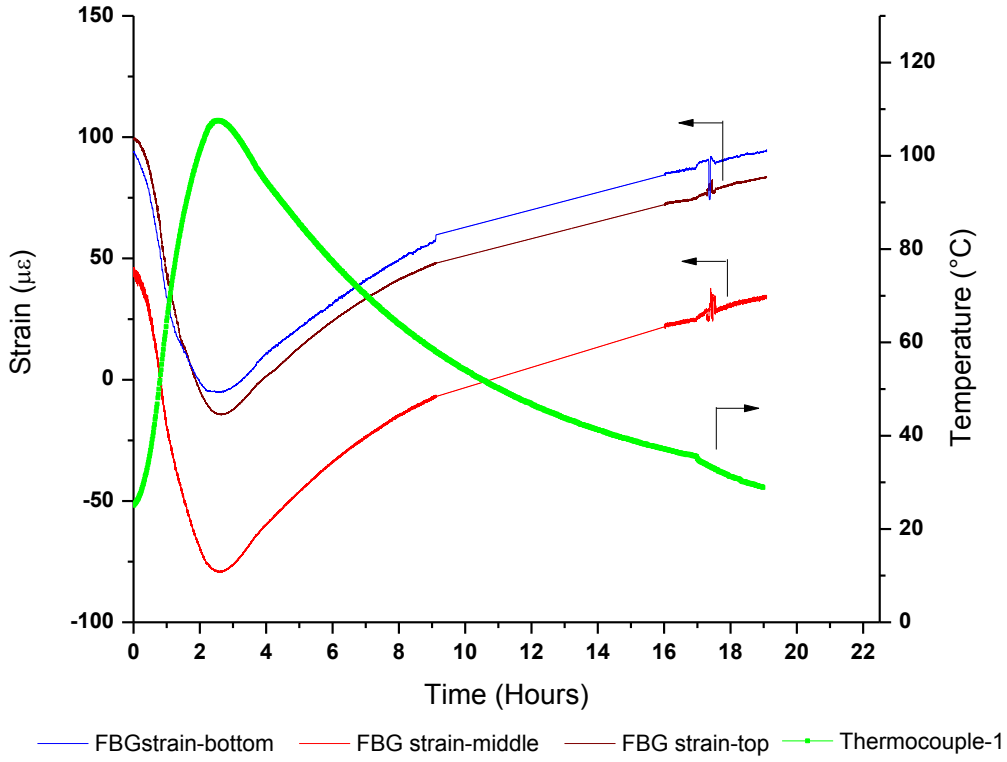

Figure 4.34 The strain recorded by the FBG sensors during the post-cure temperature cycle of the CFRP composite.

The strain at the bottom, middle and top plies at the start of the temperature cycle were 94.17, 44.05 and 99.33 με respectively. As observed previously in Figure 4.30 during the initial heating phase (zone (c)), a change in the slope is also observed here at 70 °C. The reason for this was attributed to the Tg of the acrylate coating on the optical fibre being exceeded. The recorded strain values at different stages of processing are summarised in Table 4.7.

Table 4.7 Summary of the strain recorded by the FBG sensors during the post-cure temperature cycle of the CFRP composite.

Sensor number	Sensor type	At the start of the temperature cycle (με)	Start of isothermal dwell at 107.6 °C (με)	End of isothermal dwell at 107.6 °C (με)	Residual strain at 30 °C (με)
1	FBG strain-bottom	94.17	-4.16	-5.07	95.00
2	FBG strain-middle	44.05	-77.07	-78.31	34.39
3	FBG strain-top	99.33	-11.73	-13.81	83.51

On comparing the data presented in Tables 4.5 and 4.7, it is seen that the residual strain recorded in the second heat cycle is slightly higher. The reasons for this are not known at present and further work is required.

The temperature measured using the embedded FBG temperature sensor and the K-type thermocouple are presented in Figure 4.35 and a good correlation is observed between the two devices.

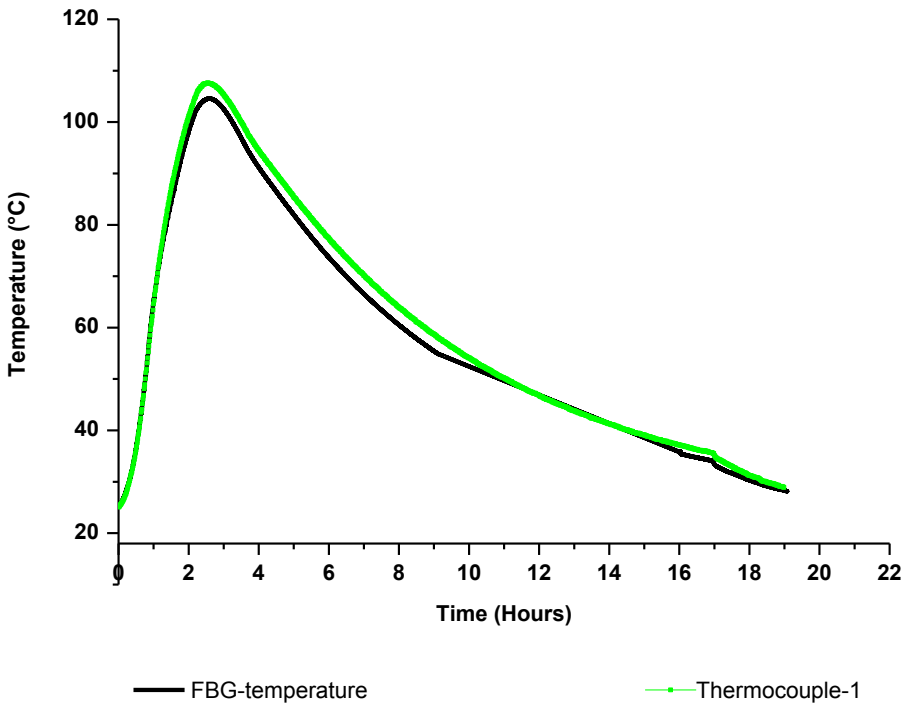

Figure 4.35 Responses of the FBG temperature sensor and the thermocouple during the post-cure temperature cycle of the CFRP composite.

4.5.4.3 Pressure cycle

The effect of the applied pressure on the cured composite was studied and the data are presented in Figure 4.36. Temperature in the autoclave was maintained at 25 °C however, the vacuum was not applied in this instance. The composite was subjected to a pressure of 0.48 MPa for 30 minutes and the pressure was released. It is clear from Figure 4.36 that the effect of the applied pressure on the output of the embedded FBG sensors within the cured composite was negligible.

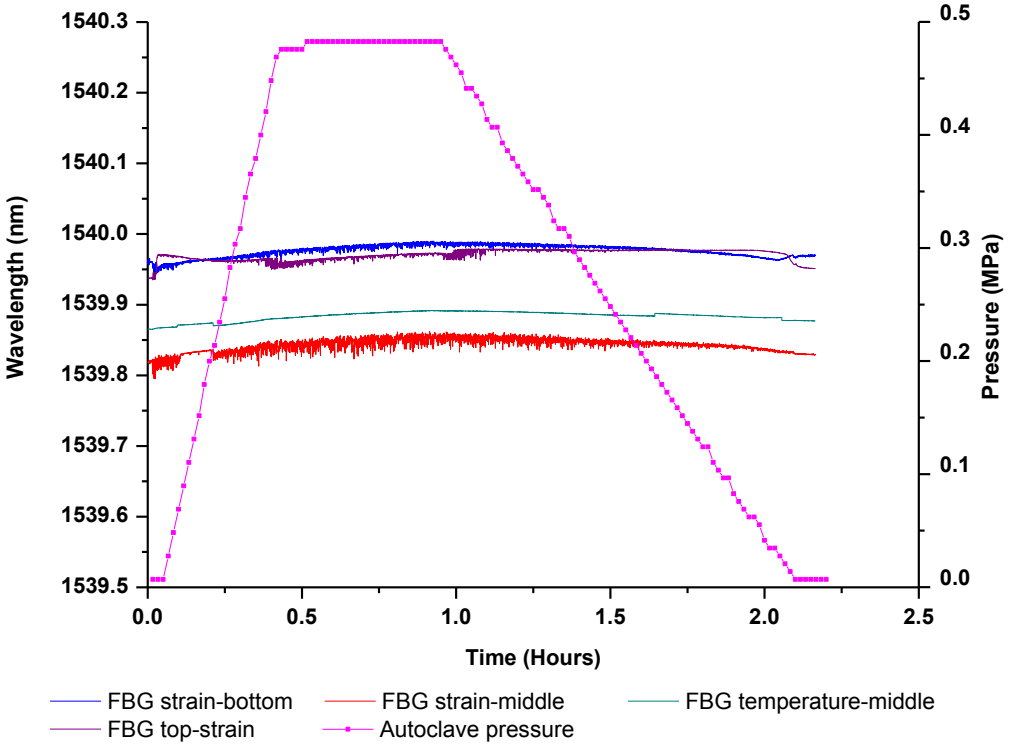

Figure 4.36 Responses of the FBG sensors during the pressure cycle of the CFRP composite.

4.5.4.4 Normal autoclave cure cycle

The cured CFRP composite was subjected to a normal cure cycle (120 °C for one hour). The strain induced in the composite during post-processing is shown in Figure 4.37. The strain at the bottom, middle and top plies of the composite at the start of the normal cure cycle were 81.51, 32.14 and 100.17 με respectively. The strain data recorded at the end of the cure and the first post-cure heating cycle were 85.59, 25.07, 80.16 and 95.0, 34.39, 83.51 με for the bottom, middle and top plies respectively. This variation in the three datasets is likely to be due to experimental variability.

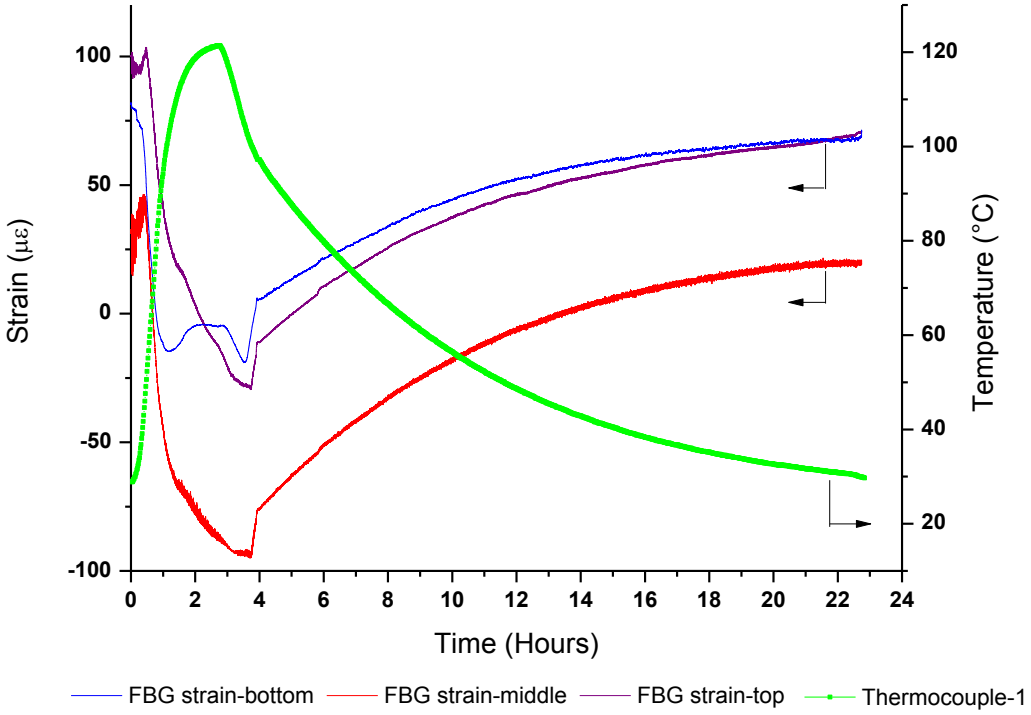

Figure 4.37 The development of strain recorded by the FBG sensors during the normal autoclave cure cycle of the CFRP composite.

In Figure 4.38, the observed trend in zone (a) is different to that observed in Figure 4.30. This highlights the variable output of the embedded FBG sensors for nominally the same composite. This discrepancy may be explained by the fact that it is not safe to assume that the effect of the vacuum bag, the applied vacuum and the subsequent loading of the composite on the tooling plate is identical. However, the acrylate-coating is a thermoplastic and therefore, its mechanical properties will change as the Tg is approached. The mode of deformation of the acrylate coating per temperature cycle may not be uniform. In addition to experimental variability, this may account for the observed discrepancy in the FBG data. On inspecting Figure 4.38, it is seen that the strain recorded by the FBG decreases in zone (b). This is consistent with the

observations made in Figure 4.30. In zone (c), a linear trend is observed for the temperature data obtained from the embedded thermocouple over the temperature range 40-88 °C. However, in the previous discussions, a change in the slope of the FBG data was observed at around 70 °C. A similar trend is seen in Figure 4.30 within zone (c) for the FBG data. This change in the slope for the FBG data is observed for the three datasets. Therefore, as concluded previously, it is assumed that this change in the slope is caused by the Tg of the acrylate being exceeded. Similar to the heating phase of the cross-linking process of the laminate, a change in the strain behaviour was observed here. A first slope-change was observed at 79.9 °C and a second slope-change was observed at 110.5 °C as shown in Figure 4.38. The recorded strain values at different stages of processing are summarised in Table 4.8. Once again variability in the output of the FBG sensor is noted.

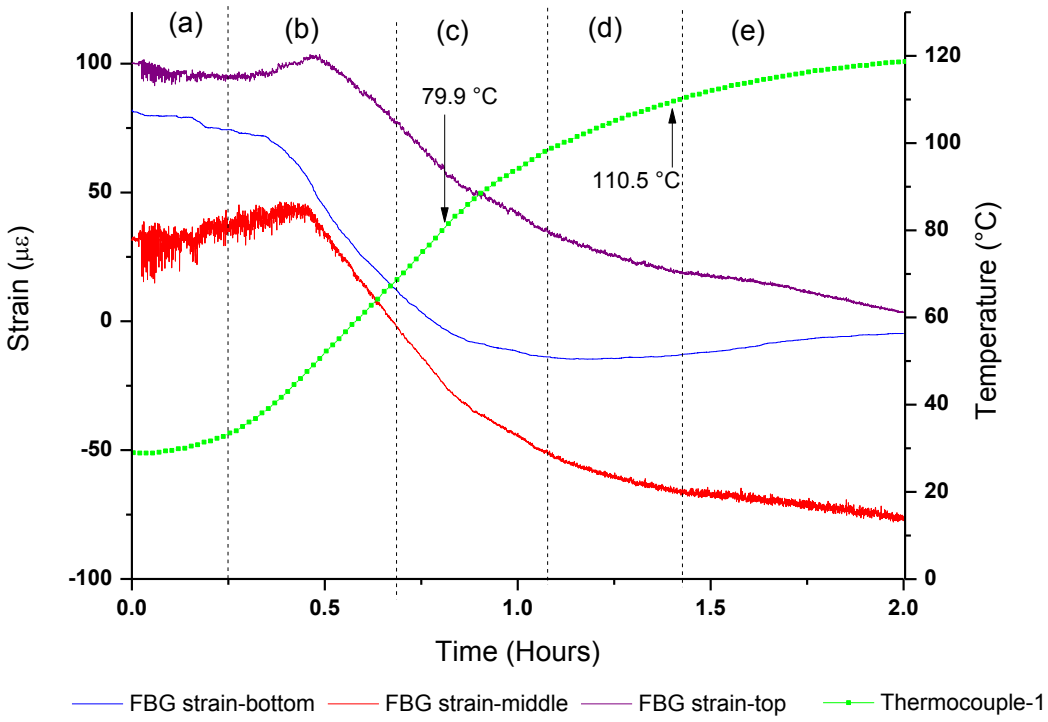

Figure 4.38 The development of strain recorded by the FBG sensors during the heating phase of a normal autoclave cure cycle.

Table 4.8 Summary of the strain recorded by the FBG sensors during the normal autoclave cure cycle of the CFRP composite.

Sensor number	Sensor type	At the start of the normal cure cycle (με)	Start of isothermal dwell at 120 °C (με)	End of isothermal dwell at 120 °C (με)	Residual strain at 30 °C (με)
1	FBG strain-bottom	81.51	-4.65	-4.07	71.36
2	FBG strain-middle	32.14	-79.47	-87.97	19.32
3	FBG strain-top	100.17	-2.23	-14.89	70.61

4.6 Process monitoring of E-glass fabric laminate using the multi-measurand sensor in the autoclave

The autoclave temperature via the in-built thermocouple, the temperature measured via the four thermocouples that were embedded in the E-glass preform and the pressure as a function of the processing time are shown in Figure 4.39. It is apparent from Figure 4.39 that the temperature profiles obtained from the embedded thermocouples are similar. The set isothermal temperature in the autoclave is attained after 54 minutes whereas the embedded thermocouples indicate that the desired temperature is achieved after 112 minutes. Moreover, the maximum temperature recorded by the embedded thermocouple is 121.8 °C; this is most likely due to the exotherm as a consequence of the cross-linking reactions illustrated in Figure 2.4. Inspecting the data from the embedded thermocouples, it is seen that the preform was above the desired isothermal temperature for 60 minutes. This general trend was observed in all the previous experiments involving the autoclave. As before, at the end of the cure cycle, the pressure was released to 0.007 MPa and the heating was terminated. The composite was then allowed to cool to 30 °C prior to performing the heating/cooling experiments.

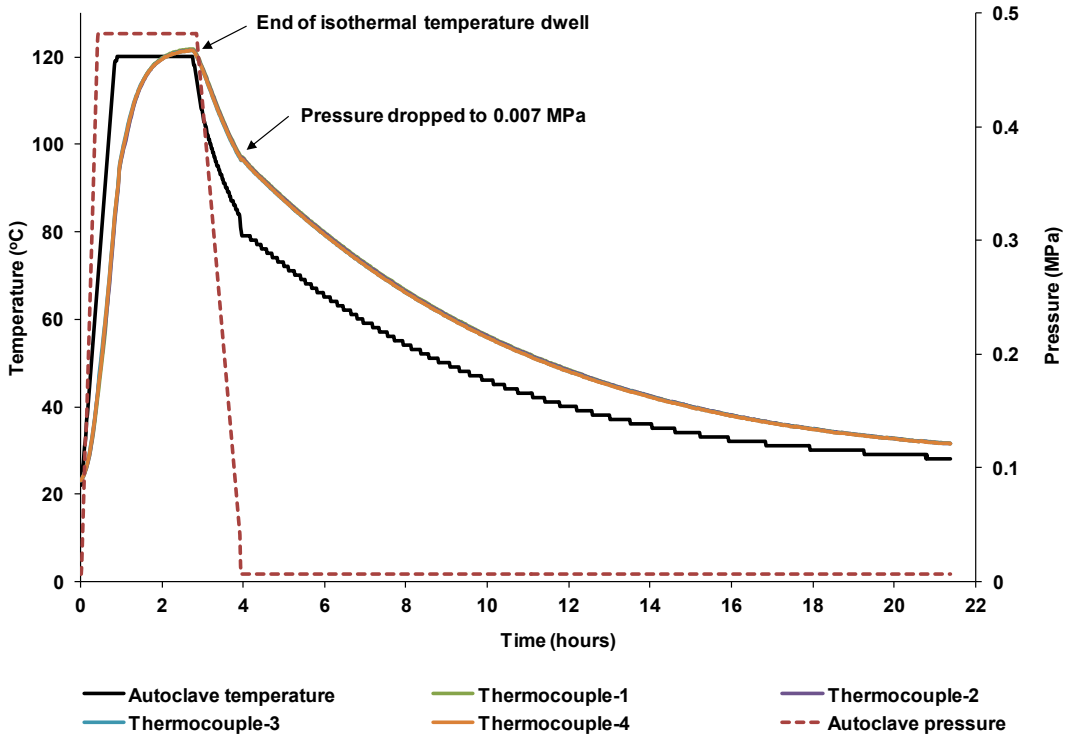

Figure 4.39 Temperature and pressure data during the processing of the eight-ply E-glass fabric laminate.

4.6.1 Comparison of the FBG response and thermocouple data

The responses of the MMS, the independent FBG temperature sensor and one of the K-type thermocouples are presented in Figure 4.40. Good correlation is observed between the three independent devices for monitoring the temperature. The consequence of the lower wavelength resolution of the FTNIR spectrometer is readily apparent in Figure 4.40 during the cooling phase. Nevertheless, this limitation can be overcome using a spectrometer with a higher wavelength resolution, and it does not detract from the uniqueness of the MMS.

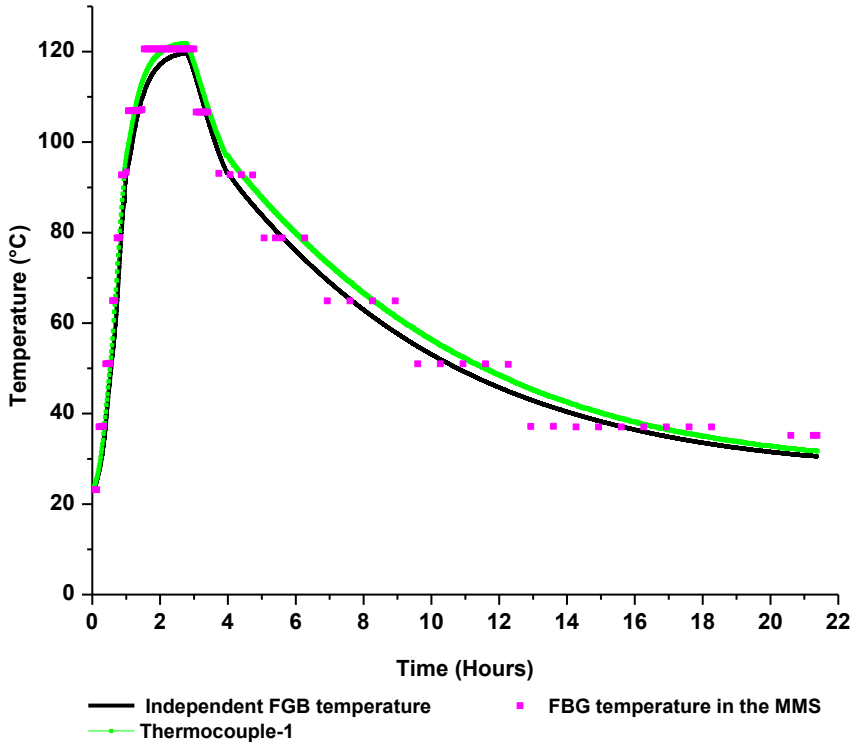

Figure 4.40 Temperature recorded by the FBG temperature sensor within the MMS, the independent FBG temperature sensor and an embedded thermocouple during the processing of the eight-ply E-glass woven fabric laminate.

4.6.2 In-situ strain monitoring during processing

The process-induced strains within the laminate were measured using the primary cavity of the MMS and the independent FBG sensor (responsive to strain and temperature). With reference to the sensor design shown in Figure 3.6, the interference signal from the primary cavity was decoupled from the Bragg reflection due to the reflective coating on the end of the fibre with the inscribed FBG. This is a unique feature of the MMS

design. With regard to previous designs of integrated EFPI/FBG sensors, it was necessary to decouple the two measurands.

The output of the FBG temperature and the EFPI strain sensor of the embedded MMS at the start of the processing cycle is shown in Figures 4.41 (a and b).

The absolute cavity length of the primary cavity was measured using the Fabry-Perot interference fringes obtained via the FTNIR spectrometer. The cavity length as a function of the processing time was obtained using Equation 2.5 and the development of strain was calculated using Equation 2.7.

The influences of strain and temperature on the independent fibre Bragg grating were calculated using Equation 2.9. The thermo-optic coefficient of the annealed FBG sensors used in these experiments was 5.45 x 10^{-6} $^{o}C^{-1}$ [53, 57]. The thermal expansion coefficient and photo-elastic coefficient of the fused silica fibre was taken to be 0.55 x 10^{-6} $^{o}C^{-1}$ and 0.22 respectively [8].

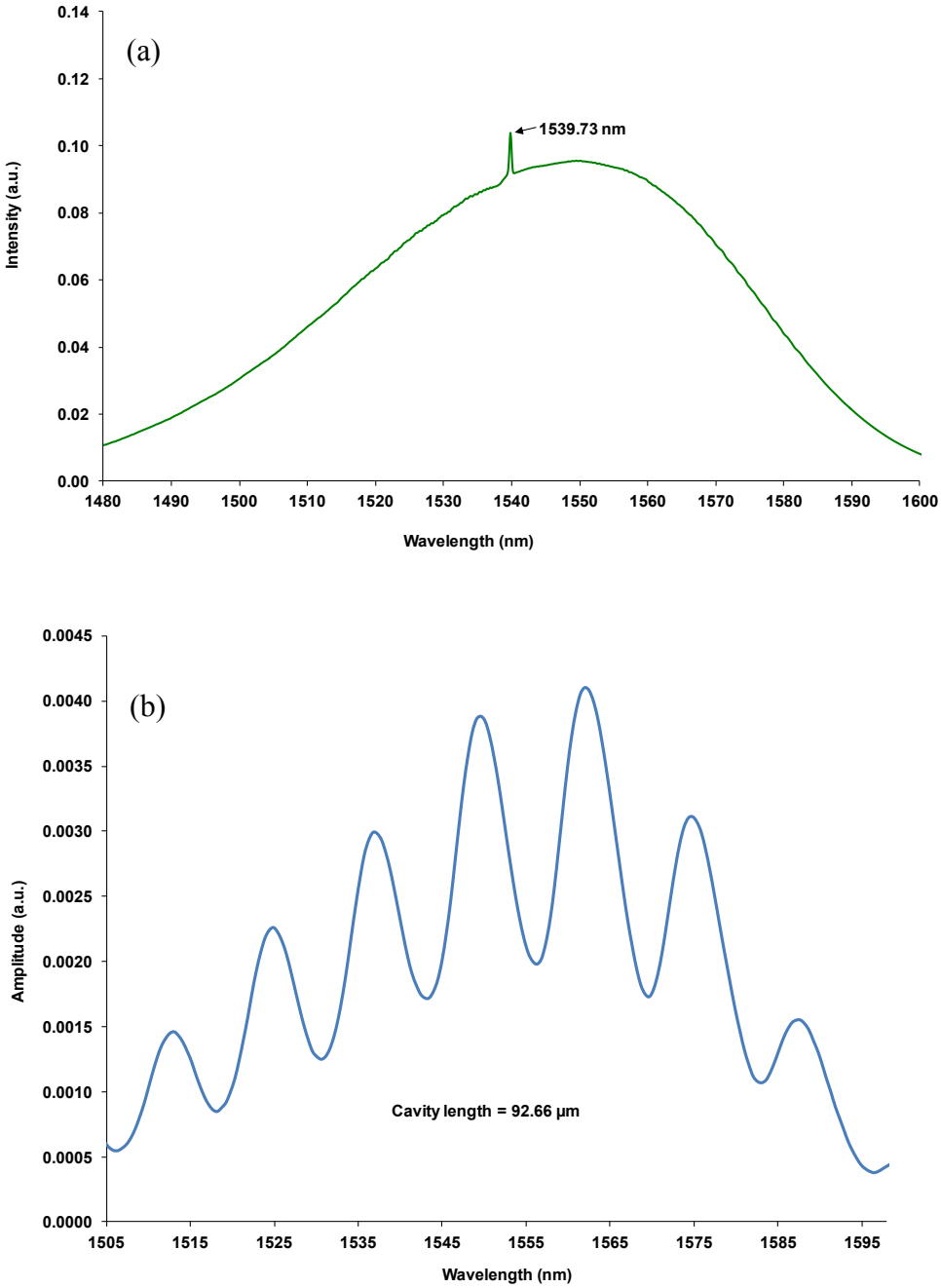

Figures 4.41 (a and b) The response of the integrated FBG temperature and the EFPI strain sensor of the MMS at the start of the processing cycle. The interrogation of the sensor was carried out using the FTNIR spectrometer. (a) Peak wavelength obtained from the FBG temperature sensor and (b) interference fringes obtained from the EFPI sensor.

The development of strain during processing of the impregnated E-glass preform in the autoclave is shown in Figure 4.42. The evolution of the strain via the embedded MMS (EFPI sensor) during cross-linking was interrogated using the FTNIR spectrometer. The strain development in the preform was also measured using an independent FBG strain sensor via the FiberPro interrogation unit. An initial strain was recorded by the sensors at the start of the processing cycle due to the effect of vacuum de-bulking.

In Figure 4.42, as the temperature was increased from ambient, a tensile strain was recorded initially due to thermal expansion. However, at 45 °C, this trend reversed and a decrease in the strain was recorded, and this continued until 90 °C. Between 45-90 °C, the maximum/minimum strains recorded by the EFPI (MMS) and the independent FBG were 305.09/93.21 με and 345.67/167.96 με respectively. After 90 °C, the previously observed trend in the tensile strain was resumed up to the dwell period.

The following factors may have been responsible for the observed trend in the strain profile: (i) the glass transition temperature of the acrylate coating on the optical fibre as discussed previously. Therefore, the loss of coupling efficiency between the optical fibre and the resin (matrix) may have occurred above the T_g of the acrylate coating; (ii) deformation of the acrylate coating: it is possible that the acrylate coating may have deformed during the period when the pressure was applied and the subsequent relaxation above its T_g. The shrinkage of the resin is unlikely to be a primary factor because this behaviour was observed when the cured composite was reheated and

cooled three times (without pressure or vacuum in the autoclave). The sudden drop in the strain recorded by the EFPI sensor coincides with the period when the pressure in the autoclave was released.

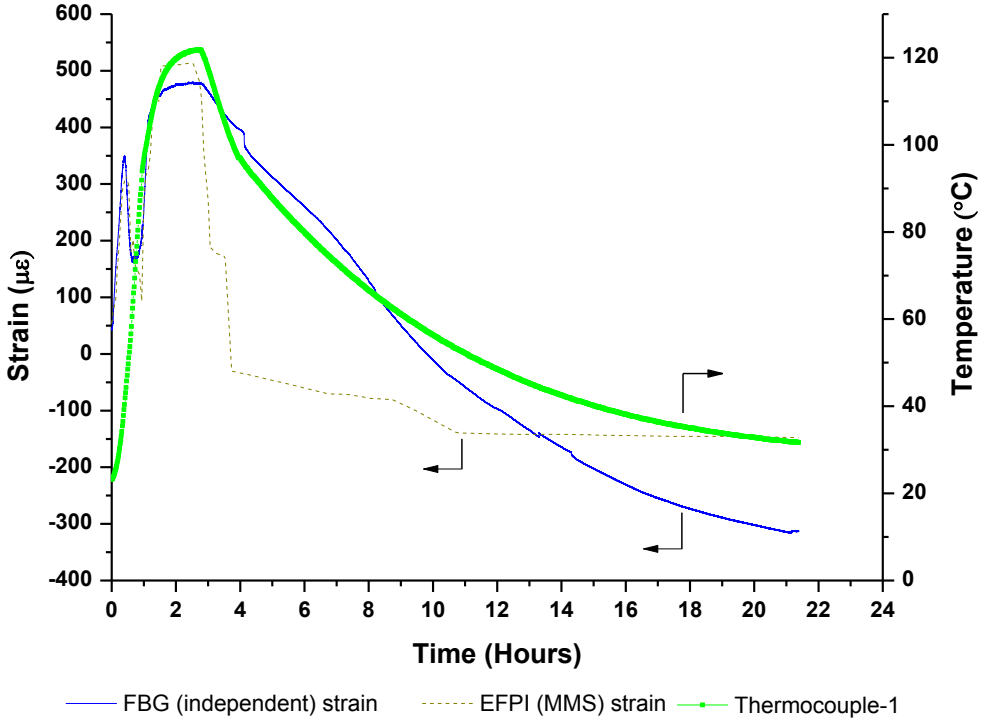

Figure 4.42 The evolution of strain during the processing of the eight-ply woven E-glass fabric laminate. The strain data were measured using the EFPI (MMS) and the independent FBG sensors.

The cross-linking data obtained from the chemical sensing device (secondary cavities) using the FTNIR spectrometer is presented in Figure 4.45. It is seen that the conversion attained is 95% after 40 minutes. Hence, it can be assumed that the stripped regions (capillary for the EFPI sensor and the stripped region where the FBG was inscribed) were bonded to the matrix. During the cooling phase, a reduction in the previously

recorded strain was observed, as expected. The residual fabrication strain recorded at 30 °C measured using EFPI (MMS) and FBG (independent sensor) sensors were found to be -147.49 and -313.98 με respectively. The measured strain at different stages of processing are summarised in Table 4.9. The temperature at which the strain data from the FBG sensors for the CFRP composite decreased was around 40 °C and in the current case, for the E-glass fabric laminate is at 45 °C. Therefore, this provides further support to the view that this decrease is primarily due to the acrylate coating. It will be seen later that this observation was repeated when this composite was subjected to three heating/cooling cycles. Residual strain data reported by other researchers for glass fibre composites are summarised in Appendix B.

Table 4.9 Summary of the strain at different stages of processing of the fabric laminate.

Sensor type	Before embedding (με)	After de-bulking (με)	At first observed drop in strain at 45 °C (με)	Min. at drop (με)	Max. at first recovery (με)	At the end of isothermal dwell at 120 °C (με)	Strain when pressure is released (με)	Residual strain at 30 °C (με)
EFPI (MMS) strain	0.00	53.36	305.09	93.21	508.25	478.02	-30.00	-147.49
Independent FBG strain	0.00	40.65	345.67	167.96	459.72	477.00	396.00	-313.98

4.6.3 Monitoring the cross-linking of the fabric laminate

Typical spectra obtained during the cross-linking of the LY3505/XB3403 resin system at 120 °C are shown in Figure 4.43. The depletion of the amine and epoxy functional groups as a function of the processing time is readily apparent from the spectra. See Table 2.4 for a summary of the peak assignments for epoxy/amine resin system in the

near-IR region. With reference to Table 2.4, the epoxy peak at 6060 cm^{-1}, the primary amine peak at 4938 cm^{-1} and the secondary amine peak at 6481 cm^{-1} were selected for the quantitative cross-linking analysis. The peak area of the epoxy, primary and secondary amine peaks was calculated by determining the appropriate positions for the baseline. A C-H reference peak centred at 4680 cm^{-1} was used to normalise the areas of the epoxy, primary and secondary peaks.

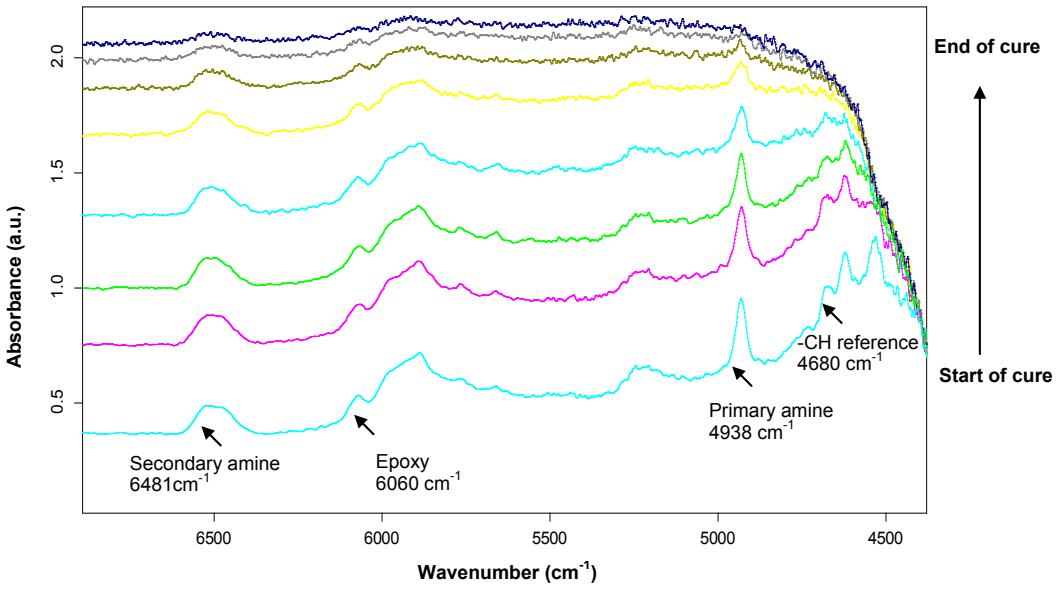

Figure 4.43 Typical NIR spectra of the resin system obtained from the chemical sensor of the MMS during the cross-linking of the eight-ply woven E-glass fabric laminate at 120 °C.

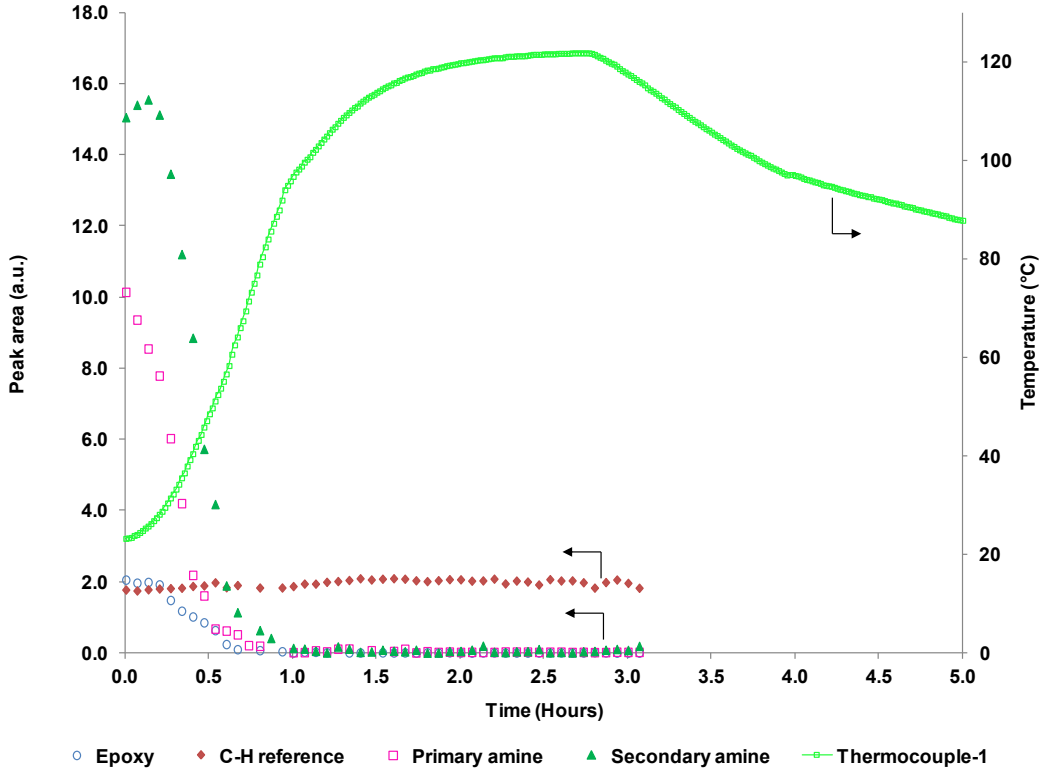

Figure 4.44 Peak area of the epoxy, primary amine, secondary amine and C-H reference functional groups during the cross-linking process.

The depletion of the epoxy, primary and secondary amine peaks as a function of the processing time is presented in Figure 4.44. The relative rate of conversion of the primary amine is faster than that observed for the epoxy group; this may be attributed to the evaporation of the low molecular weight amine at 120 °C. Nevertheless, the MMS was successful in tracking the depletion of the active functional groups in the resin system.

The degree of conversion of the epoxy, primary and secondary amines was calculated from the peak area of the spectra shown in Figure 4.43 using Equation 2.11 and the analysis is presented in Figure 4.45.

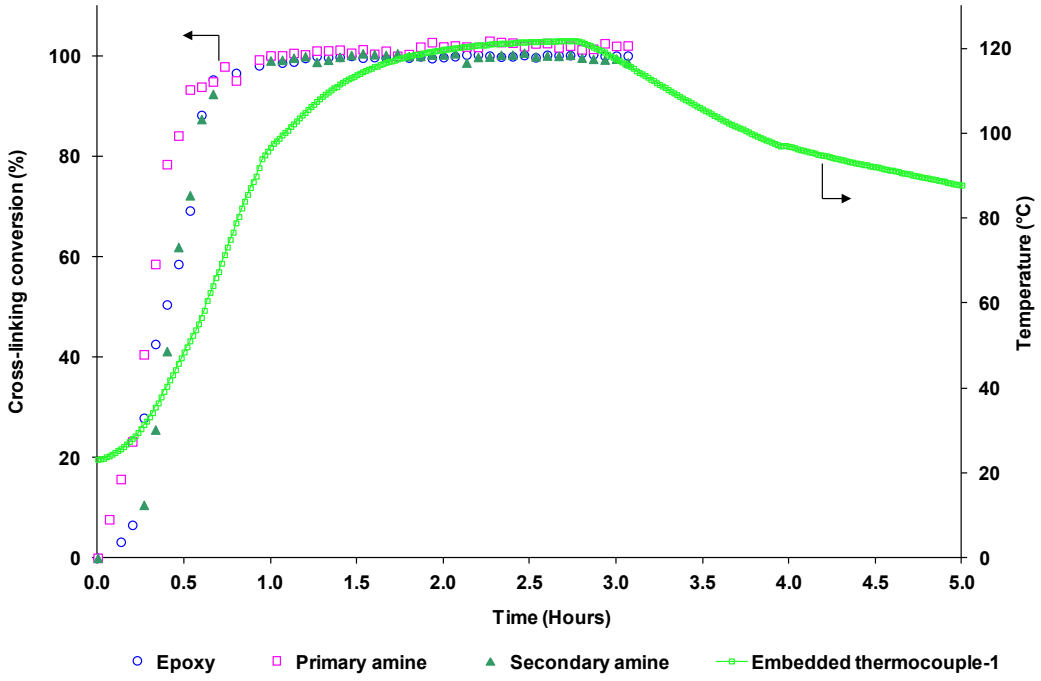

Figure 4.45 The degree of conversion of the epoxy, primary amine and secondary amine functional groups obtained via the chemical sensor of the MMS. The cross-linking was carried out at 120 °C.

4.6.3.1 Validation of the chemical sensor via cuvette-based experiments

The outputs of the secondary cavities (chemical sensor) on the MMS were compared with the isothermal cure kinetic data generated from cuvette-based experiments, in conjunction with conventional transmission FTNIR spectroscopy. Cross-linking monitoring at 50, 60 and 70 °C were carried out simultaneously using the chemical

sensor and conventional transmission FTNIR spectroscopy. The cross-linking temperatures and the duration of the experiments are summarised in Table 4.10. The epoxy peak at 4530 cm^{-1} was selected for the quantitative cross-linking analysis. It is acknowledged that the analysis of the epoxy peak at 6060 cm^{-1} was used in the experiments involving the impregnated E-glass fabric laminate via the MMS. This was because the peak at 4530 cm^{-1} was not prominent over the full cure cycle. Hence, the peak 6060 cm^{-1} was used. Time constraints did not permit the analysis of the peak at 6060 cm^{-1} in the cuvette-based experiments. The area of the epoxy peak was calculated using the methodology described in Section 4.6.3. A C-H reference peak centred at 4623 cm^{-1} was used to normalise the area of the epoxy peak.

A typical transmission spectra for the LY3505/XB3403 resin system obtained using the chemical sensor and conventional transmission FTNIR spectroscopy at the start of the cross-linking reaction at 50 °C is shown in Figure 4.46. Overlaid spectra of the epoxy and C-H reference peak of the resin system during cross-linking at 50 °C obtained using the chemical sensor is shown in Figure 4.47. With reference to Figure 4.47, the depletion of the epoxy functional group as a function of time is readily apparent. The cross-linking conversion data for the epoxy functional group obtained using the chemical sensor was compared with the data obtained using the conventional transmission FTNIR spectroscopy at each temperature and is presented in Figure 4.48. With reference to Figure 4.48, a good correlation was observed between the two data sets and this demonstrates that the optical fibre-based chemical sensor can be used for real-time process monitoring.

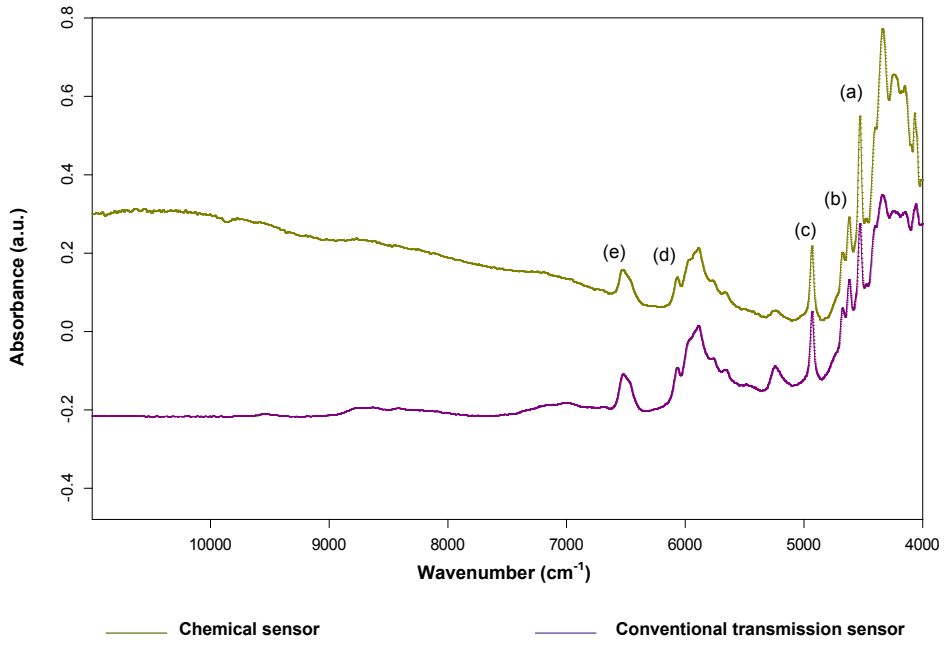

Figure 4.46 A typical transmission spectra for the LY3505/XB3403 resin system obtained using the chemical sensor and conventional transmission spectroscopy at the start of the cross-linking reaction at 50 °C. (a) epoxy peak at 4530 cm^{-1} (b) C-H reference peak at 4623 cm^{-1} (c) primary amine peak at 4938 cm^{-1} (d) epoxy peak at 6060 cm^{-1} and (e) secondary amine peak at 6481 cm^{-1}.

Table 4.10 The cross-linking temperatures and the duration of the cuvette-based experiments.

Temperature	Sensor type	Cross-linking time (Hours)
50 °C	Chemical	15.0
	Conventional	
60 °C	Chemical	8.0
	Conventional	
70 °C	Chemical	7.0
	Conventional	

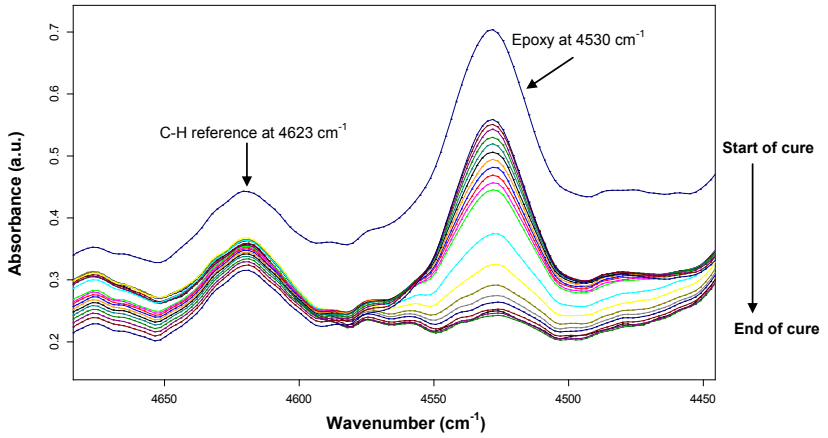

Figure 4.47 Typical overlaid spectra for the epoxy and C-H reference peak of the LY3505/XB3403 resin system during cross-linking at 50 °C. Spectra obtained using the chemical sensor.

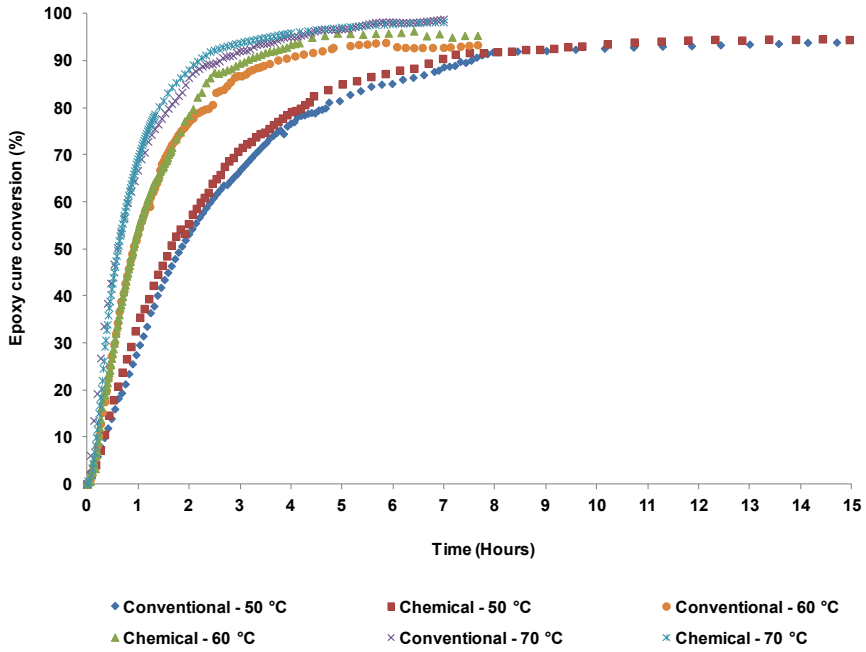

Figure 4.48 Comparison of the cross-linking conversion of the epoxy functional group during the cure of LY3505/XB3403 resin system at 50, 60 and 70 °C obtained using the chemical sensor and conventional transmission FTNIR spectroscopy.

4.6.4 Refractive index monitoring via the Fresnel reflection sensor on the MMS

In situations where inferring the extent of cross-linking reactions in a qualitative manner will suffice (as opposed to the requirement for quantitative kinetic data via infrared spectroscopy), the Fresnel sensing element shown in Figure 3.6 provides a route for inferring the refractive index of the resin system. The amplitude of the interferogram obtained via the FTNIR spectrometer, resulting from the Fresnel reflections, is a function of the refractive index of the resin and the temperature.

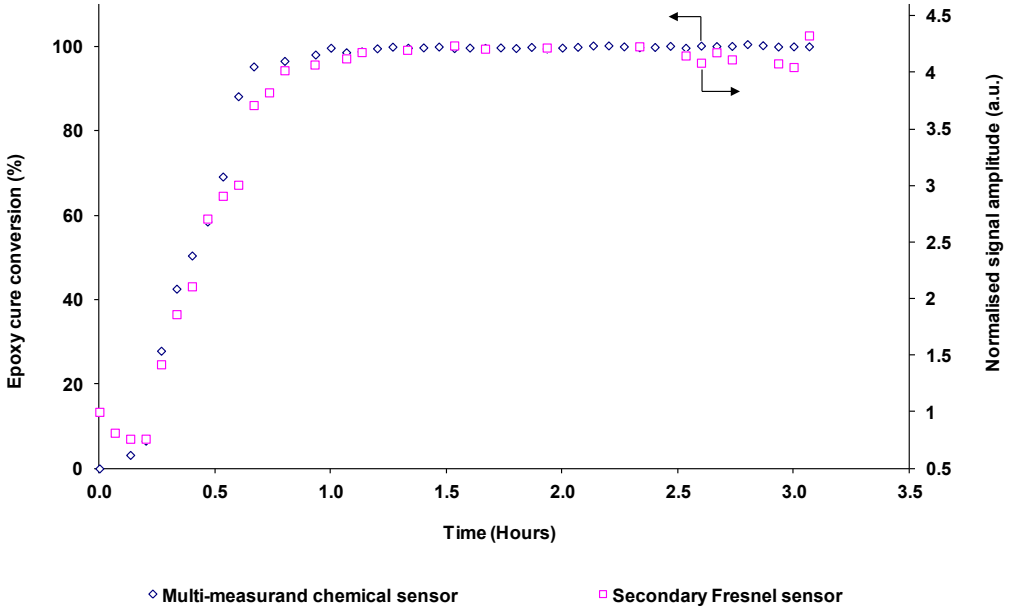

Figure 4.49 Correlation between the epoxy conversion presented in Figure 4.45 and the magnitude of the amplitude of the FTNIR interferogram measured using a secondary Fresnel reflection sensor during the processing of an eight-ply woven E-glass fabric laminate.

The initial drop in the signal amplitude is due to temperature-induced reduction of the resin density whilst the subsequent increase is due to increasing optical density via

cross-linking process. Figure 4.49 shows the correlation between the conversion shown in Figure 4.45 and the amplitude of the interferogram.

4.6.5 Post-processing of the E-glass fabric composite

The cured fabric composite was subjected to three heating/cooling cycles in the autoclave and the development of strain was monitored simultaneously using the EFPI (MMS) and the independent FBG sensors. The maximum temperature recorded by the embedded thermocouple located in the mid-ply of the composite is 112 °C. The composite was kept at this temperature for 30 minutes without using the pressure and vacuum. After this, the heating was terminated and the composite was allowed to cool to 30 °C. The measured strain in the composite using the EFPI (MMS) and the independent FBG sensors during the 1st and 2nd heating/cooling cycle is cross-plotted in Figures 4.50 and 4.51. The strain recorded by the EFPI (MMS) and the independent FBG sensor at the start of the 1st and 2nd heating/cooling cycle were -154.33/-123.30 με and -169.65/-117.65 με respectively. As observed previously, during the initial cross-linking cycle, a drop in the strain value was also observed between approximately 58-73 °C. This was due to the combined effects of the glass transition temperatures of the acrylate coating on the optical fibre and the resin system. The laminate was subjected to a third heating/cooling cycle and the strain was monitored using the independent FBG sensor. As shown in Figure 4.52, the strain behaviour during the heating phase of the third temperature cycle was found to be similar to the first two temperature cycles. The strain recorded by the independent FBG sensor at the start of the 3rd heating/cooling

cycle was -188.40 με and the residual strain when the laminate was cooled back to 30 °C was found to be -240.95 με.

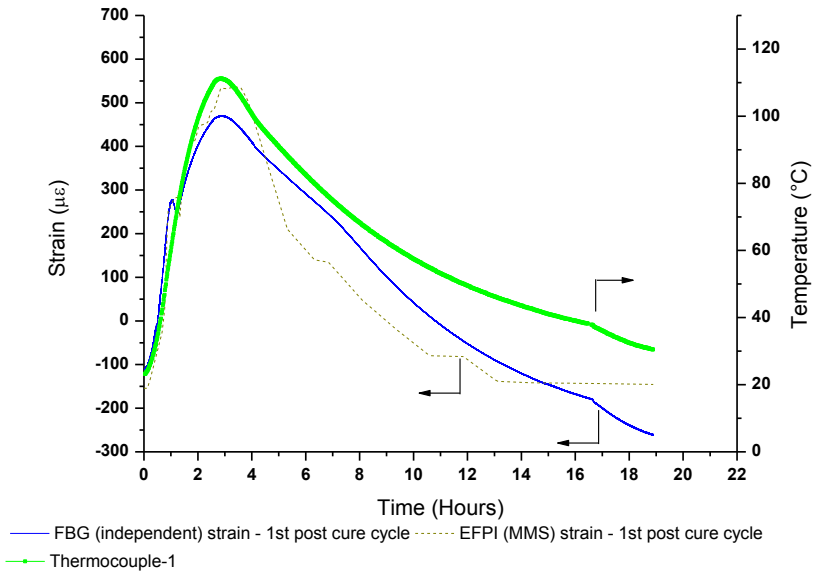

Figure 4.50 The strain recorded by the EFPI (MMS) and the independent FBG sensor during the first post cure temperature cycle of the eight-ply woven fabric preform.

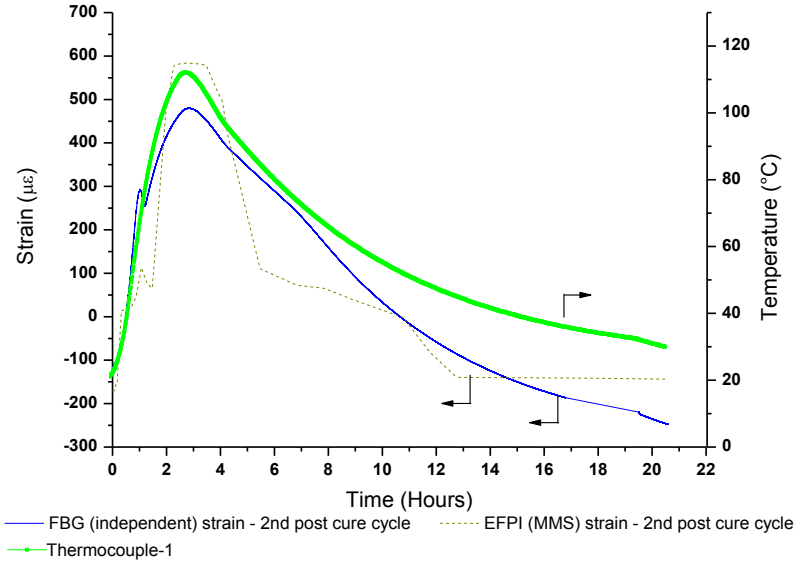

Figure 4.51 The strain recorded by the EFPI (MMS) and the independent FBG sensor during the second post cure temperature cycle of the eight-ply woven fabric preform.

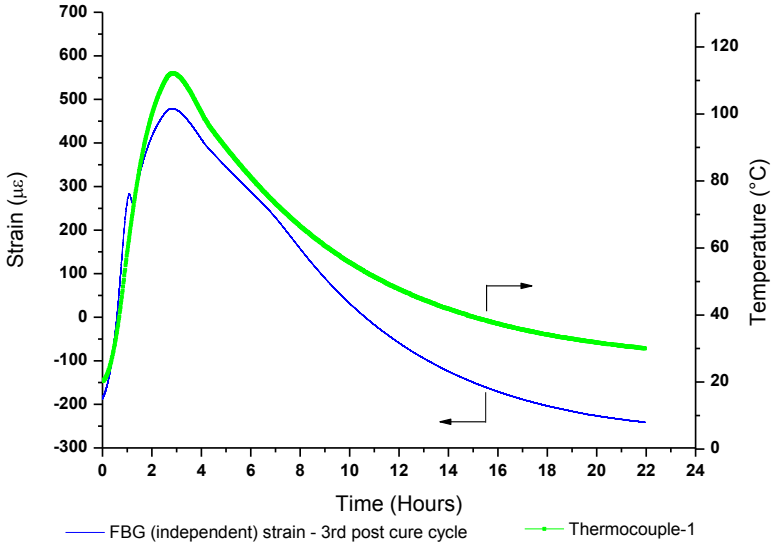

Figure 4.52 The strain recorded by the independent FBG sensor during the third post cure temperature cycle of the eight-ply woven fabric preform.

The DSC traces of the acrylate coating on the optical fibre, silica optical fibre and the LY3505/XB3403 resin system is presented in 4.53. The samples were heated from 30-180 °C at a heating rate of 20 °C min^{-1}. The average Tg of the acrylate coating and the resin system were found to be 78.6 ± 0.9 and 79.6 ± 0.1 °C respectively. These represent an average of four measurements. As expected, a glass transition temperature was not observed for the silica optical fibre over this temperature regime.

With reference to Figure 4.53, the change in strain caused by the acrylate-coating and the resin system as they pass through their respective Tgs is readily apparent in the FBG data. The strain values of the composite at different stages of the 1st, 2nd and 3rd temperature cycles are summarised in Table 4.11. With reference to Table 4.11, the residual strain recorded by the independent FBG sensor was higher than the EFPI

(MMS) sensor when the composite was cooled back to 30 °C. The reasons for this are not known at present. It is observed in Table 4.11 that the trend in the residual strain measured at 30 °C for the EFPI (MMS) and the FBG sensors is similar.

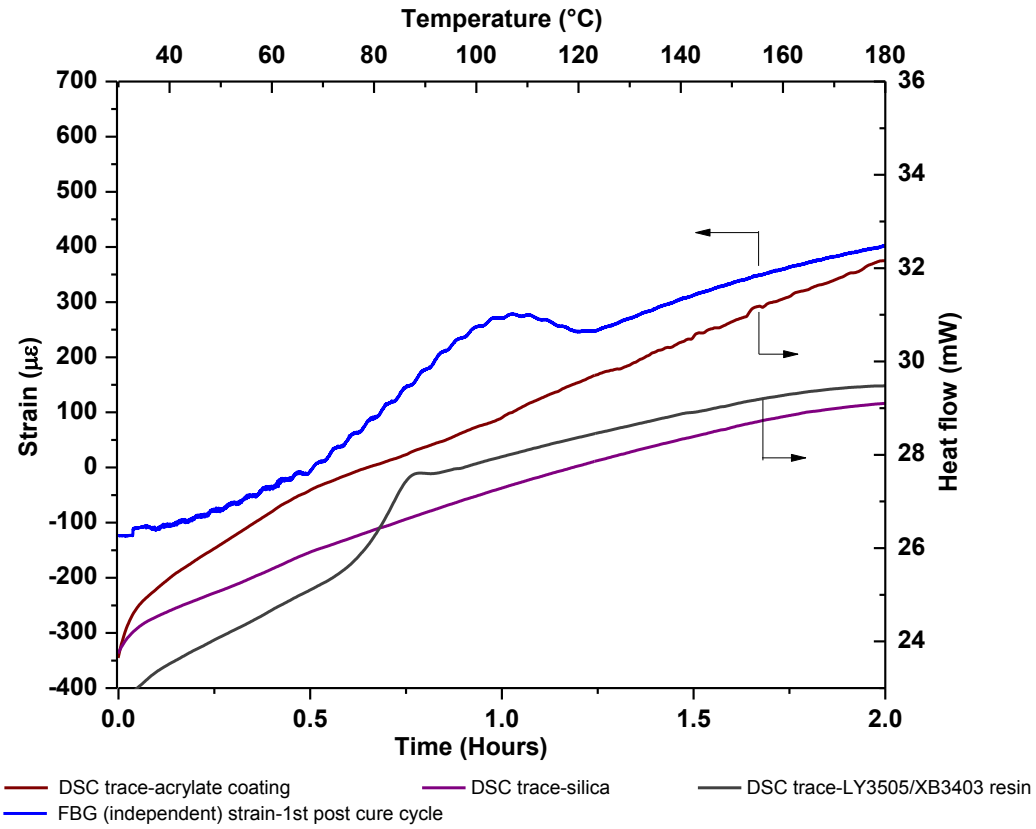

Figure 4.53 DSC traces of the acrylate-coating on the optical fibre, silica optical fibre and the LY3505/XB3403 resin system. The strain recorded by the independent FBG sensor during the first post-cure temperature cycle is also cross-plotted.

Table 4.11 Summary of the strain of the fabric composite at different stages of 1st, 2nd and 3rd temperature cycles.

Temperature cycles	At the beginning of temperature cycle (με)	Max. before drop in strain (με)	Local min. before rise in strain (με)	At the end of isothermal dwell at 112 °C (με)	Residual strain at 30 °C (με)
1st temperature cycle					
EFPI (MMS) strain	-154.33	283.8	237.33	533.33	-145.60
Independent FBG strain	-123.3	271.61	246.72	468.24	-260.93
2nd temperature cycle					
EFPI (MMS) strain	-169.65	112.75	64.61	583.63	-143.85
Independent FBG strain	-117.65	292.7	255.5	479.71	-248.37
3rd temperature cycle					
Independent FBG strain	-188.4	281.98	263.93	478.95	-240.95

4.7 Strain anomalies of acrylate-coated photo-sensitive fibres

The anomalies observed previously with regard to the output from the acrylate-coated optical fibres with Bragg gratings were investigated further.

Acrylate-coated FBGs, stripped FBGs (where the acrylate-coating were removed along the whole length of the optical fibre) and polyimide-coated FBGs were embedded in the mid-ply of unidirectional CFRP and E-glass woven fabric laminates. The sensors were interrogated using the FiberPro interrogation unit. The cross-linking schedule (temperature and pressure) used for the CFRP and fabric laminates were identical to that described previously.

4.7.1 Unidirectional CFRP laminate

Two eight-ply CFRP laminates were prepared: (a) with embedded acrylate-coated and stripped FBGs and (b) with acrylate and polyimide-coated FBGs. The strain behaviour recorded by the sensors during the processing and post-processing of the laminates are discussed separately in the following section.

(a) CFRP laminate embedded with acrylate-coated and stripped FBGs

The strain recorded by the acrylate-coated FBGs and the stripped FBGs during the cross-linking of an eight-ply unidirectional CFRP laminate is shown in Figure 4.54. The evolution of strain during the heating phase of the cross-linking cycle is shown in Figure 4.55.

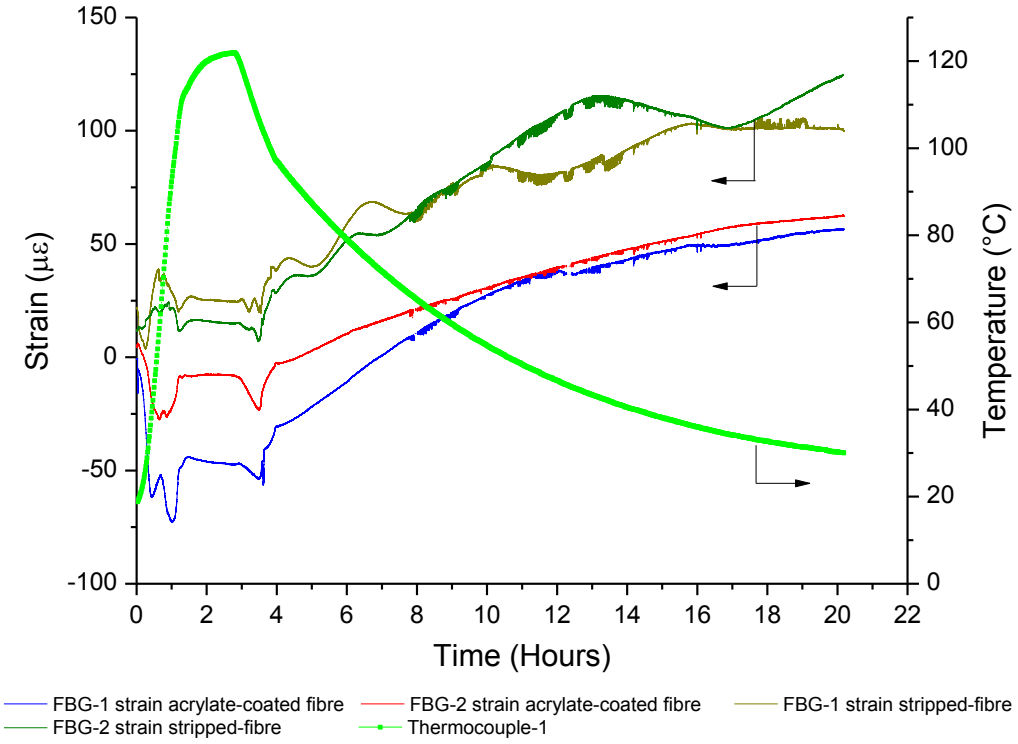

Figure 4.54 The evolution of strain recorded by the acrylate-coated and stripped FBGs during the processing of the eight-ply unidirectional CFRP laminate.

In zone (a), both the acrylate-coated optical fibres showed a decrease in the strain from the onset of the experiment but one of the sensors showed a larger decrease. One of the stripped optical fibres did not show any significant change in the strain in zone (a) but the other showed a decrease. In zone (b), both the acrylate-coated optical fibres showed a significant decrease in the measured strain. However, the output from the stripped optical fibres was different with one showing no change, and the other, an increase in value (stripped FBG-1). In Figure 4.24, the trends observed for the fifteen sensors in zone (b) were variable (some decreasing, some increasing); however, all the sensors

showed a decrease in strain in zone (c). In Figure 4.55 only one of the acrylate-coated optical fibres showed a significant decrease in the strain with the other showing no significant change. It was anticipated that both the acrylate-coated fibres will show a significant change within zone (c). Thus, introducing some uncertainty into the hypothesis that the decrease in strain is caused by the acrylate-coating, as it passes its Tg.

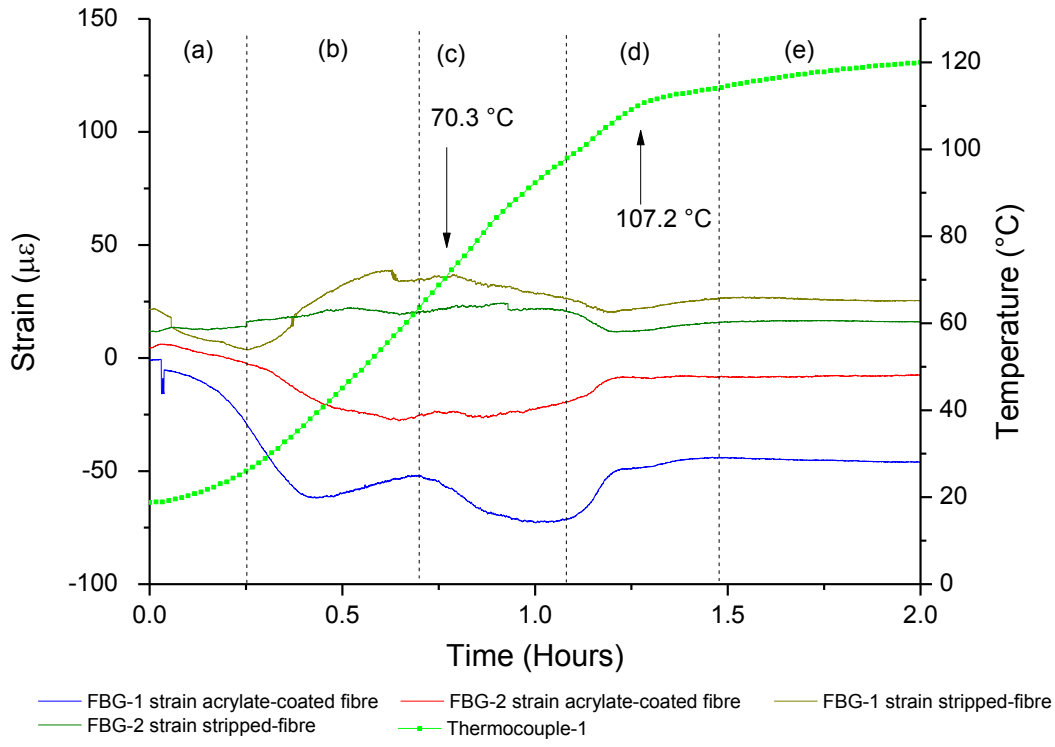

Figure 4.55 The evolution of compressive- and tensile-strain recorded by the acrylate-coated and stripped FBGs during the heating phase of the cross-linking cycle.

The strain data obtained from the acrylate-coated and the stripped FBGs at different stages of the cross-linking cycle are summarised in Table 4.12.

Table 4.12 Summary of the strain recorded by the acrylate-coated and the stripped FBGs at different stages of processing of the CFRP laminate.

Sensor type	Before embedding (με)	After de-bulking (με)	At zone (c) in strain at 70.3 °C (με)	At zone (d) at 107.2 °C (με)	At the end of isothermal dwell at 120 °C (με)	Residual strain at 30 °C (με)
FBG-1 acrylate-coated fibre	0.00	-0.92	-51.80	-49.65	-47.32	56.36
FBG-2 acrylate-coated fibre	0.00	4.58	-24.30	-8.88	-8.29	62.45
FBG-1 stripped fibre	0.00	21.48	---	---	24.42	99.75
FBG-2 stripped fibre	0.00	11.74	---	---	14.88	127.72

As with the previous cases, a post cure heating/cooling cycle was carried out on this composite. The development of strain of the laminate during the post cure temperature cycle is shown in Figure 4.56. The acrylate-coated fibres showed the change in slope of the FBG strain output in the region 40-68.7 °C. However, it was not possible to analyse the stripped optical fibres in this region because the signal-to-noise was high. The strain values recorded by the acrylate-coated and the stripped FBGs at different stages of the temperature cycle are summarised in Table 4.13.

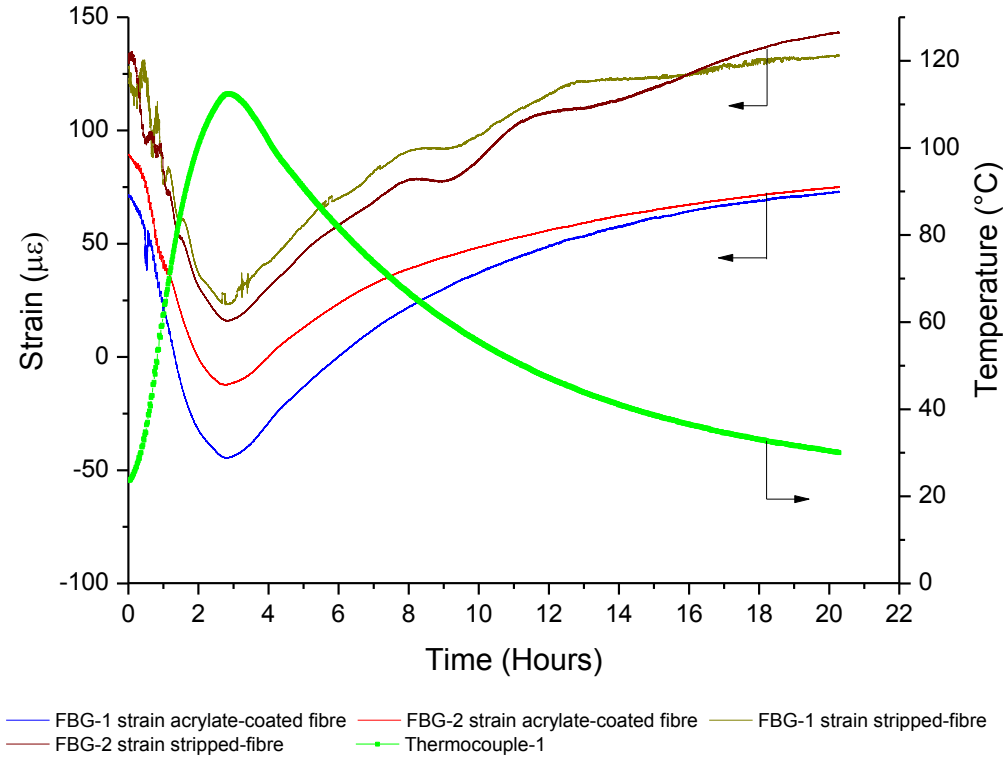

Figure 4.56 The evolution of strain obtained from the acrylate-coated and the stripped FBGs during the post-cure temperature cycle of the CFRP composite.

Table 4.13 Summary of the strain recorded by the acrylate-coated and the stripped FBGs during the post-cure temperature cycle of the CFRP composite.

Sensor type	At the start of the temperature cycle (με)	At 1st slope-change at 68.7 °C (με)	At the end of isothermal dwell at 112.4 °C (με)	Residual strain at 30 °C (με)
FBG-1 acrylate-coated fibre	71.35	16.06	-42.90	78.76
FBG-2 acrylate-coated fibre	89.10	38.15	-10.80	80.68
FBG-1 stripped fibre	121.06	---	27.38	139.38
FBG-2 stripped fibre	132.80	---	17.39	147.45

(b) CFRP laminate embedded with acrylate- and polyimide-coated FBGs

Because of the difficulties in interpreting the FBG strain data from the stripped optical fibres, a further experiment was carried out by embedding the acrylate and polyimide-coated FBGs during the processing of an eight-ply unidirectional CFRP laminate. The data are presented in Figure 4.57. The enlarged view of Figure 4.57 is shown in Figure 4.58.

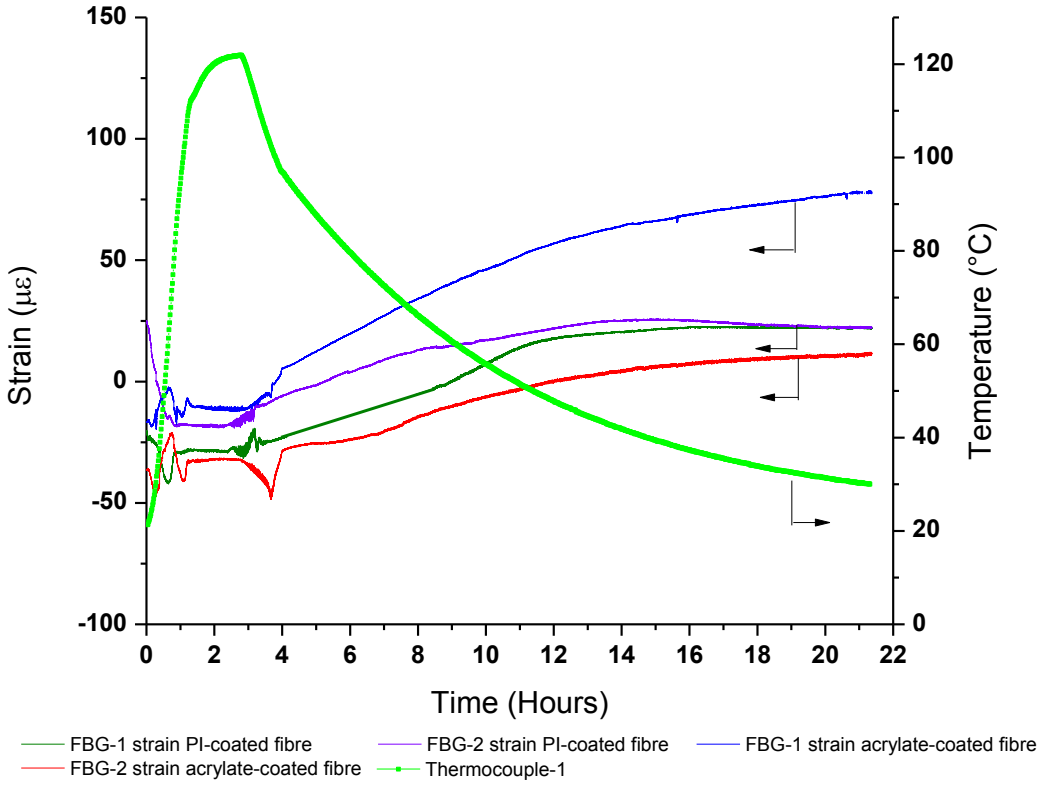

Figure 4.57 The evolution of strain recorded by the acrylate- and polyimide-coated FBGs during the processing of the eight-ply unidirectional CFRP laminate.

With reference to Figure 4.58, the polyimide-coated FBGs showed a relatively steady decrease in the strain as a function of heating in zones (a-c). The acrylate-coated fibres, on the other hand showed a steady-state values in zone (a) followed by an increase in

zone (b) and a decrease in zone (c). In conclusion, this suggests that the acrylate-coating may indeed be responsible for the decrease in the measured strain values in zone (c); this corresponds to a temperature range of 69-98 °C. In zone (d), both the acrylate-coated fibres and one of the polyimide-coated fibres showed a distinct transition in the temperature range 98-114 °C. The onset of cross-linking of the VTM 264 resin system from Figure 4.26 was 110 °C. The strain data at different stages of the cross-linking cycle is summarised in Table 4.14.

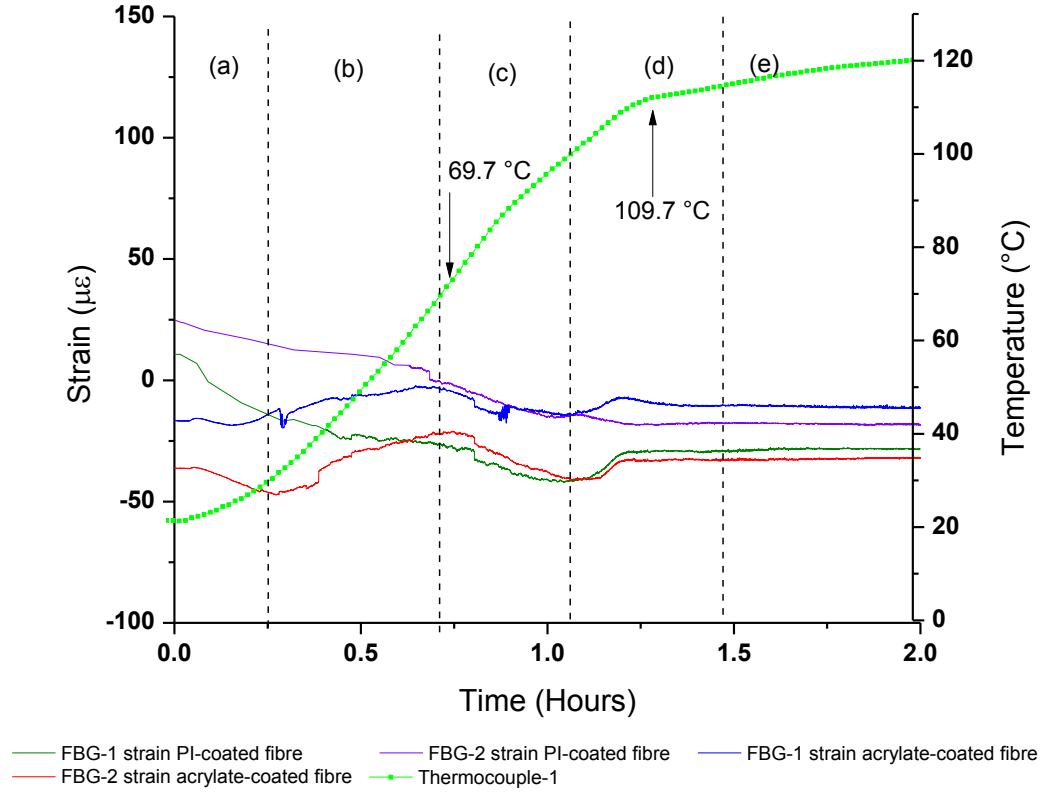

Figure 4.58 The strain recorded by the acrylate- and polyimide-coated FBGs during the heating phase of the processing cycle.

Table 4.14 Summary of the strain recorded by the acrylate- and polyimide-coated FBGs at different stages of processing of the CFRP laminate.

Sensor type	Before embedding (με)	After de-bulking (με)	At zone (c) in strain at 69.7 °C (με)	At zone (d) in strain at 109.7 °C (με)	At the end of isothermal dwell at 120 °C (με)	Residual strain at 30 °C (με)
FBG-1 PI-coated fibre	0.00	10.69	---	-7.51	-11.93	21.80
FBG-2 PI-coated fibre	0.00	24.89	---	-18.12	-17.39	22.28
FBG-1 acrylate-coated fibre	0.00	-16.49	-3.26	-29.86	-27.94	77.43
FBG-2 acrylate-coated fibre	0.00	-36.14	-21.23	-33.39	-33.39	11.90

The cured composite was subjected to a temperature cycle in the autoclave. The maximum temperature recorded by the embedded thermocouple at the middle of the laminate was 113.2 °C. The development of strain recorded by the acrylate and polyimide-coated FBGs during the temperature cycle is shown in Figure 4.59. From Figure 4.59, the strain anomalies caused by the acrylate coating of the FBGs were readily apparent during the heating phase of the temperature cycle as discussed previously. Both the acrylate-coated fibres showed a change in slope in the temperature range 40-70 °C (the temperature rise was linear over this range). However, one of the polyimide-coated fibres also showed a small change in the slope over this temperature range. Although not absolutely conclusive, the indications are that acrylate have some role to play in the observed decrease in the strain data. The strain values recorded by the acrylate- and polyimide-coated FBGs at different stages of the temperature cycle are summarised in Table 4.15.

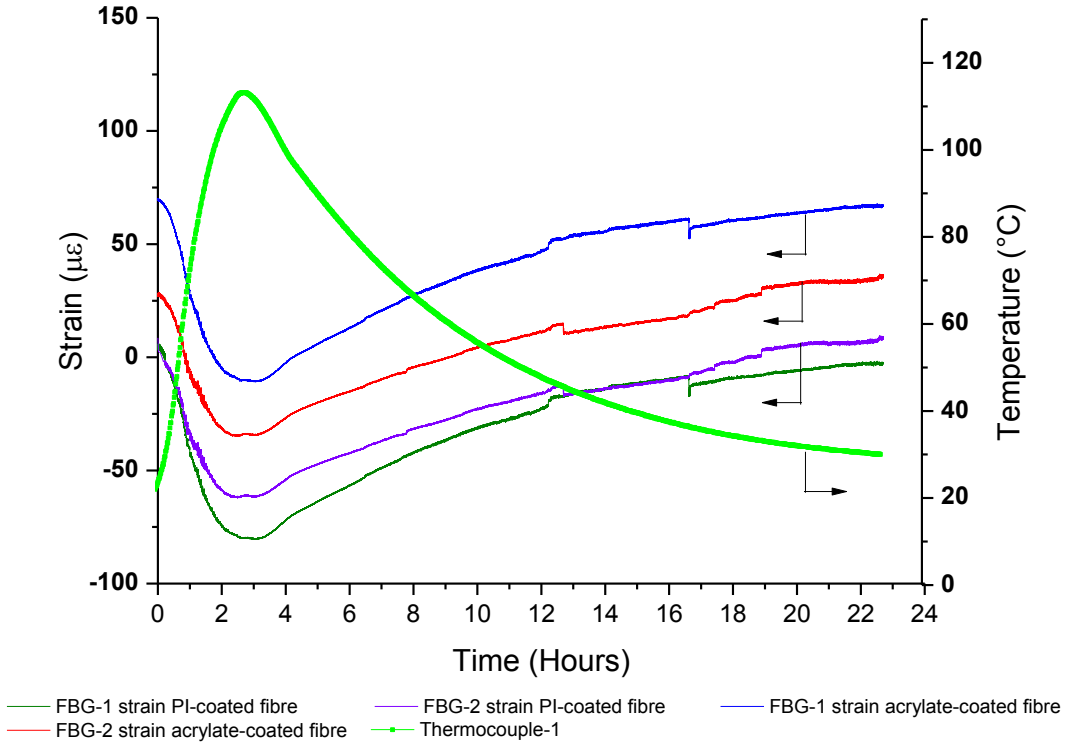

Figure 4.59 The evolution of strain recorded by the acrylate and polyimide-coated FBGs during the post cure temperature cycle of the CFRP composite.

Table 4.15 Summary of the strain values recorded by the acrylate- and polyimide-coated FBGs during the post cure temperature cycle of the CFRP composite.

Sensor type	At the start of the temperature cycle (με)	At 1st slope-change at 69.9 °C (με)	At the end of isothermal dwell at 113.1 °C (με)	Residual strain at 30 °C (με)
FBG-1 PI-coated fibre	5.31	---	-80.15	-2.33
FBG-2 PI-coated fibre	8.54	---	-61.21	8.66
FBG-1 acrylate-coated fibre	69.60	25.71	10.18	67.27
FBG-2 acrylate-coated fibre	27.23	-8.86	-33.47	35.89

4.7.2 E-glass woven fabric laminate

The evolution of strain recorded by the acrylate and polyimide-coated FBGs and the stripped FBGs during the cross-linking of an eight-ply E-glass woven fabric laminate with the LY3505/XB3403 resin system is shown in Figure 4.60. The enlarged view of Figure 4.60 is shown in Figure 4.61.

The acrylate-coated optical fibre with inscribed FBG showed a steady rise in strain in zones (a and b) but only up to 45 °C, after which a significant decrease was observed up to 70 °C. After this point, an exponential increase was seen. The general profile of the strain for the polyimide, stripped and the acrylate-coated optical fibres in zones (c-e) were similar. In the case of two stripped optical fibres, steady-state strain values were recorded. This further supports the belief that the acrylate-coating has an influence on the measured strain by the FBGs as the Tg is approached. It is emphasised that the grating itself was not acrylate-coated and therefore, it is proposed that the reduction in strain transfer from the matrix to the optical fibre acts over the whole length of the embedded fibre. The strain anomaly for the acrylate-coated optical fibre in zone (b) was not observed for the polyimide or stripped optical fibres. The strain data recorded by the acrylate- and polyimide-coated FBGs and stripped FBGs at different stages of the cross-linking cycle is summarised in Table 4.16.

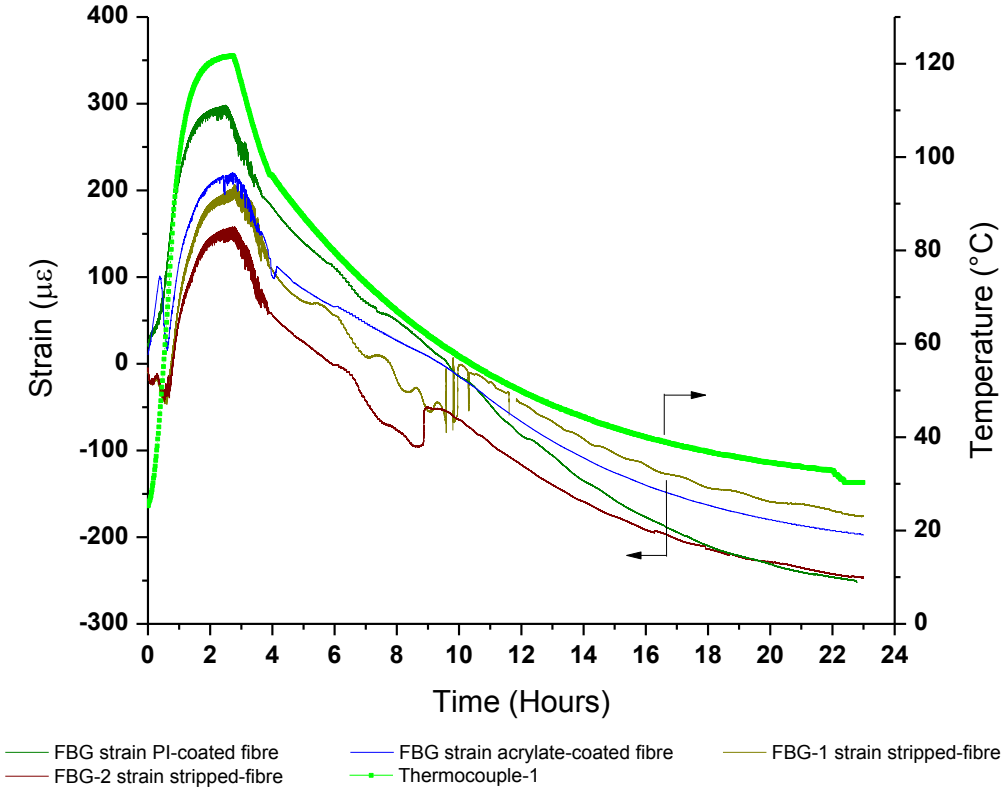

Figure 4.60 The evolution of strain recorded by the acrylate- and polyimide-coated FBGs and stripped FBGs during the processing of the eight-ply woven E-glass fabric laminate.

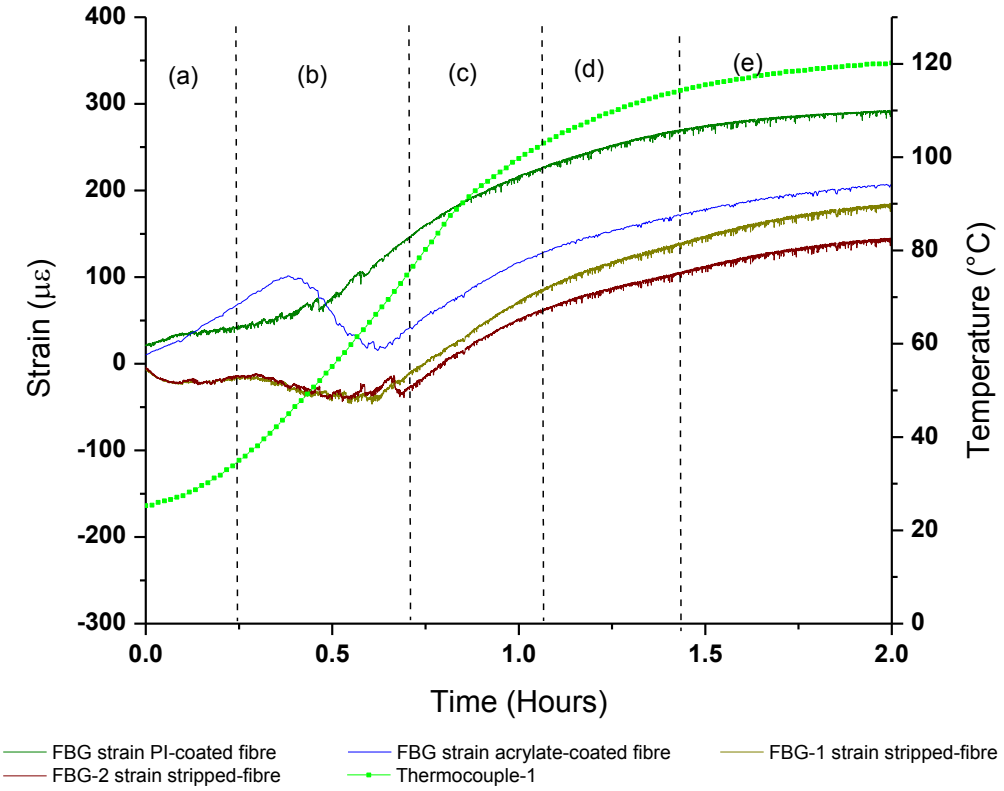

Figure 4.61 The evolution of strain recorded by the acrylate and polyimide-coated FBGs and stripped FBGs during the heating phase of the processing cycle.

Table 4.16 Summary of the strain recorded by the acrylate- and polyimide-coated FBGs and stripped FBGs at different stages of processing of the fabric laminate.

Sensor type	Before embedding (με)	After de-bulking (με)	At first observed drop in strain at 45 °C (με)	Min. at drop (με)	Max. at first recovery (με)	At the end of isothermal dwell at 120 °C (με)	Residual strain at 30 °C (με)
FBG PI-coated fibre	0.00	20.77	---	---	283.47	296.44	-251.80
FBG acrylate-coated fibre	0.00	10.22	101.35	15.35	197.89	220.55	-197.76
FBG-1 stripped-fibre	0.00	-6.41	---	---	172.02	208.88	-176.09
FBG-2 stripped fibre	0.00	-3.75	---	---	128.35	149.16	-246.70

5 CONCLUSIONS AND RECOMMENDATIONS FOR FUTURE RESEARCH

5.1 Conclusions

The key focus of this research programme was to design and deploy a multi-measurand optical fibre sensor for the autoclave-based processing of composite materials. The multi-measurand sensor reported in this study was based on the EFPI strain sensor design but with the added functionality to monitor temperature, refractive index and the relative concentrations of specified chemicals. A unique feature of the multi-measurand sensor was that the interrogation of the four measurands was carried out using a multiport fibre-coupled FTNIR spectrometer. Another advantage of the current design is that unlike conventional EFPI/FBG combination sensors, it negates the need for deconvoluting the EFPI/FBG signals.

Prior to the deployment of the multi-measurand sensor for process monitoring, a systematic study was carried out to optimise the sensor design and the process parameters. The output characteristics of the individual sensors and their associated instruments were studied in detail. The optical fibre sensors used in this research programme were: (i) extrinsic Fabry-Perot interferometric sensor, (ii) fibre Bragg grating sensor, (iii) chemical sensor, (iv) Fresnel sensor and (v) multi-measurand sensor.

A unique advantage of the optical fibre sensor systems is that in addition to process monitoring, the same devices can be used for structural health monitoring purposes. In the context of the current work, the processing and post-processing of unidirectional CFRP and woven E-glass fabric performs were monitored using embedded FBG (strain and temperature) and multi-meaurand sensors.

The overall conclusions drawn from the results reported in Chapter 4 are summarised below.

5.1.1 Optimisation of the multi-measurand sensor

(i) End-face quality of the capillary: This was important in the fabrication of MMS as one end-face of the capillary was used as the reflective surface for the chemical sensor. Therefore, a systematic procedure was adopted to ensure the quality and consistency of the cleaved end-face of the capillary. The ultrasonic and electric arc-cleaning techniques used on the cleaved capillary were found to be satisfactory in achieving the repeatability and consistency.

(ii) FTNIR spectroscopy-based interrogation and data acquisition parameters: The optimum resolution and number of scans for the individual sensors were defined. An ASE light source was used for the primary EFPI and FBG sensors whereas FTNIR spectrometer internal light source was used for the secondary chemical and Fresnel sensors. This was necessary as the spectrometer was designed to operate with multi-mode optical fibres. The EFPI and FBG sensors were interrogated at a resolution of 4

cm^{-1} (0.96 nm) and 1 cm^{-1} (0.24 nm) respectively over 16 scans. The chemical and Fresnel sensors were interrogated at a resolution of 4 cm^{-1} over 64 scans.

(iii) Annealing the gold/palladium coatings: A series of experiments were carried out to establish the annealing conditions for the Au/Pd-coated end-face of the FBG sensor and the capillary. The stabilisation of the reflective coating on the cleaved optical fibres and the effect of reflective coating on the output of EFPI and FBG sensors on temperature cycles were investigated. The thermally-induced changes in the cavity length of the EFPI sensors were relatively low due to the fact that the free-ends of the silica fibres and the capillary undergo thermal expansions in opposite directions. The temperature sensitivity for the FBG sensors measured via the FTNIR spectrometer was in the range of 9.5 – 10.2 pm $^{o}C^{-1}$. Based on the findings from these experiments, the annealing condition was chosen as 150 °C for 12 hours.

(iv) Effect of plasma exposure on FBG sensor: It was necessary that the FBG sensors had to undergo a plasma exposure as part of the sputter-coating of their cleaved end-faces. It was found that the output of the FBG sensors was not affected by the plasma exposure.

(v) Effect of clamping stress on the response of the FBG sensor: Clamping stress exerted by the magnetic clamps of the micro-translation stage on FBG peak wavelength during fabrication was studied. An appropriate clamping stress was required to establish good contact and alignment of the optical fibre with the phase-mask during the fabrication of the sensor. No residual stress was observed on the sensor once the clamp was removed.

(vi) Secondary fibre alignment on the translation stage: It was essential to establish optimum alignment of the secondary fibres with the gold-coated end-face of the capillary as part of the fabrication of the chemical sensor. Very good alignments of the secondary fibres were achieved over a gap length of 500 μm set-gap.

5.1.2 Process monitoring of a CFRP laminate using multiplexed FBGs

The evolution of strain and temperature during the cross-linking of the eight-ply unidirectional CFRP laminate were monitored using multiplexed FBG sensors. Capillary-sealed FBG sensors were used to de-couple temperature from strain. The sensors were embedded at different locations between the 4^{th} and 5^{th} plies of the laminate in line with the fibre direction and interrogated using FiberPro. Two tensile-compressive strain transitions were observed during the heating phase of the cross-linking cycle: the first transition was due to the deformation caused by the glass transition temperature of the acrylate-coating on the optical fibre sensors and the second transition was due to the onset of the glass transition temperature of the VTM264 resin system. The glass transition temperatures of the acrylate-coating on the optical fibres and the resin system were measured using DSC. The final residual strain values at different locations in the mid-plane of an eight-ply CFRP laminate were found to be different. The sensors were successful in monitoring the localised mid-plane strain of the laminate. Data obtained from the FBG temperature sensors showed good correlation with the data obtained from the embedded thermocouples.

5.1.3 Process monitoring of a CFRP laminate using FBG and Fresnel sensors

FBG (strain and temperature) sensors and Fresnel sensors were embedded between the 1st and 2nd, 4th and 5th and 7th and 8th plies of the eight-ply unidirectional CFRP laminate. The development of strain and temperature was monitored using FBG sensors whereas the cure progression was monitored using the Fresnel sensors. A lower tensile residual strain was observed in the mid-plane of the laminate as compared to the bottom and top plies when the laminate was cooled back to 30 °C. Similar findings were observed from the data obtained from the Fresnel reflection sensors. However, the Fresnel reflections recorded by the sensors were not only a representative of the cross-linking process but a resultant of the processing parameters as well.

The cured CFRP composite was subjected to (a) vacuum cycle (b) temperature cycle (c) pressure cycle and (d) normal cure cycle. It was observed that there was little/no influence of vacuum and pressure on the cured composite. The strain developed during the temperature cycle and the normal cure cycle showed similar behaviour of the cross-linking cycle.

5.1.4 Process monitoring of fabric laminates using the MMS

A multi-measurand sensor was embedded between the 4th and 5th plies of the eight-ply E-glass woven fabric laminate and the evolution of strain, temperature, Fresnel reflection and the relative concentration of the resin system during the processing of the laminate were monitored simultaneously. An independent FBG (strain and temperature) sensor was also embedded alongside the MMS and interrogated using an FBG

interrogation unit. MMS was capable for monitoring all the four measurands successfully.

At the time of writing, the author is not aware of any previous publications where an embedded multi-measurand sensor was used to monitor four measurands simultaneously using a single interrogation unit. Similar to the CFRP laminate, strain anomalies was observed here as well during the heating phase of the cross-linking cycle. This was possibly due to the deformation/relaxation caused by the glass transition temperature of the acrylate-coating of the optical fibre sensors and the LY3505/XB3403 resin system. FBG temperature (MMS) showed good correlation with the data obtained from independent FBG temperature sensor and embedded thermocouples. However, the lower wavelength resolution of the FTNIR spectrometer had an effect on tracking minor changes of the FBG peak wavelength as a function of temperature.

The chemical sensor (MMS) successfully tracked the depletion of the epoxy, primary and secondary amine functional groups in the resin system. The epoxy cross-linking conversion data obtained from the chemical sensor was compared with the data obtained from the Fresnel sensor and a good correlation was observed.

The outputs of the secondary cavities (chemical sensor) on the MMS were compared with isothermal cure kinetic data generated from cuvette-based experiments in conjunction with conventional transmission near-infrared spectroscopy. The experiment was carried out at 50, 60 and 70 °C. The epoxy cross-linking conversion data obtained

using the chemical sensor was compared with the data obtained using the conventional transmission spectroscopy at each temperature and good agreements between the two data sets were observed.

The cured fabric composite was subjected to temperature cycles and the development of strain was monitored simultaneously using EFPI (MMS) sensor and the independent FBG sensor. Similar to the cross-linking cycle, strain anomalies were observed in the heating phase of the three temperature cycles.

5.1.5 Strain anomalies of acrylate-coated photo-sensitive fibres

It was essential to study the strain anomalies caused by the acrylate-coating of the photo-sensitive fibres. Acrylate-coated FBGs, stripped FBGs and polyimide-coated FBGs were embedded in the eight-ply unidirectional CFRP and woven fabric laminates. The evolution of strain during the processing and post-processing of the laminates were monitored. It was found that the strain anomalies were absent when the strain recorded using PI-coated FBGs. This further confirmed the strain anomalies may have been caused by the acrylate-coating of the optical fibre especially during the heating phase of the cross-linking cycle.

5.2 Recommendations for future research

Following are the suggestions for continuing the research:

(i) MMS sensor design: In the current MMS design, the strain was measured using the EFPI sensor. An additional secondary optical fibre with a fibre Bragg grating secured on the primary single-mode SMF-28^{TM} optical fibre would help to cross-correlate the strain data recorded by the EFPI and the FBG sensors. Currently this was done by embedding independent FBG strain and temperature sensors in close proximity to the MMS sensor.

(ii) High resolution FTNIR spectrometer for MMS interrogation: The optimum resolution of the FTNIR used in this study was 1 cm^{-1} (0.24 nm). However, this resolution was not sufficient to track the minor peak wavelength shift of the FBG temperature sensors effectively as opposed to the 1 pm resolution of the independent FBG interrogation unit (FiberPro).

(iii) Process monitoring of other composites manufacturing techniques: In addition to the autoclave-based process monitoring, it would be beneficial to extend the use of optical fibre sensors for other manufacturing techniques such as pultrusion, filament winding and resin transfer moulding.

(iv) Process monitoring of rubber compounds/fabrics used for the manufacture of aircraft tyres: There is a growing demand in the tyre industry for the static and dynamic monitoring of tyre manufacturing process parameters. The measurands of interest are

strain, temperature, cross-linking kinetics and pressure. Currently these are monitored using the basic conventional techniques. The optical fibre sensor technology would be really beneficial in this area to tackle the design/production-related issues and this will be particularly useful for the development of next-generation light weight aircraft radial tyres.

REFERENCES

1. Boger, L., Wiichmann, M.H.G., Meyer, L.O. and Shulte, K. “Load and health monitoring in glass fibre reinforced composites with an electrically conductive nanocomposite epoxy matrix”, Composites Science and Technology, 68, (2008), 1886-1894.
2. Fernando, G. F., Crosby, P. A. and Liu, T. "The application of optical fibre sensors in advanced fibre reinforced composites: Chapter 2 - Introduction and issues", Optical Fibre Sensor Technology, Volume III, Edited by K. T. V. Grattan and B. T. Meggitt. Publisher: Kluwer Academic Publishers (1999), ISBN 0412825708.
3. Hull, D. “An introduction to composite materials”, (1981), Cambridge University Press.
4. Fernando, G.F. and Degamber, B. “Process monitoring of fibre reinforced composites using optical fibre sensors”, International Materials Reviews, 51, (2006), 65-106.
5. Fernando, G.F. “Fibre optic sensor systems for monitoring composite structures”, RP Asia Conference, (2005).
6. Kim, K.S. and Hahn, H.T. “Residual stress development during processing of graphite/epoxy composites”, Composites Science and Technology, 36, (1989), 121-132.
7. Jones, F.R. “Laminates – residual thermal and related strains”, Handbook of Polymer-Fibre Composites, Jones, F.R. Ed., ISBN 0-582-06554-2, (1994), 254-260.

8. Leng, J. and Asundi, A. “Structural health monitoring of smart composite materials by using EFPI and FBG sensors”, Sensors and Actuators A, 103, (2003), 330-340.
9. Brydson, J.A. “Plastic Materials”, 6th edition, (1995), Butterworth Heinemann.
10. Rao, Y-J. “In-fibre Bragg grating sensors”, Measurement Science and Technology, 8, (1997), 355-375.
11. Rao, Y-J. “Recent progress in applications of in-fibre Bragg grating sensors”, Optics and Lasers in Engineering, 31, (1999), 297-324.
12. Marand, E., Baker, K.R. and Graybeal, J.D. “Comparisons of reaction mechanisms of epoxy resins undergoing thermal and microwave cure from in-situ measurements of microwave dielectric properties and infrared spectroscopy”, Macromolecules, 25, (1992), 2243-2252.
13. Smith, I.T. “The mechanism of cross-linking of epoxide resins by amines”, Polymer, 2, (1961), 95-108.
14. Gough, L.J. and Smith, I.T. “A Gel point method for the estimation of overall apparent activation energies of polymerisation”, Journal of Applied Polymer Science, 3, 9, (1960), 362-364.
15. Jones, F. R. “Epoxy resins” in Handbook of Polymer-Fibre Composites, Jones, F.R. Ed., ISBN 0-582-06554-2, (1994), 86-96.
16. Bar, H., Narkis, M. and Boiteux, G. “The electrical behaviour of thermosetting polymer composites containing metal plated ceramic filler”, Polymer Composites, 26, (2005), 12-19.

17. Almusallam, A. A., Khan, F. M., Dulaijan, S. U. and Al-Amoudi, O. S. B. "Effectiveness of surface coatings in improving concrete durability", Cement and Concrete Composites, 25, (2003), 473-481.
18. Abdel-Magid, B., Ziaee, S., Gass, K. and Schneider, M. "The combined effect of load, moisture and temperature on the properties of E-glass/epoxy composites", Composite Structures, 71, (2005), 320-326.
19. Colpo, F., Humbert, L., Giaccari, P. and Botsis, J. "Characterisation of residual strains in an epoxy block using an embedded FBG sensor and the OLCR technique", Composites: Part A, 37, (2006), 652-661.
20. Mika, T. F. and Bauer, R. S. "Curing agents and modifiers", in May, C. A., Ed. Epoxy Resins: Chemistry and Technology", 2nd Edition, California, USA, CRC Press, (1988), 465-550.
21. Martin, G. C., Tungare, A. V. and Gotro, J. T. "Modelling rheological and dielectric properties during thermoset cure", in Craver C. D. and Provder T., Ed. Polymer Characterisation, Washington, America Chemical Society, (1990), 235-248.
22. Etches, J.A. and Fernando, G.F. "Evaluation of embedded optical fibre sensors in composites: EFPI sensor fabrication and quasi-static evaluation", Polymer Composites, (2008), 1-10.
23. Degamber, B. and Fernando, G.F. "Microwave processing of thermosets: non-contact cure monitoring and fibre optic temperature sensors", Journal of Plastics, Rubber and Composites, (2003), 32(8/9): 327-33.

24. Fernando, G.F., Liu, T., Crosby, P., Doyle, C., Martin, A., Brooks, D., Ralph, B. and Badcock, R. “A multi-purpose optical fibre sensor design for fibre reinforced composite materials”, Measurement Science and Technology, 8, (1997), 1065-79.

25. Crosby, P., Powell, G.R., Fernando, G.F., Spooncer, R.C., France, C.M. and Waters, D.N. “*In-situ* cure monitoring in advanced composites using evanescent wave spectroscopy”, Journal of Smart Materials and Structures, 5, (1996), 415-28.

26. Oliveira, R.D., Lavanchy, S. and Mansion, J.-A.E. “Experimental investigation of the effect of the mould thermal expansion on the development of internal stresses during carbon fibre composite processing”, Composite Part-A, 39, (2008), 1083-1090.

27. Oliveira, R.D., Ramos, C.A. and Marques, A.T. “Health monitoring of composite structures by embedded FBG and interferometric Fabry-Perot sensors”, Computers and Structures, 86, (2008), 340-346.

28. Fernlund, G., Rahman, N., Courdji, R., Bresslauer, M., Poursartip, A., Willden, K. and Nelson, K. “Experimental and numerical study of the effect of cure cycle, tool surface, geometry, and lay-up on the dimensional fidelity of autoclave-processed composite parts”, Composites - Part A: Applied Science and Manufacturing, 33, 3, (2002), 341-351.

29. Shah, D.U. and Schubel, P.J. “Evaluation of cure shrinkage measurement techniques for thermosetting resins”, Polymer Testing, 29, 6, (2010), 629-639.

30. Wild, G. and Hinckley, S. “Acousto-ultrasonic optical fibre sensors: Overview and state of the art”, IEEE Sensors Journal, 8, 7, (2008).

31. Jinno, M., Sakai, S., Osaka, K. and Fukuda, T. ‘‘Smart autoclave processing of thermoset resin matrix composites based on temperature and internal strain monitoring’’, Advanced Composite Materials, 12 (1), (2003), 57-72.
32. Zhao, J.H., Shi, Y.K., Shan, N. and Yuan, X.Q. “Stabilised fibre-optic extrinsic Fabry-Perot sensor system for acoustic emission measurement”, Optics and Laser Technology, 40, (2008), 874-880.
33. Clark, P., Boriniski, J., Gunther, M. and Poland, S. “Modern fibre optic sensors”, Smart Materials Bulletin, (2001), 8-11.
34. King, M.H. “Smart structures through embedding optical fibre strain sensing”, Smart Materials Bulletin, (2001).
35. Park, J-M., Lee, S-Il., Kwon, O-Y., Choai, H-S. and Lee, J-H. “Comparison of non-destructive micro failure evaluation of Bragg grating and acoustic emission piezo-electric sensors using fragmentation test”, Composites: Part- A, 34, (2003), 203-216.
36. Murukeshan, V.M., Chan, P.Y., Ong, L.S. and Seah, L.K. “Cure monitoring of smart composites using fibre bragg gratings based embedded sensors”, Sensors and Actuators, 79, (2000), 153-161.
37. Lawrence, C.M., Nelson, D.V., Bennett, T.E. and Spingarn, J.R. ‘‘An embedded fibre optic-sensor method for determining residual stresses in fibre-reinforced composite materials’’, Journal of Intelligent Material Systems and Structures, 9, (1998), 788-799.
38. Ehlers, J–E., Rondan, N.G., Huynh, L.K., Pham, H., Marks, M. and Truong, T.N. “Theoretical study on mechanisms of the epoxy – amine curing reaction”, Macromolecules, 40, (2007), 4370-4377.

39. Narendran, N., Zhou, C., Letcher, S. and Shukla, A. “Fibre optic sensor for non-destructive evaluation”, Optics and Lasers in Engineering, 22 (1995), 137 – 148.
40. Singh, M., Tuck, C.J. and Fernando, G.F. “Multiplexed optical fibre fabry – perot sensors for strain metrology”, Smart Materials and Structures, 8, (1999), 549-553.
41. Silva, S.F.O., Frazao, O., Santos, J.L., Araujo, F.M. and Ferreira, L.A. “Fibre Bragg grating structure in a braid twisted configuration for sensing applications”, Journal of Optics A: Pure and Applied Optics, 10, (2008).
42. Lachenal, G., Stevenson, I., Durand, A., Seytre, G.and Bertrand, D. “Ambiguity in assignment of near infrared vibrational bands for polymerisation monitoring of epoxy system”, Macromolecular Symposia, 265, (2008), 249-259.
43. George, G.A., Cash, G.A. and Rintoul, L. “Cure monitoring of aerospace epoxy resins and prepregs by FTIR emission spectroscopy”, Polymer International, 41, (1996), 169-182.
44. Chen, R., Fernando, G.F., Butler, T. and Badcock, R.A. “A novel ultrasound fibre optic sensor based on a fused tapered optical fibre coupler”, Measurement Science and Technology, 15, (2004), 1490-1495.
45. Kuang, K.S.C., Kenny, R., Whelan, M.P., Cantwell, W.J. and Chalker, R.R. “Embedded fibre Bragg grating sensors in advanced composite materials”, Composite Science and Technology, 61, (2001), 1379-1387.
46. Mulle, M., Collombet, F., Olivier, P. and Grunevald, Y-H. ‘‘Assessment of cure residual strains through the thickness of carbon-epoxy laminates using FBGs Part 1: Elementary specimen’’, Composites: Part A, 40, (2009), 94-104.

47. Montanini, R. and D'Acquisto, L. ''Simultaneous measurement of temperature and strain in glass fibre/epoxy composites by embedded fibre optic sensors: I. Cure monitoring'', Smart Materials and Structures, 16, (2007), 1718-1726.

48. Kang, S.G., Kang, D.H. and Kim, C.G. ''Real-time monitoring of transverse thermal strain of carbon fibre reinforced composites under long-term space environment using fibre optic sensors'', NDT&E International, 42, (2009), 361-368.

49. Antonucci, V., Girordano, M., Cusano, A., Nasser, J. and Nicolais, L. ''Real time monitoring of cure and gelification of a thermoset matrix'', Composites Science and Technology, 66, (2006), 3273-3280

50. Kang, H-U., Kang, D-H., Bang, H-J., Hong, C-S. and Kim, C-G. ''Cure monitoring of composite laminates using fibre optic sensors'' Smart Materials and Structures, 11, (2002), 279-287

51. Dewynter-Marty, V., Ferdinand, P., Bocherens, E., Carbone, R., Beranger, H., Bourasseau, S., Dupont, M. and Balageas, D. "Embedded Fiber Bragg Grating sensors for industrial composite cure monitoring", Journal of Intelligent Material Systems and Structures, 9, 10, (1998), 785-787.

52. Ito, Y., Minakuchi, S., Mizutani, T. and Takeda, N. "Cure monitoring of carbon-epoxy composites by optical fiber-based distributed strain-temperature sensing system", Advanced Composite Materials, 21, 3, (2012), 259-271.

53. Yoon, H.J., Costantini, D.M., Limberger, H.G., Salathe, R.P., Kim, C.G. and Michaud, V. "In-situ strain and temperature monitoring of adaptive composite materials", Journal of Intelligent Material Systems and Structures, 17, (2006), 1059-1067.

54. Bogetti, T.A. “Process-induced stress and deformation in thick-section thermoset composite laminates”, Journal of Composite Materials, 26, 5, (1992), 626-660.

55. Kang, H.K., Kang, D.H., Hong, C.S. and Kim, C.G. “Simultaneous monitoring of strain and temperature during and after cure of unsymmetric composite laminate using fibre-optic sensors”, Smart Materials and Structures, 12, (2003), 29-35.

56. Liu, T., Wu, M., Rao, Y., Jackson, D.A. and Fernando, G.F. “A multiplexed optical fibre based extrinsic Fabry Perot sensor system for in-situ strain monitoring in composites”, Smart Materials and Structures, 7, (1998), 550-556.

57. Pal, S., Sun, T., Grattan, K.T.V., Wade, S., Collins, S.F., Baxter, G.W., Dussardier, B. and Monnom, G. “Non-linear termperature dependance of Bragg gratings written in different fibres, optimised for sensor applications over a wide range of temperatures”, Sensors and Actuators A, 112, (2004), 211-219.

58. Rao, Y.J., Henderson, P.J., Jackson, D.A., Zhang, L. and Bennion, I. “Simultaneous strain, temperature and vibration measurement using a multiplexed in-fibre-Bragg-grating/fibre-Fabry-Perot sensor system”, Electronics Letters, 33, 24, (1997), 2063-2064.

59. Rao, Y.J., Ran, Z.L., Liao, X. and Deng,H.Y. “Hybrid LPFG/MEFPI sensor for simultaneous measurement of high-temperature and strain”, Optics Express, 15, (2007), 14936-14941.

60. Liu, T., Fernando, G.F., Zhang, Z.Y., and Grattan, K.T.V. “Simultaneous strain and temperature measurements in composites using extrinsic Fabry-Perot interferometric and intrinsic rare-earth doped fiber sensors”, Sensors and Actuators A-Physical, 80, 3, (2000), 208-215.

61. Liu, T., Fernando, G.F., Rao, Y.J., Jackson, D.A., Zhang, L. and Bennion, I. "Simultaneous strain and temperature measurements in composites using a multiplexed fiber Bragg grating sensor and an extrinsic Fabry-Perot sensor," Proceedings of SPIE, 3042, (1997), 203-212.
62. Powell, G.R., Crossby, P.A., Waters, D.N., France, C.M., Spooncer, R.C.and Fernando, G.F. "*In-situ* cure monitoring using optical fibre sensors - a comparative study", Smart Materials and Structures, 7, (1998), 557-568.
63. Martin, A., Badcock, R., Nightingale, C. and Fernando, G.F. "A novel optical fibre based strain sensor", IEEE Photonics Technology Letters, 9, (1997), 982-984.
64. Zhao, J-H., Shi, Y., Shan, N. and Yuan, X. "Stabilised fibre optic extrinsic Fabry-Perot sensor system for acoustic emission measurement", Optics and Laser Technology, 40, (2008), 874-880.
65. Read, I., Foote, P.and Murray, S. "Optical fibre acoustic emission for damage detection in carbon fibre composite structures", Measurement Science and Technology, 13, (2002), N5-N9.
66. Vieira, A., Oliveira, R.D., Frazao, O., Baptista, J.M. and Marques, A.T. **"**Effect of the recoating and the length on fibre Bragg grating sensors embedded in polymer composites", Materials and Design, 30, (2009), 1818-1821.
67. Lee, J-R. and Tsuda, H. "A novel fibre Bragg grating acoustic emission sensor head for mechanical tests", Scripta Materialia, 53, (2005), 1181-1186.
68. Chen, R., Fernando, G.F., Butler, T. and Badcock, R.A. "A novel ultrasound fibre optic sensor based on a fused tapered optical fibre coupler", Measurement Science and Technology, 15, (2004), 1490-1495.

69. Degamber, B. and Fernando, G.F. “Fibre optic dilato-spectroscopic sensor: simultaneous thermal, spectral and physical analyses of materials”, Smart Materials and Structures, 15, (2006), 1054-1062.

70. Haddad, E., Kruzelecky, R., Zou, J., Wong, B., Mohammad, N., Thatte, G., Jamroz, W. and Riendeau, S. “Innovative embedded fibre sensor system for spacecraft’s health in-situ monitoring”, Proceedings of 9th International Conference: Protection of materials and structures from space environment, Edited by Kleiman, J.I., (2009), 463-474.

71. Betz, D.C., Thursby, G., Culshaw, B. and Staszewski, W.J. “Acousto-ultrasonic sensing using fibre Bragg gratings”, Smart Materials and Structures, 12, (2003), 122-128.

72. Hsieh, C.S., Wu, T.L. and Cheng, W.H. “An optimum approach for fabrication of low loss fused tapered couplers”, Materials Chemistry and Physics, 69, (2001), 199-203.

73. Surgeon, M. and Wevers, M. “Modal analysis of acoustic emission signals from CFRP laminates”, NDT&E International, 32, (1999), 311-322.

74. Guan B-O., Tam, H-Y., Ho, S-L., Chung, W-H. and Dong, X-Y. “Simultaneous strain temperature measurement using a single fibre Bragg grating”, Electronics Letters, 36, 12, (2000), 1018-1019.

75. James, S.W., Dockney, M.L. and Tatam, R.P. “Simultaneous independent temperature and strain measurement using in-fibre Bragg grating sensors”, Electronics Letters, 32, 12, (1996), 1133-1134.

76. Bremer, K., Lewis, E., Mossi, B., Leem, G., Lochmann, S. and Muller, L. "Conception and preliminary evaluation of an optical fibre sensor for simultaneous measurement of pressure and temperature", Journal of Physics: Conference Series, 178, (2009), 1-4.
77. Bae, H. and Yu, M. "Miniature Fabry-Perot pressure sensor created by using UV-moulding process with an optical fibre based mould", Optics Express, 20, (2012) 14573-14583.
78. Poisson, N., Lachenal, G. and Sautereau, H. "Near and mid-infrared spectroscopy studies of an epoxy reactive system", Vibration Spectroscopy, 12, (1996), 237-247.
79. Mijovic, J. and Andjelic, S. "Monitoring of reactive processing by remote mid infra-red spectroscopy", Polymer, 37, (1996), 1295-1303.
80. Mahendran, R. S., Wang, L., Machavaram, V. R., Chen, R., Kukureka, S. N. and Fernando, G. F. "Fibre optic sensor design for chemical process and environmental monitoring", Optics and Laser Engineering, 47, (2009), 1069-1076.
81. Majumdar, M., Gangopadhyay, T.K., Chakraborty, A.K., Dasgupta, K. and Bhattacharya, D.K. "Fibre Bragg gratings in structural health monitoring-Present status and applications", Sensors and Actuators A, 147, (2008), 150-164.
82. Thursby, G., Culshaw, B., Botsev, Y., Arad, E., Zeyde, R., Tur, M. and Kressel, I. "The use of fibre Bragg gratings to detect ultrasound in anisotropic materials", Proceedings of SPIE, 6933, (2008).
83. Finzel, M. C., Delong, J. and Hawley, M. C. "Effect of stoichiometry and diffusion on an epoxy/amine reaction mechanism", Polymer Science: Part A, 33, (1995), 673-689.

84. George, G. A., Cole-Clarke, P., St. John, N. A. and Friend G. “Real-time monitoring of the cure reaction of a TGDDM/DDS epoxy resin using fibre optic FTIR”, Journal of Applied Polymer Science, 42, (1991), 643-657.

85. Harris, D. and Fernando, G. F. “Simultaneous acquisition of data on refractive index, strain, temperature and cross-linking kinetics”, International Conference on Composite Materials, ICCM-17, Edinburgh, UK, (2009).

86. Lam, K.Y. and Afromowitz, M.A. “Fiber-optic epoxy composite cure sensor. I. Dependence of refractive index of an autocatalytic reaction epoxy system at 850 nm on temperature and extent of cure”, Applied Optics, 34, 25, (1995), 5635-5638.

87. Machavaram, R. V., Badcock, R. A. and Fernando, G. F. “F-2-laser ablation of Fabry-Perot cavities in optical fibres: chemical sensors”, Journal of Optics A: Pure and Applied Optics, 14, 3, (2012).

88. Dunkers, J.P., Lenhart, J.L., Kueh, S.R., Van Zanten, J.H., Advani, S.G. and Parnas, R.S. “Fiber optic flow and cure sensing for liquid composite molding”, Optics and Lasers in Engineering, 35, 2, (2001), 91-104.

89. Crosby, P.A., Powell, G.R., Fernando, G.F., France, C.M., Waters, D.N. and Spooncer, R.C. “Cure monitoring of epoxy resins using optical fibre sensors”, Sensors and their Applications VII, Institute of Physics, Dublin, (1995).

90. Cusano, A., Breglio, G., Giordano, M., Calabro, A., Cutolo, A. and Nicolais, L. “An optoelectronic sensor for cure monitoring in thermoset-based composites”, Sensors and Actuators A, 84, (2000), 270-275.

91. Vacher, S., Molimard, J., Gagnaire, H.and Vautrin, A. “A Fresnel reflection optical fiber sensor for thermoset polymer cure monitoring”, Polymers and Polymer Composites, 12, (2004), 269-276.

92. Liu, Y.M., Ganesh, C., Steele, J.P.H.and Jones, J.E. “Fiber optic sensor development for real-time *in-situ* epoxy cure monitoring”, Journal of Composite Materials, 31, (1996), 87-102.

93. Aduriz, X.A., Lupi, C., Boyard, N., Bailleul, J.L., Leduc, D., Sobotka, V., Lefevre, N., Chapeleau, X., Boisrobert, C. and Delaunay, D. “Quantitative control of RTM6 epoxy resin polymerisation by optical index determination”, Composite Science and Technology, 67, (2007), 3196-3201.

94. Mouritz, A.P., Gellert, E., Burchill, P. and Challis, K. “Review of advanced composite structures for naval ships and submarines”, Composite Structures, 53, (2001), 21-41.

95. Wang, L., Pandita, S. D., Machavaram, V. R., Malik, S. A., Harris, D. and Fernando, G. F. “Characterisation of the cross-linking process in an E-glass fibre/epoxy composite using evanescent wave spectroscopy”, Composite Science and Technology, 69, (2009), 2069-2074.

96. Ferreira, L.A., Lobo Ribeiro, A.B., Santos, J.L. and Farahi, F. “Simultaneous displacement and temperature sensing using white light interrogated low-finesse cavity in line with a fibre Bragg grating”, Smart Materials and Structures, 7, (1998), 189-198.

97. Machavaram, V. R., Badcock, R. A. and Fernando, G. F. “Fabrication of intrinsic fibre Fabry-Perot cavities in silica optical fibres via F2-laser ablation”, Measurement Science and Technology, 18, (2007), 928-934.

98. Machavaram, V. R., Badcock, R. A. and Fernando, G. F. “Fabrication of intrinsic Fabry-Perot sensors in silica fibres using hydrofluoric acid etching”, Sensors and Actuators, A- Physical, 138, (2007), 248-260.

99. Li, L., Tong, X.L., Zhou, C.M., Wen, H.Q., Lv, D.J., Ling, K. and Wen, C.S. “Integration of miniature Fabry-Perot fiber optic sensor with FBG for the measurement of temperature and strain”, Optics Communications, 284, (2011), 1612-1615.

100. Jin, X.D., Sirkis, J.S., Chung, J.K. and Venkat,V.S. “Embedded in-line fibre etalon/Bragg grating hybrid sensor to measure strain and temperature in a composite beam”, Journal of Intelligent Material Systems and Structures, 9, (1998), 171-181.

101. Cusano, A., Bregelio, G., Giordano, M., Nicolais, L. and Cutolo, A. “Multifunction fibre optic sensing system for smart applications”, IEEE Transactions on Mechatronics, 9, (2004), 40-49.

102. Chen, J., Su, Z. and Cheng, L. “Identification of corrosion damage in submerged structures using fundamental anti-symmetric lamb waves”, Smart Materials and Structures, 19, (2010).

103. Ramadas, C., Balasubramaniam, K., Joshi, M. and Krishnamurthy, C.V. “Interaction of primary anti-symmetric lamb waves with symmetric delaminations: numerical and experimental studies”, Materials and Structures, 18, (2009).

104. Bogetti, T.A. “Process-induced stress and deformation in thick-section thermoset composite laminates”, Journal of Composite Materials, 26, 5, (1992), 626-660.

105. Groot, P.J.D., Wijnen, P.A.M. and Janssen, R.B.F. “Real-time frequency determination of emission for different fracture mechanisms in carbon/epoxy composites”, Composites Science and Technology, 55, (1995), 405-412.

106. Ghorbanpour, M. and Falamaki, C. “ A novel method for the production of highly adherent Au layers on glass substrates used in surface Plasmon resonance analysis: substitution of Tr or Ci intermediate layers with Ag layer followed by an optimal annealing treatment”, Journal of Nanostructure in Chemistry, (2013).

107. SC7640 auto/manual high resolution sputter coater operating manual, Quorum Technologies, Document number OM-SC7640, 01/02, 16-26.

108. Proszynski, A., Chocyk, D. and Gladyszewski, G. “Stress modification in gold metal thin films during thermal annealing”, Optica Applicata, 39, 705, (2009).

Appendix A

A list of publications by the author to-date is given below:

Published/Presented

1. Nair, A.K., Machavaram, V.R., Mahendran, R.S., Pandita, S.D., Paget, C., Barrow, C. and Fernando, G.F. "Process monitoring of fibre reinforced composites using a multi-measurand fibre-optic sensor", Sensors and Actuators B: Chemical, *in-press*.
2. Machavaram, V.R., Nair, A.K., Mahendran, R.S., Wang, L., Harris, D., Paget, C., Barrow, C., Gupta, B.D. and Fernando, G.F. ''Process monitoring of fibre reinforced composites: A tribute'', European Workshop on the Use of Optical Fibres for the Monitoring of Composites Manufacturing Process, Toulouse, France (November 2012).
3. Nair, A.K., Machavaram, V.R., Paget, C., Barrow, C., Gupta B.D. and Fernando, G.F. ''A multi-measurand fibre optic sensor system for process and health monitoring of fibre reinforced composites'', The Ninth International Conference on Condition Monitoring and Machinery Failure Prevention Technologies, London, UK (June 2012).
4. Nair, A.K. and Fernando, G.F. ''Optical sensors for chemical monitoring'', Siemens Discovery Day, University of Birmingham, UK (February 2012).
5. Nair, A.K., Machavaram, V.R., Harris, D., Mahendran, R.S., Fernando, G.F., Paget, C., Barrow, C. and Gupta, B.D. ''Process and health monitoring of fibre reinforced composites using multi-measurand fibre optic sensor'', SAMPE/BCS

Annual Students Seminar, London, UK (January 2012).

6. Nair, A.K., Machavaram, V.R., Harris, D., Mahendran, R.S., Fernando, G.F., Paget, C. and Gupta, B.D. ‘‘Multi-measurand process and health monitoring of fibre reinforced composites’’, Proceedings of the Frontiers in Optics and Photonics Conference, New Delhi, India (December 2011).
7. Fernando, G.F., Mahendran, R.S., Machavaram, V.R., Wang, L., Harris, D., Tomlin, A., Nair, A.K., Pandita, S.D., Malik, S.A., Hellmann, S., Paget, M., Ballard, S., Kukureka S.N. and Gupta, B.D. ‘‘Process monitoring of advanced fibre reinforced composites using novel multi-measurand optical fibre sensor’’, International Conference on Fibre Optics and Photonics, Guwahati, India (December 2010).
8. Mahendran, R.S., Machavaram, V.R., Wang, L., Nair, A.K.R., Burns, J.M., Kukureka S.N. and Fernando, G.F. “A novel multi-functional sensor design for process monitoring”, International Conference on Composite Materials: ICCM-17, Edinburgh, UK (July 2009).

Appendix B

Summary of the residual strain values of CFRP and glass composites reported in the Literature [8, 26, 45, 46, 50, 53, 55].

Author	Laminate	Sensors embedded	Temperature de-coupling	Residual strain (με)
Mulle *et al.* (2009)	8-ply Unidirectional carbon	2 FBGs	Yes	70/75
Kuang *et al.* (2001)	8-ply Quasi-isotropic glass	1 FBG	No	362/359
	8-ply Angle-ply glass	1 FBG	No	368/289
	8-ply uNidirectional carbon	1 FBG	No	214/313
Kang *et al.* (2002)	24-ply Unidirectional glass	2 FP-FBGs	---	-40/-4200
	24-ply cross-ply glass	2 FP-FBGs	---	-280/-380
	16-ply glass fabric	2 FP-FBGs	---	-360/-350
Kang *et al.* (2003)	36-ply Unsymmetric glass	2 FP-FBGs	---	-440/-520
Oliveria *et al.* (2008)	4- ply Unidirectional carbon	1 FBG	No	19.4
	6-ply cross-ply carbon	2 FBGs	No	-89.4/-193
Yoon *et al.* (2006)	4-ply Unidirectional Kevlar	1 FBG	Yes	-800
Leng *et al.* (2003)	16-ply cross-ply carbon	1 FBG	No	-300